



CHALMERS
UNIVERSITY OF TECHNOLOGY

TUDelft



Generic and complete vehicle dynamic models for open-source platforms

VADIRAJ PATIL

*A thesis submitted in partial fulfillment for the
Master of Science programme
in
Solid and Fluid Mechanics
at the
Mechanical, Maritime and Materials Engineering Department
TU Delft*

Generic and complete vehicle dynamic models for open-source platforms

VADIRAJ PATIL



Department of Mechanics and
Maritime Sciences,
*Vehicle Engineering and
Autonomous Systems*
Chalmers University of Technology
Gothenburg, Sweden 2017

Department of Mechanical,
Maritime and Material
Engineering,
Process and Energy
TU Delft
Delft, Netherlands 2017

Generic and complete vehicle dynamic models for open-source platforms
VADIRAJ PATIL

Chalmers University of Technology
Supervisor: Dr. Ola Benderius, MSc. Pär Pettersson, Vehicle Engineering and Autonomous Systems, MSc. Arpit Karsolia, Revere Lab
Examiner: Prof.Dr. Bengt Jacobson, Vehicle Engineering and Autonomous Systems

Delft University of Technology
Supervisor: Dr. Barys Shyrokau, Intelligent Vehicles & Cognitive Robotics
Examiner (Chair): Dr.ir. Rene Pecnik, Process and Energy
Examiner : Dr.ir. Riender Happee, Intelligent Vehicles & Cognitive Robotics

P&E report number: 2838

Cover: Revere's Test vehicles Volvo FH16 and XC90

Abstract

Vehicle dynamics models are important tools for research and development within the automotive industry. The need for such models is steadily rising due to the rapid development of automated driving, as these models allow efficient design and development of the control algorithms and functions. Chalmers Revere Lab supplements research in the field of automated driving and collision avoidance. The lab maintains two test vehicles, a passenger car (Volvo XC90) and a heavy duty truck (6x4 Volvo FH16). The models provided by Volvo are confidential, complicated for implementation as reference models and do not share the same control interface as the test vehicles. The objective of this work is to develop well documented generic and complete open-source models that represent Revere's test vehicles.

The thesis aims to develop three model units per test vehicle. The three model units are a control interface model, a quick simulation model for online prediction and an advanced model for offline simulation prior to track testing. In addition to model development, an investigation has been made on the level of modelling details suitable for automated driving for non-critical highway and city driving on dry asphalt. For instance, a clutch model was implemented to capture the behaviour of starting from a standstill for the test vehicle equipped with an automated manual transmission. The models were developed using Modelica, an object-oriented modelling tool, and Matlab/Simulink. Furthermore, a suitable model architecture was proposed for simulation of automated driving functions.

To assess the validity of the models, the simulation results were compared against experimental data. Data was collected using open-loop test maneuvers and manual driving tests. The simulation results highlight the differences between the simple and advanced model and their accuracy with respect to experimental data. As a use-case, the XC90 advanced model was simulated with a GPS-based autonomous navigation controller. Validation with experimental data showed that the vehicle model is suitable for the development of control algorithms. The simple model is faster than real-time making it suitable for online prediction and the advanced model is real-time capable which was verified with real-time toolbox on Simulink. As a suggestion for future work, the tire model can be improved to handle low-speed parking scenario and a trailer-dolly combination can be added to the tractor model for studies on combination vehicles.

Keywords: Vehicle models, Control interface, Modelica, Matlab/Simulink, Experimental validation, Open-source, Full vehicle simulation

Acknowledgements

I would like to extend my sincere gratitude towards my thesis examiner, Prof.Dr. Bengt Jacobson for all his advice, and inputs toward vehicle modelling and for always providing motivation. I am extremely grateful to my supervisor Dr.Ola Benderius for being my mentor and for his encouragement all throughout the thesis and during the testing sessions at the track. Dr. Sixten Berglund from Volvo GTT and Pär Petersson one of my supervisors from Chalmers, thank you very much for taking out time and giving me inputs on powertrain modelling. Arpit, Björnborg and Fredrik thank you for helping me out with testing at AstaZero.

I would like to thank Dr. Barys Shyrokau, my supervisor at TU Delft for taking out time for all our Skype meetings and for your feedback thought the thesis. I would also like to thank the Erasmus coordinators at Chalmers and TU Delft for giving me an opportunity to conduct my thesis as an exchange student. Thank you, Dr.ir. Rene Pecnik and Dr.ir. Riender Haphee for being part of the thesis committee.

Finally my family and all my friends for the unconditional support and encouragement.

Vadiraj Patil, Delft, August 2017

Contents

List of Figures	xiii
List of Tables	xv
1 Introduction	1
1.1 Background	1
1.2 Problem definition	1
1.3 Research question	2
1.4 Deliverables	2
1.5 Tools	3
1.5.1 Modelling tools	3
1.5.2 Software packages	3
1.5.3 Functional Mock-up Interface	4
1.6 Report Outline	4
2 Vehicle modelling theory	5
2.1 Types of models	6
2.1.1 Vertical dynamics model	6
2.1.2 Longitudinal and lateral dynamics model	8
2.1.3 Full dynamics model	9
2.2 Tire model	10
2.3 Powertrain	10
2.4 Suspension	11
2.5 Steering	11
2.6 Brakes	12
2.7 Vehicle control	12
2.8 Cabin dynamics	13
2.9 Summary	13
3 Methodology	15
3.1 Model requirements	16
3.1.1 Model evaluation criterion	16
3.2 Model architecture	17
3.3 Control interface model	18
3.3.1 Control interface model FH16	18
3.3.2 Control interface model XC90	20
3.4 Simple model for actuated vehicle	21

3.4.1	Common model components	22
3.4.1.1	Wheel model	22
3.4.1.2	Vehicle body	25
3.4.1.3	Powertrain	25
3.4.2	FH16 simple model	28
3.4.2.1	Brakes model	28
3.4.3	XC90 simple model	29
3.4.3.1	Powertrain	29
3.4.3.2	Brakes model	29
3.5	Advanced model for actuated vehicles	30
3.5.1	Common model components	30
3.5.1.1	Wheel model	30
3.5.1.2	Steering	34
3.5.2	FH16	34
3.5.2.1	Vehicle body	34
3.5.2.2	Axles	40
3.5.2.3	Cab	44
3.5.2.4	Powertrain	47
3.5.3	XC90	54
3.5.3.1	Vehicle body	54
3.5.3.2	Suspension	57
3.5.3.3	Powertrain	59
3.6	Summary	60
4	Results and Discussion	63
4.1	Results FH16	64
4.1.1	Longitudinal test	64
4.1.1.1	Test 1 FH16: Slow acceleration to 8–10 m/s	64
4.1.1.2	Test 2 FH16: Step acceleration to 13–15 m/s	67
4.1.1.3	Test 3 FH16: Step acceleration of 100 %	69
4.1.1.4	Test 4 FH16: Manual driving of driving cycle 1	71
4.1.1.5	Test 5 FH16: Manual driving of driving cycle 2	73
4.1.2	Lateral test	76
4.1.2.1	Test 6 FH16: Manual lane change test	76
4.1.3	Discussion FH16	78
4.2	Results XC90	81
4.2.1	Longitudinal test	82
4.2.2	Lateral test	84
4.2.3	Discussion XC90	86
4.3	Computational efficiency	87
4.4	Use-case: GPS-based autonomous navigation	87
4.5	Summary	91
5	Conclusion and Recommendation	93
5.1	Conclusion	93
5.2	Recommendations	95

Bibliography	99
--------------	----

A Appendix 1	I
--------------	---

Contents

List of Figures

1.1	From original thesis description	2
2.1	Quarter car model (Pg.851 [6])	6
2.2	Half car model: Pitch and heave (Pg.855 [6])	7
2.3	Half car model: Roll and heave (Pg.860 [6])	7
2.4	Full car model: Vertical dynamics studies (Pg.867 [6])	8
2.5	Kinematic bicycle model[7]	9
2.6	Example of full dynamics 3D view of two track [13]	9
2.7	Classification of tire models (Pg.85 [14])	10
2.8	Classification of driving simulation (Pg.595 [18])	11
2.9	Rack and pinion steering mechanism (Pg.66 [19])	12
3.1	Methodology	15
3.2	Model architecture for simulation of automated driving functions	18
3.3	Control interface and vehicle model block diagram FH16	19
3.4	Control interface and vehicle model block diagram XC90	20
3.5	ISO 8855 coordinate system [13]	22
3.6	Single track model(Pg.153 [5])	22
3.7	Wheel and body coordinate system (Pg.147 [5])	23
3.8	Wheel torque equilibrium	24
3.9	Longitudinal tire forces for different combined slips	24
3.10	Longitudinal force balance for single track model	25
3.11	Convention for analysis of torques and speed	26
3.12	Vehicle driveline	26
3.13	Plunger spring travel vs brake pressure	29
3.14	Brush tire model side and top view (Pg.40 [15])	31
3.15	Longitudinal force vs longitudinal slip	33
3.16	Lateral force vs lateral slip	33
3.17	Self-aligning moment vs lateral slip	33
3.18	Free body diagram of longitudinal forces	36
3.19	Free body diagram for chassis (vertical and roll configuration)	38
3.20	Free body diagram for chassis (Pitch configuration)	39
3.21	Steered axle	40
3.22	Roll moment balance axle and chassis	41
3.23	Pitch moment balance axle and chassis	41
3.24	Axle free body diagram	42
3.25	Cab and chassis free body diagram	44

3.26 Engine flow diagram	47
3.27 Powertrain node diagram for advanced model	48
3.28 Torque distribution for axle configurations	50
3.29 Engine speed clutch controller	53
3.30 Clutch actuation flow diagram	53
3.31 Planar free body diagram for passenger car	55
3.32 Vertical DOF for a passenger car	57
3.33 Roll moment balance for a passenger car	58
3.34 Pitch moment balance for a passenger car	59
3.35 Driveline node diagram for XC90	59
3.36 Torque ratio vs speed ratio	60
3.37 K factor vs speed ratio	60
4.1 Actuation input for slow acceleration to 8–10 m/s	65
4.2 Longitudinal results for test 1 FH16	66
4.3 Actuation input for step acceleration to 13–15 m/s	67
4.4 Longitudinal results for test 2 FH16	68
4.5 Actuation input for step acceleration of 100 %	69
4.6 Longitudinal results for test 3 FH16	70
4.7 Recorded test inputs for the driving cycle	71
4.8 Longitudinal results of test 4 FH16	72
4.9 Recorded test inputs for the driving cycle 2	73
4.10 Longitudinal results of test 5 FH16	74
4.11 Lateral acceleration and yaw rate for driving cycle 2	75
4.12 Input for Test 6 FH16	76
4.13 Longitudinal results of test 6 FH16	77
4.14 Lateral results of test 6 FH16	78
4.15 Comparison of Engine speed and torque for test 1 and 2 FH16	79
4.16 Engine speed and torque for test 5 FH16	80
4.17 Input for Test 1 XC90	82
4.18 Longitudinal results of test 1 XC90	83
4.19 Input for Test 2 XC90	84
4.20 Longitudinal results of test 2 XC90	85
4.21 Lateral results of test 2 XC90	86
4.22 Model architecture followed with GPS based autonomous navigation	88
4.23 Trajectory in lat–lon for GPS-based autonomous navigation	89
4.24 Longitudinal velocity in m/s for GPS-based autonomous navigation	89
4.25 Controller acceleration input	90
4.26 Controller steering input	90
4.27 Comparison of vehicle steering input with model and actuation input	91

List of Tables

1.1	Pros(+) and cons(-) of approaches within <i>Modelica</i>	3
4.1	Energy consumed	81
4.2	Simple model run-times	87

List of Tables

1

Introduction

1.1 Background

Dynamics vehicle models play a vital role in research and development of vehicles ranging from bicycles to heavy road vehicles. Vehicle models serve as virtual prototypes in the development phase, giving developers an insight on the influence of design parameters on vehicle behaviour. With simulation models, developers can test and optimize their designs, control algorithms and several other functions. There are a number of applications where vehicle models are needed, for example in driving simulators, lap-time simulators, controller design for automated driving, product development. Depending on the application, these models can be represented as a point mass model or can be extended to multibody or even as inverse models with several hundred variables.

This report describes the development and validation of models of Volvo FH16 (tractor) and XC90 (passenger car). The vehicles are being maintained at Revere (Resources for vehicle research), a research lab at Chalmers University. The lab supports several projects working towards automated driving and collision avoidance research with well-equipped test vehicles and track testing. Furthermore, the lab aims to use the vehicle models to conduct simulations before track testing and provide the models to incoming project groups for their research work.

1.2 Problem definition

Revere has received two test vehicles (Volvo XC90 and Volvo FH16 Tractor) from VCC and Volvo GTT to supplement research especially in fields of active safety and automated driving. These vehicles have a special control interface for longitudinal and lateral actuation in addition to standard driver inputs. The current models which are provided by Volvo are difficult to use as reference model, and do not share the same control interface and cannot be shared with other projects due to their confidentiality. To overcome these restrictions, Revere aims to develop open-source models of the test vehicle that can facilitate current and future research.

1.3 Research question

- What level of model detail is suitable for automated driving for:
 - Non-critical highway driving (*)
 - Non-critical city driving
- What is a suitable model architecture for simulation of automated driving function ?

(*)Up to speed limits of 90 km/h for the truck and 120 km/h for the car and in good weather condition.

1.4 Deliverables

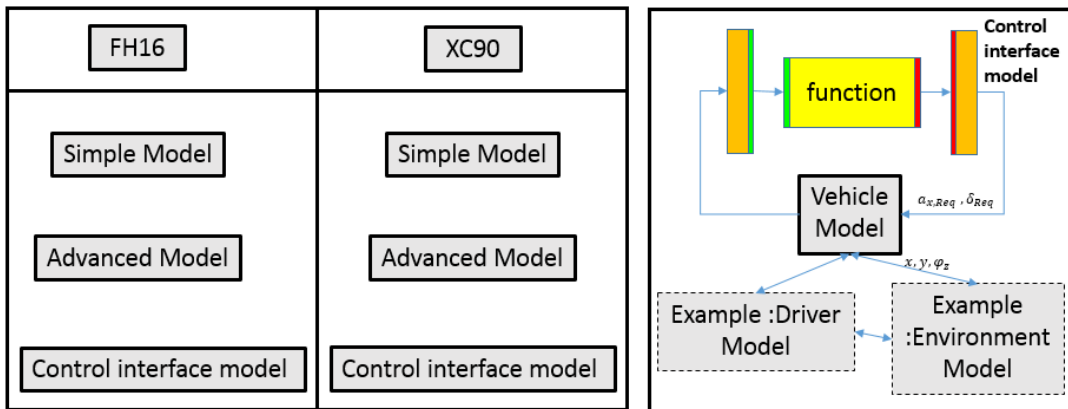


Figure 1.1: From original thesis description

The following are the deliverables of the thesis:

- Develop open-source models of test vehicles:
 - Volvo FH16
 - Volvo XC90
- For each test vehicle
 - Control interface model
 - Set 1 simple model
 - Set 2 advanced model
- Model validation through track testing.

1.5 Tools

1.5.1 Modelling tools

There are several tools available for developing physical models, such as MATLAB/Simulink, IPG CarMaker, CarSim, MSC ADAMS, Modelica-tools etc. For this work, the vehicle models are written using Modelica programming language. The primary reason for using Modelica is that it is an open source programming tool. Furthermore, it is an acausal and object-oriented programming tool. Which, makes it suitable for modelling large, complex and heterogeneous systems. It is based on declarative notation of models, where the order for solving the equations is not relevant but decided by the tool itself. MATLAB and Simulink are based on causal approach, but Simulink also offers a tool called Simscape which is based on the acausal notation.

In *Modelica*, vehicle models can be developed using three methods:

- Text based
- Graphical/block oriented using Modelica standard library
- Commercial vehicle dynamics library and graphical interface

Each approach has its own benefits and pitfalls. Developing vehicle models from scratch is a tedious and time-consuming task, but it offers a structured environment to build the models ensuring good readability and flexibility. The graphical approach uses blocks from the Modelica standard library such as mass, gear, inertia. This approach gives a good understanding on the working of the model, but as the model complexity increases, the number of blocks also increase making it difficult to understand and make changes. Using commercial vehicle dynamics library allows easy and quick generation of models using predefined components like tires, suspension, steering etc. Such a library is not open-source and difficult to develop. For this thesis, the text-based approach would be best suited for its modular and open-source nature.

Table 1.1: Pros(+) and cons(-) of approaches within *Modelica*

Text based approach	Library based approach	
	Modelica Standard Library	Vehicle Dynamics Library
+Open-source	+Open-source	-Commercial
+Modular	+Modular	+Modular
++Highly flexible	+Flexible to a certain extent	+Flexible to a certain extent
-High workload	-Workload increase with complexity	+ Simple and easy to use

1.5.2 Software packages

A number of tools are available which are based on Modelica language, to name a few Dymola from Dassault Systems, OpenModelica, JModelica, AMESim, MapleSim, Math-Modelica, and SimulationX. Dymola 2016 is used as the software to execute Modelica code and conduct preliminary simulations. To compare the model against log data, MATLAB and Simulink are used with the Modelica model imported to Simulink as an Functional mock-up Unit (FMU) which is discussed in the next section.

1.5.3 Functional Mock-up Interface

FMI is a standard that is used to generate C code from a dynamical system model which can be simulated by various modelling software. FMI toolbox generates a FMU that consists of a model interface which is a set of C functions for equation evaluation and a Model description schema which is an XML file containing model metadata and variable definition. Dymola supports the creation of FMU which can be exported as:

- Model exchange
- Co-simulation
- Both model exchange and co-simulation
- Co-simulation with Dymola solvers

The two main file types of FMU are model exchange(.me) and co-simulation(.cs). In model exchange no solver is included in the FMU hence the simulation environment solver will be used and in co-simulation the FMU includes a solver [1].

1.6 Report Outline

The introduction chapter of the report is followed by a literature study on vehicle modelling theory. It is followed by a chapter discussing the methodology of developing all the models and the equations. Following the methodology chapter the testing maneuvers and results are discussed. Finally, the conclusion and recommendations for future work are presented.

2

Vehicle modelling theory

In this chapter based on the available literature, different types of vehicle models are studied, which is followed by literature study on modelling of the important vehicle sub-units.

There are different types vehicle models, each meant for a specific purpose. The system elements or components of the vehicle model govern its behaviour. For example, a quarter model (one or two degrees of freedom (DOF) vertical model), for studies towards vertical dynamics, like active suspension as in [2] or 14DOF model that is suitable for Roll dynamics study [3]. There are other detailed vehicle models with 38 DOF [4] or multibody models available within commercial software packages with more than 100 DOF. The degree of detail required on the model is determined by the application. Before looking into different types of vehicle models it is important to know the various system elements that compose a complete vehicle model. They are:

1. Vehicle body
2. Wheel and Tires
3. Powertrain
4. Suspension
5. Steering
6. Brakes
7. Vehicle control

The above list is applicable for the passenger car having two axles and four wheels, in addition to these components there are more components that are present on a heavy vehicles like a truck such as [5]:

1. Cabin
2. Fifth wheel, coupling points and towed units
3. Multiple axles

2.1 Types of models

As discussed previously, vehicle models serve a certain purpose based on which they are classified as follows:

1. Vertical dynamics model
2. Longitudinal and lateral dynamics model
3. Full dynamics model

2.1.1 Vertical dynamics model

To investigate behaviour related to vertical dynamics of a vehicle, a quarter model can be used to study vehicle suspension as suggested in [6]. The quarter car model with one or two DOF as the name suggests is one corner of a vehicle which is represented by a spring–mass–damper as in the figure 2.1. The quarter car can be extended to a half car model with at least three DOF. In the figure 2.2, the model has wheel heave, body heave and pitch.

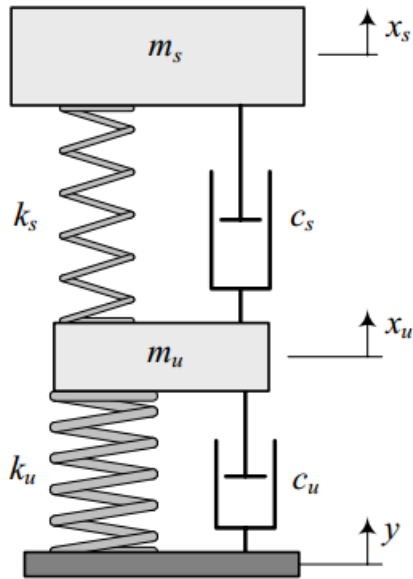


Figure 2.1: Quarter car model (Pg.851 [6])

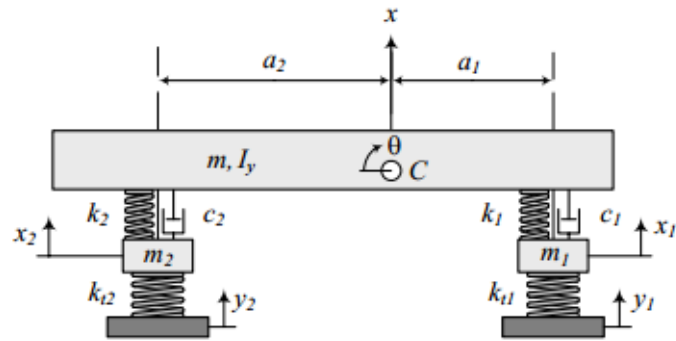


Figure 2.2: Half car model: Pitch and heave (Pg.855 [6])

When only the left and right wheel of the vehicle are considered, it would be a half car model for roll and heave studies as shown in figure 2.3. It has to be kept in mind that front and rear half of the model would be different due to different mass distribution and suspension properties.

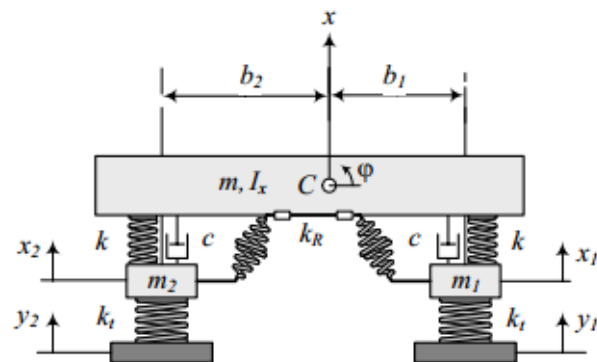


Figure 2.3: Half car model: Roll and heave (Pg.860 [6])

A full vibration model as in figure 2.4 has seven DOF body pitch, roll, heave and individual wheel displacement.

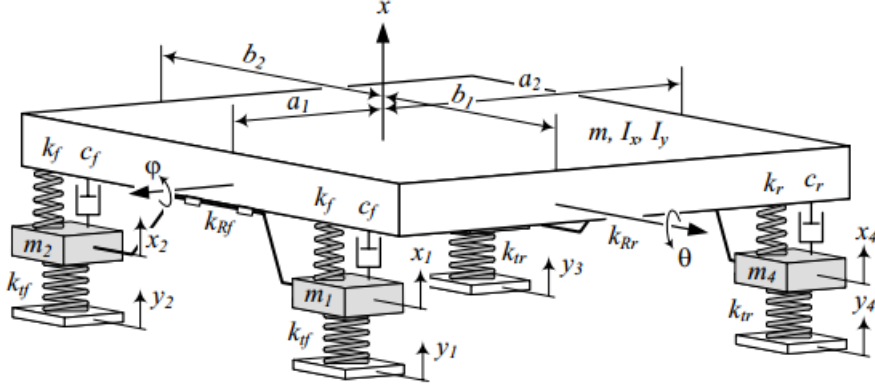


Figure 2.4: Full car model: Vertical dynamics studies (Pg.867 [6])

2.1.2 Longitudinal and lateral dynamics model

Lateral and longitudinal vehicle models exhibit planar motion, single track model is one such example. In a single track model, the left and right wheels are combined as one wheel for both the axles as shown in the figure 2.5. For such models, it is assumed that the wheel slip angles are zero at low speed. For these models, the total lateral force around a curved road of radius R is given by:

$$F_y = \frac{m \cdot v^2}{R} \quad (2.1)$$

Based on these equation, the motion equations for the kinematic model are given by,

$$\dot{x} = v \cdot \cos(\psi + \beta) \quad (2.2)$$

$$\dot{y} = v \cdot \sin(\psi + \beta) \quad (2.3)$$

$$\dot{\varphi}_z = \frac{v \cdot \cos(\beta)}{l_f + l_r} \cdot (\tan(\delta_f) - \tan(\delta_r)) \quad (2.4)$$

Where x and y are the trajectories and φ_z is the yaw angle. Due to their simplicity, such kinematic models can be used for path planning and design of control methods for automated driving [7].

The discussed kinematic model is not suitable for higher speeds since the velocity vector and wheel directions are no longer pointing in the same direction. For this reason, the lateral forces from the tires are modelled as a function of tire lateral slip, or generated from a tire model. Using these forces, equations of motion around the centre of gravity (CG) of the body can be obtained from Newton's and Euler's equilibrium equations. This is called a dynamic single-track model. Furthermore, adding longitudinal load transfer gives better results in comparison to the kinematic models and can be suitable for studies related to anti-lock braking system (ABS) and limit handling of automated driving vehicles [8]. Such a single track model is suitable for passenger cars but for combination vehicles with towed units a different model is needed. This can be found in the studies done by [9], [10].

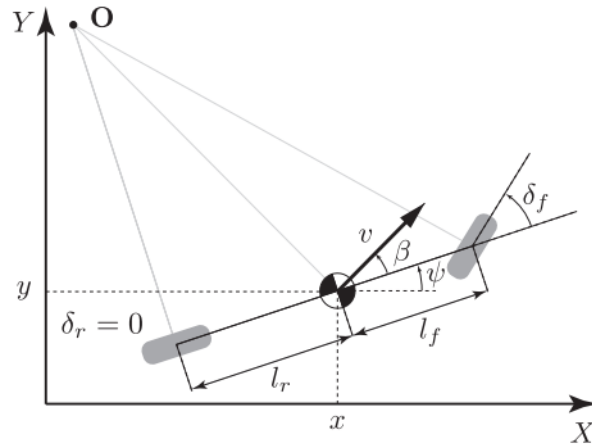


Figure 2.5: Kinematic bicycle model[7]

2.1.3 Full dynamics model

The last two sections 2.1.1 and 2.1.2 handled out of road plane (OORP) and in road plane (IRP) motion independently. A full dynamics model can be seen as a combined model taking into account OORP and IRP motion. A nonlinear eight DOF model is suitable for several vehicle dynamics studies [11] that has lateral, longitudinal, roll and yaw motion, and four wheel rotations. Adding wheel displacements in the vertical direction, body pitch and heave gives a 14 DOF model. Such a full dynamics vehicle model gives a good representation of the real vehicle and is suitable for integrated control [12].

In case of full dynamics model for a truck, additional degrees of freedom such as cabin dynamics, articulated trailer and dolly need to be taken into account [5]. In this thesis only the tractor model will be developed. Although the combination will not be studied, the tractor model would be suitable to be a part of combinations in future works.

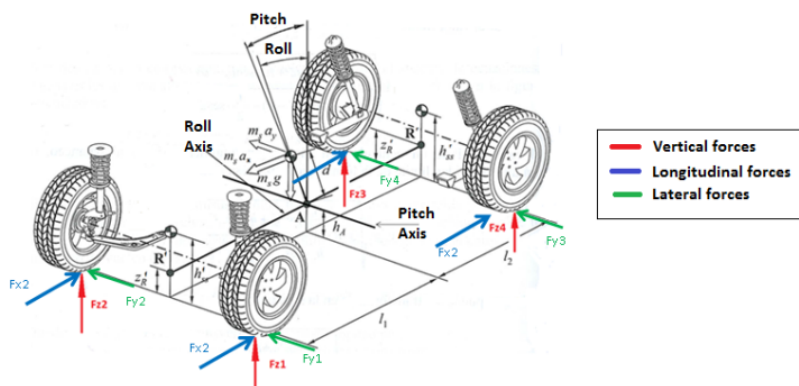


Figure 2.6: Example of full dynamics 3D view of two track [13]

2.2 Tire model

The tires are vital components for vehicle modeling since tires transmit forces from the ground to the vehicle and vice versa.

Tire models are categorized as in the figure 2.7, the models on the left are based on experimental data while the ones on the right are theoretical based [14]. Magic formula tire model is an example for experimental data based model and examples of the similarity method can be found in [14]. A Brush tire model is an example of simple physical model and FEM tire models are examples of complex physical models. The models in the middle are based on both mathematical and experimental studies. Each model has its benefits as some models are computational feasible but limited tunability for a certain combination of tire and road surfaces. While the others, describe the behaviour with greater accuracy but at a large computational cost. Some models are suitable for vehicle dynamics simulations while others are suited for studies related to tire construction.

from experimental data only	using similarity method	through simple physical model	through complex physical model
fitting full scale tyre test data by regression techniques	distorting, rescaling and combining basic characteristics	using simple mechanical representation, possibly closed form solution	describing tyre in greater detail, computer simulation, finite element method

Figure 2.7: Classification of tire models (Pg.85 [14])

In one of the previous studies on driving simulator [13] the author studied three types of tire models suitable for real-time simulation. The three models studied were Magic formula or Pacejka tire model, similarity method and brush model. Among the three models, Brush model was chosen for its simplicity and physical nature additionally only a few parameters are needed for tuning the model. Studies about the brush tire model and its comparison have been done in [15] and they discuss the compromise between modelling simplicity and tunability of the model. In this thesis for the simple model, a combined slip isotropic tire model will be used and a brush tire model for the advanced vehicle model.

2.3 Powertrain

Under this section the vehicle powertrain and its components will be discussed. A general powertrain unit for a vehicle with automatic/automated transmission consist of the following sub-components:

1. Engine
2. Main clutch or Torque converter
3. Transmission, with shift elements (couplings, clutches, brakes [16])
4. Final drive

Vehicle powertrain is a complicated system and has a great influence on the vehicle performance. Powertrain subsystem modelling has developed greatly since the 1950s [17]. Powertrain modelling has several applications, one closely related to this study is driving simulation, which can be categorized into 3 parts as suggested in [18]

1. Submicroscopic
2. Microscopic
3. Macroscopic

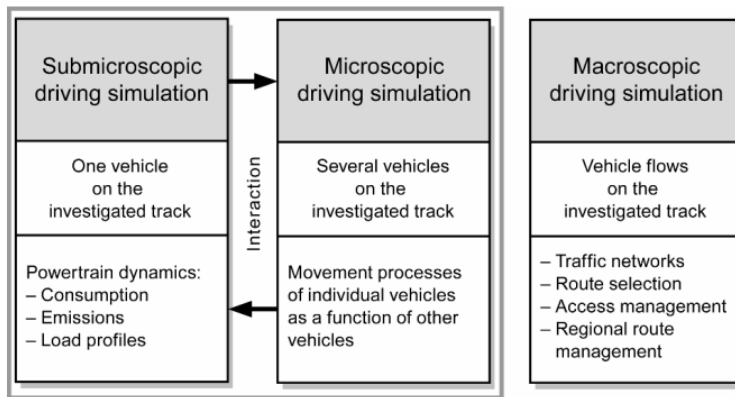


Figure 2.8: Classification of driving simulation (Pg.595 [18])

In this study a part of submicroscopic driving simulation will be studied, aiming to capture the behaviour of powertrain components present in the two test vehicle for a number of test maneuvers.

2.4 Suspension

For a full dynamics model such as an eight or 14 DOF, the transmission of forces from the wheels to the body would be governed by the suspension. The force transmitted is influenced by the kinematic and dynamic components of the suspension system such as links, springs and dampers. In this study, suspension modelling is equation based as in [13] and [19] which captures longitudinal and lateral load transfer, roll and pitch behaviour but do not include suspension kinematics and compliance. Such models have been used for studies on vehicle handling stability [20], integrated vehicle control [12] and for control of automated vehicles [21].

2.5 Steering

The steering system is responsible for providing direction to the front wheels of the vehicle and also controls the rear wheel steering angle if 4-wheel or rear-wheel steering is present on the vehicle. Some common steering mechanisms are rack and pinion or a worm and nut [6]. In the case of a rack and pinion mechanism, the steering wheel is connected to the pinion through one or two universal joints. The input to the steering wheel is transmitted through the joints to the pinion which mates with the rack. The rotational

motion of the pinion is translated into linear motion of the rack, which is connected to the steering arms. The movement of the rack causes the wheels to move via the arms. In the case of power steering, hydraulic piston arrangement or an electric motor provide torque assistance based on the driver input to reduce steering effort. Similarly, in the case of worm and nut mechanism, the rotation of the worm causes the nut to reciprocate which is connected to another gear attached to the pit arm. The pit arm motion is transmitted to the wheel through two other steering linkages. To model the steering system the dynamic effects will be captured by modelling it as first order ordinary differential equation (ODE) [22]. Detailed steering models capturing the power steering mechanism [23] will not be a part of this study.

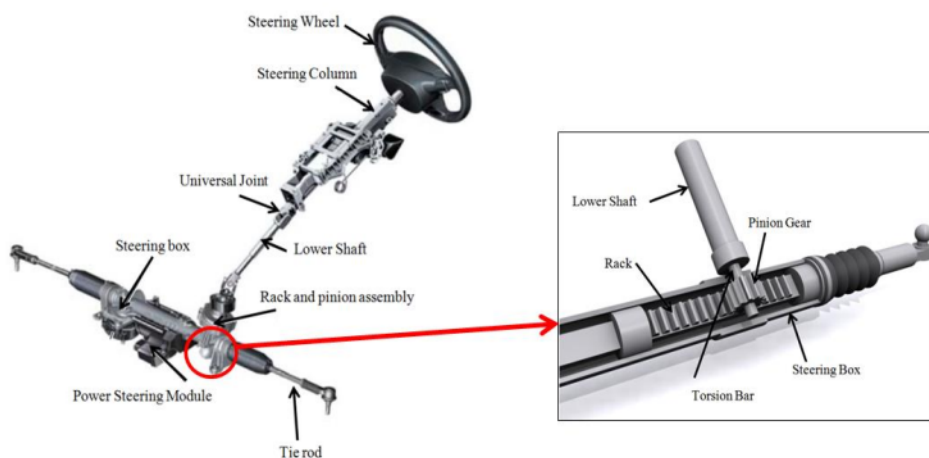


Figure 2.9: Rack and pinion steering mechanism (Pg.66 [19])

2.6 Brakes

The braking subsystem present in the tractor is based on pneumatics while the system on the passenger car is based on hydraulics. In [24] the author describes the model and working of pneumatic braking system and [25] models a hydraulic braking system on passengers. In this study based on the literature studied for braking, simplification are made on the braking mechanism and the models are developed which can be found in the next chapter.

2.7 Vehicle control

Vehicle control can typically be subdivided into control at subsystem level and at vehicle level. For example, wheel slip control in the braking subsystem or steering assist in steering subsystem. Adaptive cruise control (ACC) or stability control are examples of vehicle level control. Modelling such control units is not a part of this work but some control units in the powertrain such as the clutch control and gearshift control are modelled with certain assumptions.

2.8 Cabin dynamics

In heavy vehicles, the cabin houses the instruments and is suspended from the chassis for driving comfort. This is typically modelled by adding three DOF to the vehicle model of the tractor cabin heave, roll, and pitch. A similar model was used to design control methods to suppress cabin motion [26]. Modelling cabin dynamics is useful for studying the cabin motion and its effect on motion comfort for automated driving.

2.9 Summary

The vehicle models provided by Volvo have certain limitations like lack of flexibility in terms making changes and interface difference between the test vehicle and the models. Additionally, there are several commercial software packages that provide developed models but such model are difficult to understand and to make changes on them. As seen in the literature *Modelica* an open-source tool offers a platform to develop dynamic models that are easy to understand and well structured. In this chapter based on literature study it is observed that most vehicle models are built for a specific purpose, but there is limited information available regarding modelling detail for automated driving. For instance, most vehicle models used for control studies operate at a constant velocity, ignoring the start-up phase, but this phase is important for many automated driving functions. There is limited information on simulation architecture for developing automated driving control functions. Based on the different types of models and the required level modelling detail in the next chapter (Ch.3), the models developed in this work are discussed. A simulation architecture for the testing of automated driving function is proposed. The deliverables of this work are as follows:

- For each test vehicle
 - Control interface model
 - Simple model
 - Advanced model
- Model validation through track testing

3

Methodology

In the previous chapters Ch.1 and Ch.2 the problem definition, deliverables and the different types of vehicle models and theory regarding different system elements were studied. This chapter begins with the model requirements in section 3.1, followed by discussion on requirements testing and validation criteria. The next section 3.2 is focused towards model architecture after which the actuation control interface for both the vehicles are studied, following this are the sections 3.4 and 3.5 for the simple model and advanced model for actuated vehicles.

In this work, the models are built with an iterative approach based on real testing and modelling as shown in figure 3.1.

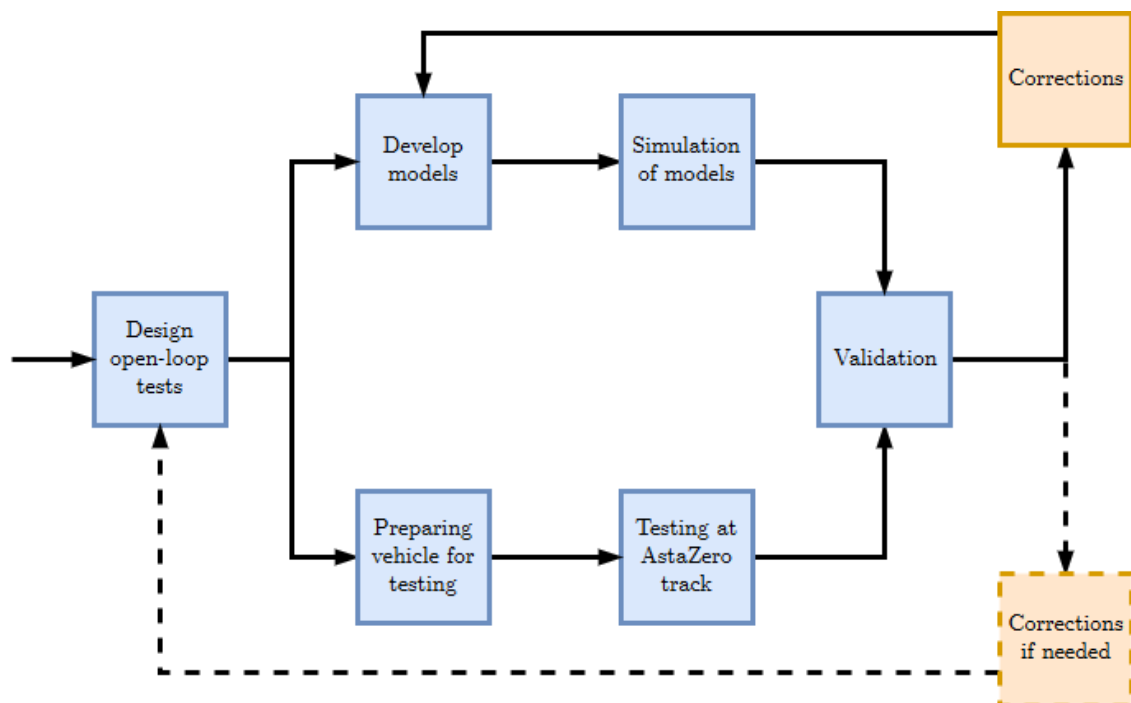


Figure 3.1: Methodology

3.1 Model requirements

In this section, the requirements on the models are discussed. These requirements state the assumptions made for developing the models and the test maneuvers. The models shall be evaluated keeping in mind these requirements set on them. The requirements below will be followed for testing and developing the vehicle models:

- Starting from standstill
- Road bank angle is 0
- Minimal road gradient (± 1 deg)
- Flat road (No road irregularities)
- Dry asphalt

Some requirements on the vehicle variables:

- Longitudinal velocity range: -15 to 80 km/h or -4 to 22 m/s (due to test area restrictions)
- Longitudinal acceleration range(m/s^2)
 - FH16 tractor: -3 to 2.5
 - XC90: -4 to 2.5
- Lateral acceleration (for both vehicles): $\pm 3 m/s^2$
- No driver model
- Parking maneuver (low speed) not covered

All the tests will be started from standstill and terminated by bringing the vehicle to standstill. The FH16 tractor 3rd axle will be raised and will be driven unloaded with no towed units for all the tests. The testing will be conducted using open-loop and manual driving. For open-loop testing, the special control interface present on the vehicle shall be used to actuate the vehicle. The inputs will be sent using .csv files to the CAN bus with MATLAB Vehicle network toolbox or OpenDLV.

3.1.1 Model evaluation criterion

To evaluate models from the collected experimental data a set of longitudinal and lateral variables shall be used. The variables for the FH16 and XC90 are:

Longitudinal variables

- x longitudinal distance covered [m]
- v_x longitudinal velocity [m/s]
- a_x longitudinal acceleration [m/s^2]

Lateral variables

- a_y lateral acceleration [m/s^2]
- ω_z yaw rate [rad/s]

Same actuation inputs are given to the real vehicles and the models. The collected results from the experiments and simulation are compared against each other. For each of the variables, the data from experiments, simple and advanced model are plotted together for comparison. Next to this plot window, a histogram of the absolute error is plotted. The absolute error is the difference between the log data and simulation data at each time step. The error will be only calculated when the input signals are given and until the maneuver is completed.

3.2 Model architecture

This section is dedicated towards design of model architecture for simulation of automated and semi-automated driving functions. An architecture is proposed to illustrate how the model can interact with function blocks for automated driving. A general architecture with the possible sub-function is discussed here, but the definition of the sub-function can vary depending on the area of focus of the research group. Similar work has been done in [27]–[29] where simulation architectures have been studied and in the work [30], [31] the architectures for real case automated driving have been studied.

The major units in the model architecture are the vehicle control function, environment model, test vehicle model and adaptation interface. The vehicle control function unit is responsible for the driving of the vehicle. A few example sub units for this unit are listed below.

- Driver model
- Driving simulator interface
- Automated driving function
- Semi-automated driving function with decision unit

The environment unit sets-up and manages models of obstacles, road, weather, traffic and the scenario. The test vehicle model unit is a virtual representation of the real vehicle and has the same interface as the real vehicle. It transmits the same signals and this will be the area of focus in this thesis. The adaptation interface is responsible for the interaction between the units. For example, if the vehicle model unit and control function unit are developed using different tools, the adaptation interface will make the necessary changes to the signals such that both units can exchange information. An example adaptation interface has been discussed in the use-case section 4.4.

Figure 3.2 shows the block diagram of the model architecture. The vehicle control function interacts with the environment model and through the adaptation interface it interacts with the vehicle model. The common signals that are sent between the vehicle control function and the vehicle model are actuation requests, required vehicle states, other vehicle variables and information such as xy position transformed to GPS coordinates. From the environment model the vehicle control function receives sensor data that is

3. Methodology

generated based on the interaction between the vehicle model and the environment. Based on this interaction the environment model accordingly manages the scenario and traffic.

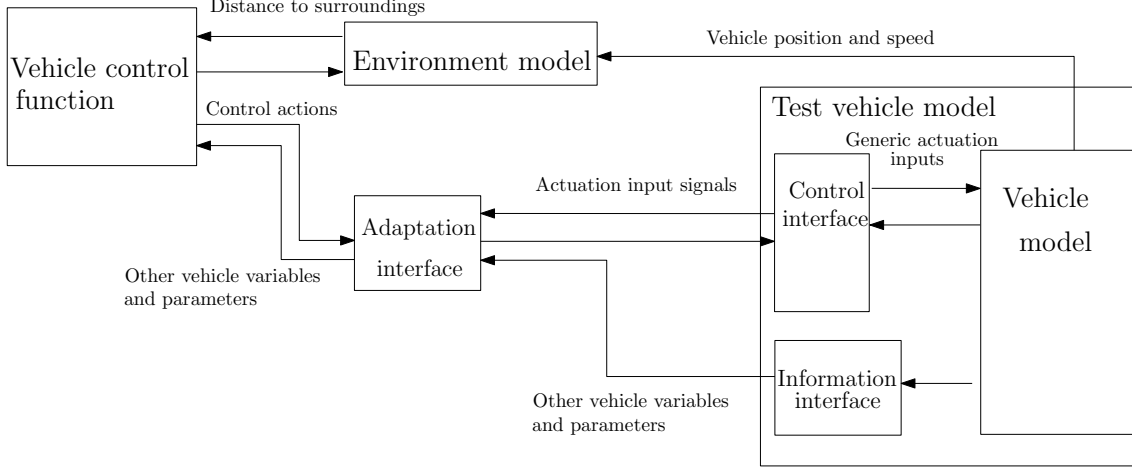


Figure 3.2: Model architecture for simulation of automated driving functions

3.3 Control interface model

The Revere test vehicles are controlled through a set of actuation signals via the control interface. For each vehicle, the control input signals are different. Before looking into the control input signals present on the test vehicles, the generic inputs to the vehicle models are listed to have a better understanding of the control interface model. The input actuation signals or request signals to the vehicle models are the following:

- Steering Wheel angle [rad]
- Accelerator pedal position [%]
- Brake pedal position [%]

For example, the Revere FH16 accepts road wheel angle as an input signal to steer the front wheels. In this case the request signal is accepted by the Volvo Dynamic Steering system (VDS) and sent to the front road wheels. So, the control interface model is a simple version of the VDS. For the models to represent the Revere FH16, it is important to have a representation of the control interface model. The control interface is modelled as a different block so that future interface upgrades will require only the control interface to be updated and not the vehicle model.

3.3.1 Control interface model FH16

In this section, the FH16 control interface model is discussed. The request signals to the interface model for automated driving mode are:

- Road wheel angle request [rad]
- Accelerator pedal position request [%]

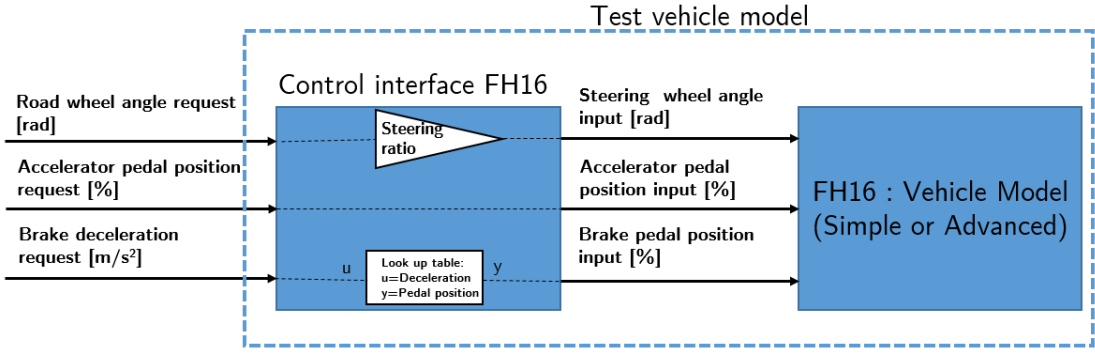


Figure 3.3: Control interface and vehicle model block diagram FH16

- Brake deceleration request [m/s^2]

Figure 3.3 shows the block diagram for the control interface. Road wheel angle is multiplied by the steering ratio to obtain the steering wheel angle. The mapping between brake deceleration and brake pedal position is done using the relation between brake plunger spring travel and brake pressure as in figure 3.13 based on the assumptions used to design the brakes system. A plunger spring is present at the foot brake valve and the brake pedal. The brake pedal travel is related to the plunger spring travel by a ratio B_{pst} . It is assumed that for a maximum brake pressure of 12 bar the corresponding maximum braking torque generated is 22-25 KNm. Using this relation, the braking torque values for the remaining pressure values are interpolated which gives the relationship between plunger spring travel and braking torque. To calculate the braking torque from the brake deceleration request B_{dec} , the vehicle is assumed as a free rolling wheel of radius r_w and a lumped mass m_{lump}

$$T_{breq} = m_{lump} \cdot B_{dec} \cdot r_w \quad (3.1)$$

$$B_{ped,req} = f(T_{breq}) \cdot B_{pst} \quad (3.2)$$

Now that the brake deceleration B_{dec} is related to the torque a look-up table is set-up to determine the travel of the plunger spring. Ratio B_{pst} gives the final mapping to brake pedal travel $B_{ped,req}$. As the vehicle model and control interface both accept accelerator pedal position, no change is made to this signal.

3.3.2 Control interface model XC90

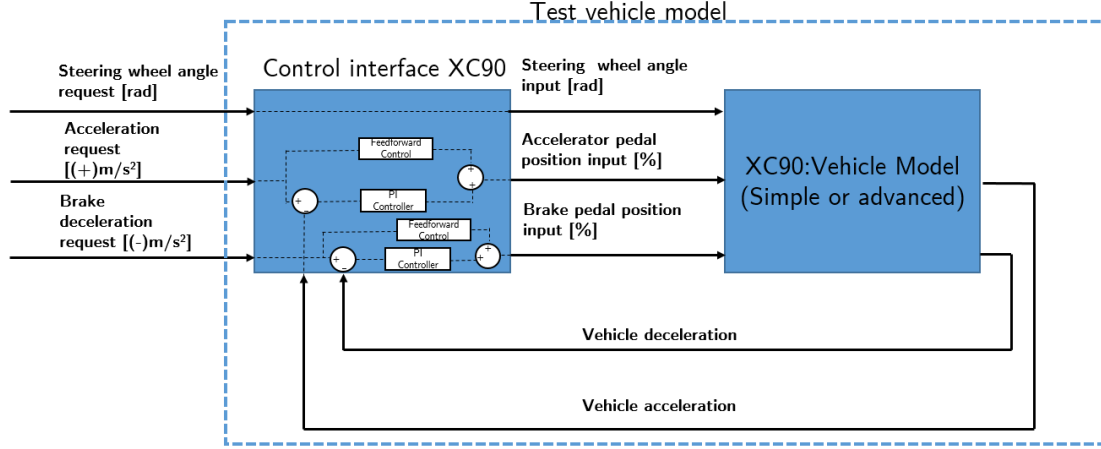


Figure 3.4: Control interface and vehicle model block diagram XC90

For XC90 the request signals available for automated driving mode are:

- Steering wheel angle request [rad]
- Acceleration request [m/s^2]
- Brake deceleration request [m/s^2]

The Revere XC90 control interface accepts steering wheel angle in radians (rad) which is same as on the model hence no mapping is required. In the case of longitudinal request signals, the vehicle accepts acceleration value. If positive, the vehicle velocity increases and if negative the vehicle decelerates. Firstly, acceleration will be looked into followed by deceleration.

Accelerator pedal mapping

To determine the accelerator pedal position from the requested acceleration, an equivalent wheel torque needs to be calculated. To determine the torque, the vehicle is assumed to be a lumped inertia of mass m in the form of a rotating disc with no slip. A force balance equation is written taking into account the air drag F_d , rolling resistance torque T_{roll} (which will be explained in the later section), lumped inertia of the wheel J_w and inertia of the powertrain J_{tot} . The torque at the wheel $T_{w,req}$ is given as :

$$T_{w,req} = ((m + \frac{J_w + J_{tot}}{r_w^2}) \cdot a_{req} - F_d) \cdot r_w - T_{roll} \quad (3.3)$$

$$J_{tot} = J_e \cdot (i_g \cdot i_f)^2 \quad (3.4)$$

$$T_{e,req} = \frac{T_{w,req}}{i_g \cdot i_f} \quad (3.5)$$

$$T_{e,max} = f(\omega_e) \quad (3.6)$$

$$A_{ped} = \frac{T_{e,req}}{T_{e,max}} \cdot 100 \quad (3.7)$$

From the above equations the engine request torque $T_{e,req}$ is determined based on the acceleration request a_{req} . Based on the engine speed ω_e the maximum torque $T_{e,max}$ available is determined. Assuming a linear relationship between the pedal position and request torque, the pedal position A_{ped} is obtained. While in reality, the vehicle will have an inverse pedal map and fuel map that will the relationship between the torque and pedal position. Since such data is difficult to obtain a linear assumption is made. A PI controller is added to make up for any discrepancies from the assumption made on the engine map. The controller is tuned to follow the reference acceleration with pedal position as the output from the controller [32].

Deceleration mapping

Similar to the acceleration mapping the brake deceleration is used to determine the desired or requested braking torque. A proportional controller is used to generate the brake pedal position, with the controller tracking the reference brake torque. A first order filter is implemented to make the pedal inputs to the vehicle model more realistic with appropriate time constants.

3.4 Simple model for actuated vehicle

The methodology adopted for modelling simple vehicle model of the test vehicle is discussed here. Firstly, the modelling assumptions made and the model components that are common to both vehicles are discussed followed by the vehicle specific assumptions and the model components. The next section 3.4.1 discusses all the common components and the components that are differently modelled are studied under the respective vehicle subheading.

A single track model is used for the simple model. The single track model has following states:

- Longitudinal motion, represented by the states v_x and x
- Lateral motion, represented by the states v_y and y
- Yaw motion, represented by the states ω_z and φ_z
- 2 wheel rotation of front and rear wheel (ω_f and ω_r), another related state is ω_{engine}

Based on the above states for the single track model the model components are as follows:

- Wheel
- Vehicle body
- Powertrain

Steering model is a part of the wheel model and is realized by transformations from body to wheel coordinate system (explained in the wheel model section).

The sign convention followed for the single track model is ISO 8855 as in figure 3.5. Forward in x axis is positive, left is positive in y axis and upwards in z axis is positive. As shown in the figure 3.6, l_f is the distance from CG to front axle and l_r is the distance from CG to rear axle with L being the wheelbase.

3. Methodology

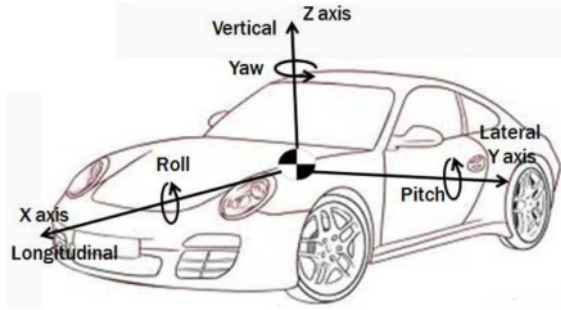


Figure 3.5: ISO 8855 coordinate system [13]

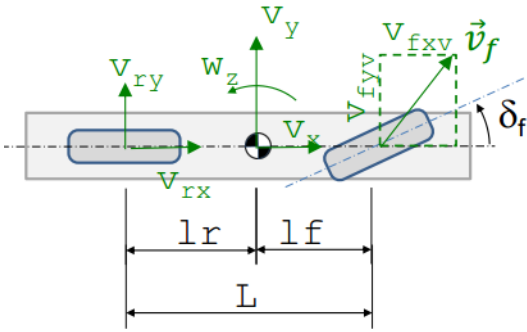


Figure 3.6: Single track model(Pg.153 [5])

3.4.1 Common model components

3.4.1.1 Wheel model

The wheel model contains the wheels dynamics equation and tire model equations. The velocity of the wheel centre is transformed to body coordinate system as given by equations (3.8) and (3.9). Figure 3.7 shows the orientation of wheel and vehicle velocities.

The tire model used is an isotropic combined slip model. It is called isotropic because the cornering stiffness c_p and friction coefficients μ are assumed to be same in lateral and longitudinal direction. The tire forces are given by the functions F_{xy} and f_{sxy} of normal load and friction coefficient. This describes the relation between wheel slip and tire forces as given in equation (3.15). Longitudinal force is F_{xw} proportional to longitudinal slip s_x , similarly Lateral force F_{yw} proportional to lateral slip s_y and the effective combined slip is s_{xy} . v_{xw} is the wheel longitudinal velocity, v_{yw} the lateral velocity, angular velocity of wheel is ω_w and wheel radius is r_w . The tire forces are shown in the figure 3.9, F_{xw} vs s_x with varying lateral slip s_y from -1 to 1 rad for a $\mu = 0.9$ and F_z of 34000 N. The forces and velocities with subscript w are in wheel coordinate system and with v are in vehicle coordinate system.

$$v_{xw} = v_{xv} \cdot \cos\delta + v_{yv} \cdot \sin\delta \quad (3.8)$$

$$v_{yw} = -v_{xv} \cdot \sin\delta + v_{yv} \cdot \cos\delta \quad (3.9)$$

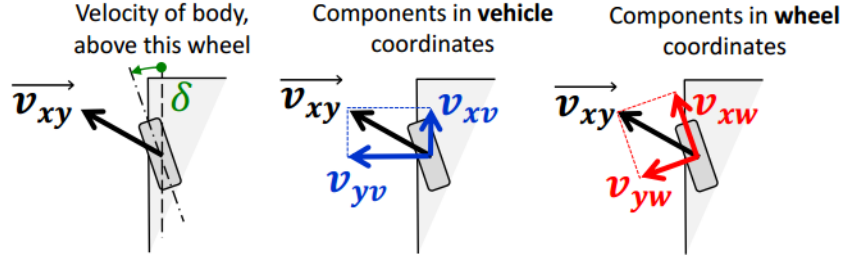


Figure 3.7: Wheel and body coordinate system (Pg.147 [5])

$$s_x = -\frac{v_{xw} - r_w \cdot \omega_w}{\max(\text{abs}(r_w \cdot \omega_w), 0.01)} \quad (3.10)$$

$$s_y = -\frac{v_{yw}}{\max(\text{abs}(r_w \cdot \omega_w), 0.01)} \quad (3.11)$$

$$(3.12)$$

$$s_{xy} = \sqrt{s_x^2 + s_y^2} \quad (3.13)$$

$$f_{sxy} = \frac{2}{\pi} \cdot \arctan\left(\frac{2 \cdot c_p \cdot s_{xy}}{\pi}\right) \quad (3.14)$$

$$F_{xy} = \mu \cdot F_z \cdot f_{sxy} \quad (3.15)$$

$$F_{xw} = \frac{(r_w \cdot \omega_w - v_{xw}) \cdot F_{xy}}{\sqrt{(r_w \cdot \omega_w - v_{xw})^2 + v_{yw}^2}} \quad (3.16)$$

$$F_{yw} = \frac{-v_{yw} \cdot F_{xy}}{\sqrt{(r_w \cdot \omega_w - v_{xw})^2 + v_{yw}^2}} \quad (3.17)$$

Another equation to add is the wheel dynamics which is a balance of all the torques acting on the wheel, the wheel inertia is given by I_w , the torque delivered to the wheel by the driveline T_{prop} and brake torque T_{brk} . T_{roll} is the rolling resistance and f_r is the rolling resistance coefficient.

$$I_w \cdot \dot{\omega}_w = T_{prop} - T_{brk} - F_{xw} \cdot r_w - T_{roll} \quad (3.18)$$

$$T_{roll} = f_r \cdot m \cdot g \cdot r_w \quad (3.19)$$

The forces F_{xw} and F_{yw} are the tire longitudinal and lateral force which are in the wheel coordinate system and a similar transformation as velocity gives forces in the vehicle coordinate system.

$$F_{xv} = \cos(\delta) \cdot F_{xw} - \sin(\delta) \cdot F_{yw} \quad (3.20)$$

$$F_{yv} = \sin(\delta) \cdot F_{xw} + \cos(\delta) \cdot F_{yw} \quad (3.21)$$

3. Methodology

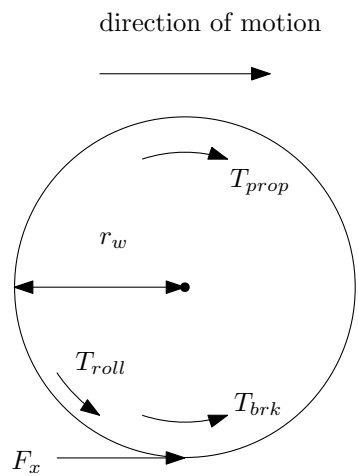


Figure 3.8: Wheel torque equilibrium

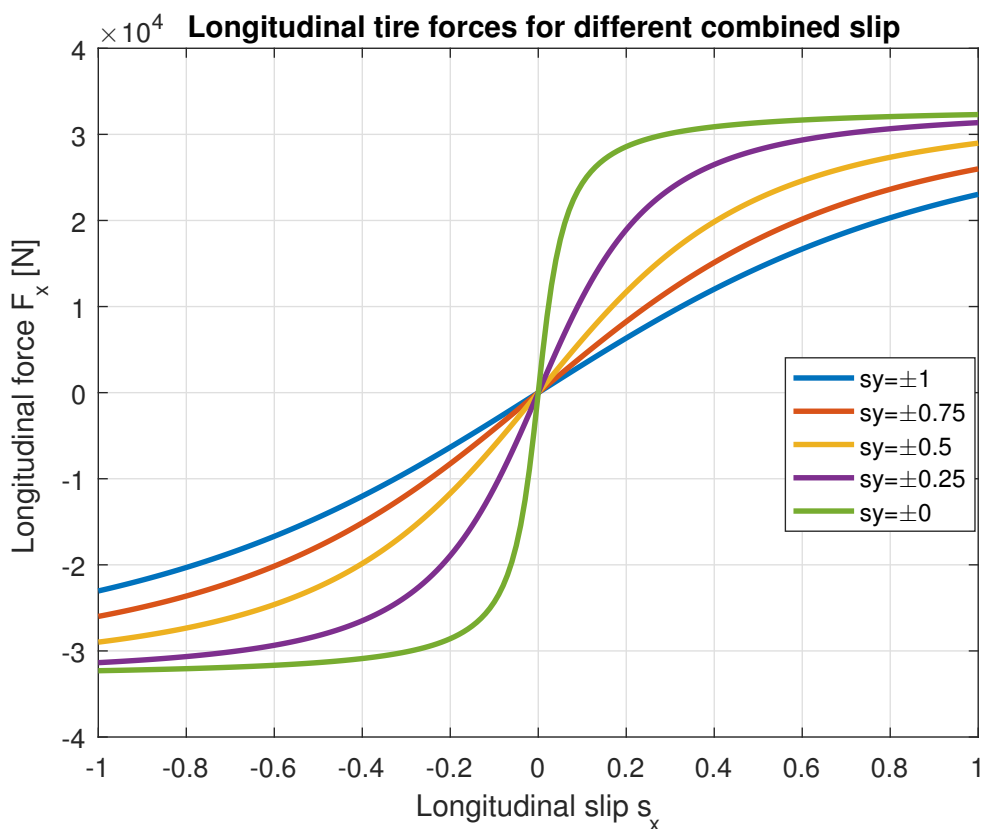


Figure 3.9: Longitudinal tire forces for different combined slips

3.4.1.2 Vehicle body

In this section, the forces and moments acting about the vehicle CG are determined using Newton's laws of motion. The vehicle body as based on the assumptions made on the single track model possesses three DOF- longitudinal, lateral and yaw motion. The first set of equation cover the longitudinal motion and figure 3.10 shows all the longitudinal forces.

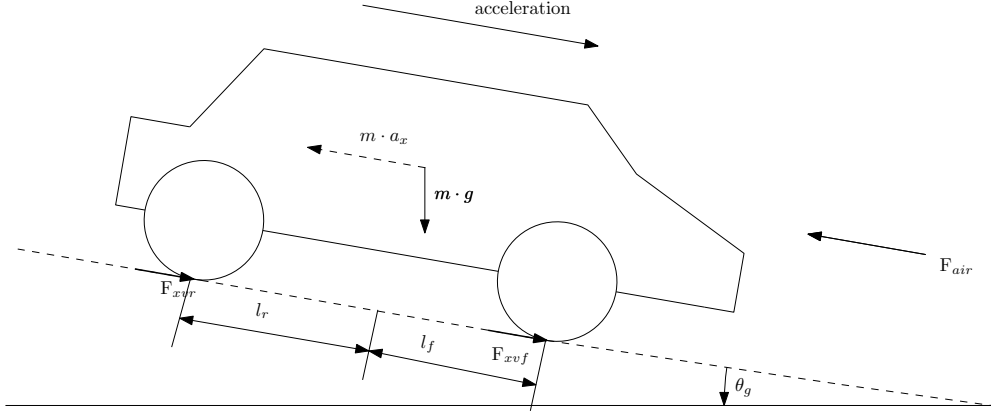


Figure 3.10: Longitudinal force balance for single track model

$$F_x = F_{xvf} + F_{xvvr} - F_d - F_g \quad (3.22)$$

$$F_d = \frac{1}{2} \cdot \rho \cdot C_d \cdot A \cdot v_{xw}^2 \quad (3.23)$$

$$F_g = m \cdot g \cdot \sin(\theta_g) \quad (3.24)$$

$$F_x = m \cdot a_x \quad (3.25)$$

The total longitudinal force on the vehicle body is given by F_x which is the sum of the longitudinal forces on the tires F_{xvf} and F_{xvvr} for front and rear respectively and the resistive forces acting at CG of the vehicle F_d is the aerodynamic drag or the air resistance, and F_g is the gradient resistance.

Similarly based on Newton's law the lateral dynamics equations are obtained. The total lateral forces is given by sum of the lateral tire forces F_{yvf} from the front and F_{yvvr} from the rear. The rotational inertia about the z axis of the vehicle is I_{zz} , yaw velocity is given by ω_z .

$$I_{zz} \cdot \dot{\omega}_z = l_f \cdot F_{yvf} - l_r \cdot F_{yvvr} \quad (3.26)$$

$$m \cdot (\dot{v}_{yv} + v_{xv} \cdot \omega_z) = F_{yvf} + F_{yvvr} \quad (3.27)$$

$$a_x = \dot{v}_{xv} - v_{yv} \cdot \omega_z \quad (3.28)$$

$$a_y = \dot{v}_{yv} + v_{xv} \cdot \omega_z \quad (3.29)$$

3.4.1.3 Powertrain

The powertrain model consists of engine and transmission models. Equations (3.30) to (3.31) represent the engine torque generation and remaining equations until (3.49) represent all other parts of the powertrain. The modelling is done based on the recommendations in the work [16]. Nodal approach is used to represent the power flow. A simple

3. Methodology

example shows the torques from components on either side of the node that is represented by double arrow head, the power and speed flow is from left to right and is considered as the positive direction.

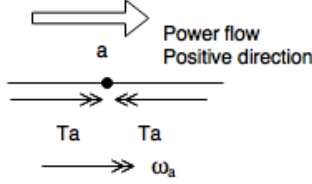


Figure 3.11: Convention for analysis of torques and speed

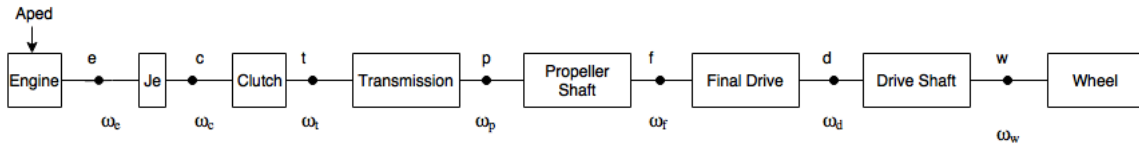


Figure 3.12: Vehicle driveline

The engine is modelled as a look-up table which generates the engine torque $T_{e,max}$ as a function of engine speed ω_e . Based on the acceleration pedal input A_{ped} , a proportional amount of torque $T_{e,aped}$ is determined. An acceleration limiter is modelled in the engine which limits the torque based on restrictions imposed on vehicle acceleration. E_{factor} is the fraction by which the engine torque is reduced, a_{xlower} and a_{xupper} are the acceleration limits. The acceleration limiter is implemented to prevent large instantaneous torque being delivered by the engine for large acceleration pedal inputs. The torque is limited when the vehicle acceleration exceeds the set limits and if it is below then the engine torque remains unchanged.

$$T_{e,max} = f(\omega_e) \quad (3.30)$$

$$T_{e,aped} = A_{ped} \cdot 0.01 \cdot (T_{e,max}) \quad (3.31)$$

$$T_e = \begin{cases} \text{if } \dot{v}_{xv} > a_{xupper} \text{ then} \\ \quad E_{factor} \cdot T_{e,aped} \\ \text{else if } \dot{v}_{xv} < a_{xlower} \text{ then} \\ \quad T_{e,max} \\ \text{else} \\ \quad T_{e,aped} \cdot \left[\frac{(\dot{v}_{xv} - a_{xlower}) \cdot (E_{factor} - 1)}{a_{xupper} - a_{xlower}} + 1 \right] \end{cases} \quad (3.32)$$

Following the engine model is the clutch model which is a torque balance between the engine torque T_e and clutch torque T_c . For this model, the clutch is modelled as a solid disc always connecting the engine and transmission where the speed of the clutch disc is given by ω_c , torque by T_c and the engine flywheel inertia is J_e .

$$J_e \cdot \dot{\omega}_e = T_e - T_c \quad (3.33)$$

$$\omega_e = \omega_c \quad (3.34)$$

Since the FH16 has automated transmission and the XC90 has automatic transmission a simple gear shifting logic based on velocity is designed. Up and dw are arrays that contain velocity based gear shift points. The function `pre` is a built-in function in *Modelica*, that retains the value of the variable from the previous time step this is comparable to the memory block in *MATLAB* and *Simulink*. The torque transmitted by the transmission unit is T_t and the speed is ω_t .

$$T_c = T_t \quad (3.35)$$

$$\omega_c = \omega_t \quad (3.36)$$

$$\text{agear} = \begin{cases} \text{when } v_{xv} > \text{up}[\text{pre}(\text{agear})] \text{ then} \\ \text{pre}(\text{agear})+1 \\ \text{else when } v_{xv} < \text{dw}[\text{pre}(\text{agear})] \text{ then} \\ \text{pre}(\text{agear})-1 \\ \text{else} \\ \text{pre}(\text{agear}) \\ \text{end when} \end{cases} \quad (3.37)$$

The following equation models the propeller shaft transmitting a torque of T_p and angular speed of ω_p . The torque from the transmission is multiplied by the gear ratio while the speed ω_t is stepped down by the gear ratio i_{gear} . The gearbox is assumed to have an efficiency of η_{tr} to account for losses.

$$T_p = \eta_{tr} \cdot T_t \cdot i_{gear} \quad (3.38)$$

$$\frac{\omega_t}{i_{gear}} = \omega_p \quad (3.39)$$

The propeller shaft connects the transmission to the final drive. The torque at the final drive is T_f and speed is ω_f .

$$T_f = T_p \quad (3.40)$$

$$\omega_p = \omega_f \quad (3.41)$$

$$\quad (3.42)$$

The torque from the final drive to the drive shaft is T_d that is multiplied by the final drive ratio i_{final} and speed of the shaft ω_d is divided by the same ratio. The efficiency of the final drive is given by η_{fd} .

$$T_d = T_f \cdot \eta_{fd} \cdot i_{final} \quad (3.43)$$

$$\frac{\omega_f}{i_{final}} = \omega_d \quad (3.44)$$

Equation (3.45) is the torque transmitted to the wheel and the remaining equations are for the reverse gear. To implement the reverse gear, an input is accepted r_{gear} . If this value is 1 then a torque proportional to the pedal input is transmitted to the wheels to drive in the reverse direction. The drive shaft connects the final drive to the wheel. The torque at wheel is given by T_w , speed is ω_w and final torque that is responsible for driving

3. Methodology

the vehicle forwards and backwards is given by T_{prop} .

$$T_w = T_d \quad (3.45)$$

$$\omega_w = \omega_d \quad (3.46)$$

$$rev_{trq} = -1 \cdot r_c \cdot max(T_t, 0) \cdot i_{gear} \cdot i_{final} \quad (3.47)$$

$$r_c = \text{if } r_{gear} > 0 \text{ then } 1 \text{ else } 0 \quad (3.48)$$

$$T_{prop} = \text{if } r_{gear} == 1 \text{ then } rev_{trq} \text{ else } \max(T_w, 0) \quad (3.49)$$

3.4.2 FH16 simple model

The vehicle parameters of the simple model are accordingly changed for the FH16 tractor, using the parameters from previous work done in [33], the workshop manual and the OEM model. The FH16 engine delivers torque to the two rear axles, for the project the third axle is lifted hence the model has two axles front and rear, with the power being delivered to rear axle.

3.4.2.1 Brakes model

The FH16 has a conventional pneumatic braking system. It is modelled based on the relationship between the plunger spring travel and brake pressure is used to model the brakes. The plunger spring travel S_{travel} is associated with the B_{ped} brake pedal position [%] with a ratio B_{pst} and brake pedal travel. The ratio relates the spring travel to the pedal position and this is normalized to 0-100. Based on the pedal position the braking pressure is determined from the spring travel and brake pressure data as in figure 3.13. Assuming that a conventional truck generates a maximum brake torque of 22-25 kNm for maximum brake pressure of 12 bar, the intermediate torque requests are linearly interpolated. A first order delay is added to capture the simple dynamics of the braking system [24]. The time constant k_b is set to $2 s^{-1}$ for the simulations on the first order ODE.

$$B_p = f(S_{travel}) \quad (3.50)$$

$$B_{ped} = B_{pst} \cdot S_{travel} \quad (3.51)$$

$$T_{max} = 22 \text{ to } 25 \text{ KNm} \quad (3.52)$$

$$T_{req} = \frac{B_p \cdot T_{max}}{B_{pmax}} \quad (3.53)$$

$$\dot{T}_b = k_b \cdot (T_{req} - T_b) \quad (3.54)$$

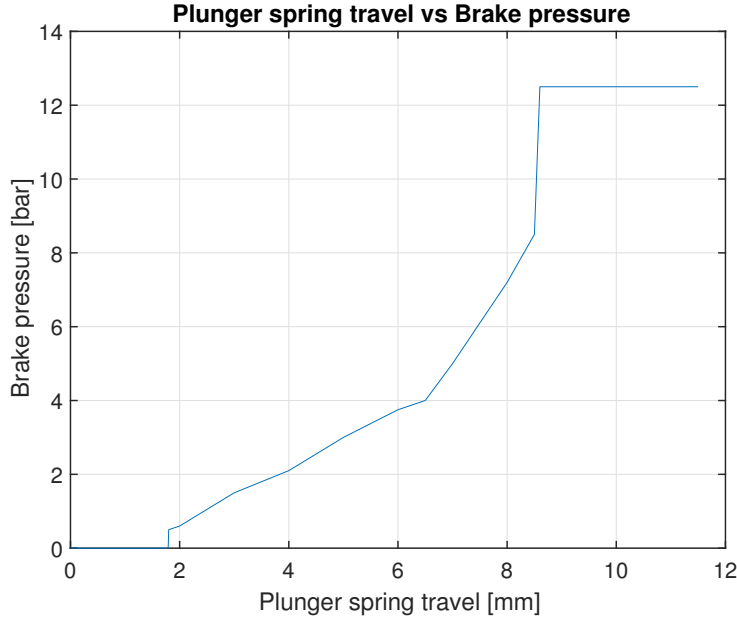


Figure 3.13: Plunger spring travel vs brake pressure

3.4.3 XC90 simple model

The simple model for the XC90 is also modelled with the same general components and the parameters are accordingly modified to the vehicle parameters available, but with some changes to the driveline model and the brakes model.

3.4.3.1 Powertrain

The additional change to the general powertrain model previously discussed is that the drive torque is sent to the front and the rear wheels. The Revere XC90 has an electronically controlled all-wheel drive system, modelling such a system is not captured in this thesis. It is assumed that the rear axle receives 10% more torque than the front axle.

$$T_{wf} = 0.4 \cdot T_d \quad (3.55)$$

$$T_{wr} = 0.6 \cdot T_d \quad (3.56)$$

$$\omega_d = \frac{\omega_{wf} + \omega_{wr}}{2} \quad (3.57)$$

$$J_w \cdot \dot{\omega}_{wf} = T_{df} - T_{bf} - F_{xf} \cdot r_w \quad (3.58)$$

$$J_w \cdot \dot{\omega}_{wr} = T_{dr} - T_{br} - F_{xr} \cdot r_w \quad (3.59)$$

The wheel dynamic equation appear as in equation 3.58 and 3.59.

3.4.3.2 Brakes model

The braking system on the XC90 is hydraulic braking system. A simplification is made for modelling the braking system. It is assumed that the requested braking torque on the wheel T_{req} is function of the brake pedal input B_{ped} and the maximum braking torque

3. Methodology

T_{bmax} . To model a constant delay in the system, the wheel brake torque T_b is modelled as a first order system [25].

$$T_{req} = 0.01 \cdot T_{bmax} \cdot B_{ped} \quad (3.60)$$

$$\dot{T}_b = k_b \cdot (T_{req} - T_b) \quad (3.61)$$

3.5 Advanced model for actuated vehicles

Advanced models for both the test vehicles take into account additional details of the vehicle in order to give a better representation. The vehicle models of the two test vehicle are composed of the following components:

- Wheel model
- Steering
- Chassis (vehicle body)
- Suspension
- Powertrain
- Brakes

In addition to the above components the FH16 has the following components:

- Cab
- Multiple axles

The components that are modelled with the same equations for both the vehicles are described first to avoid repetition of the equations. This is followed by the entities unique for each of the test vehicle which are studied under the respective vehicle sub heading. For the advanced model the braking subsystem is kept same as in the simple model.

3.5.1 Common model components

3.5.1.1 Wheel model

To have a better representation of the tire forces compared to the simple model, a brush tire model is used for the advanced models. A brush tire model gives a better physical representation of the tire force when compared to the isotropic combined slip tire model, where the force is given by an arctan curve as in figure 3.9. The brush tire model is anisotropic in nature with different cornering stiffness for lateral and longitudinal forces.

In a brush tire model the contact patch of the tire of length a is divided in two regions namely sliding and adhesion region. In the former the force generation is governed by sliding friction while in the later by static friction.

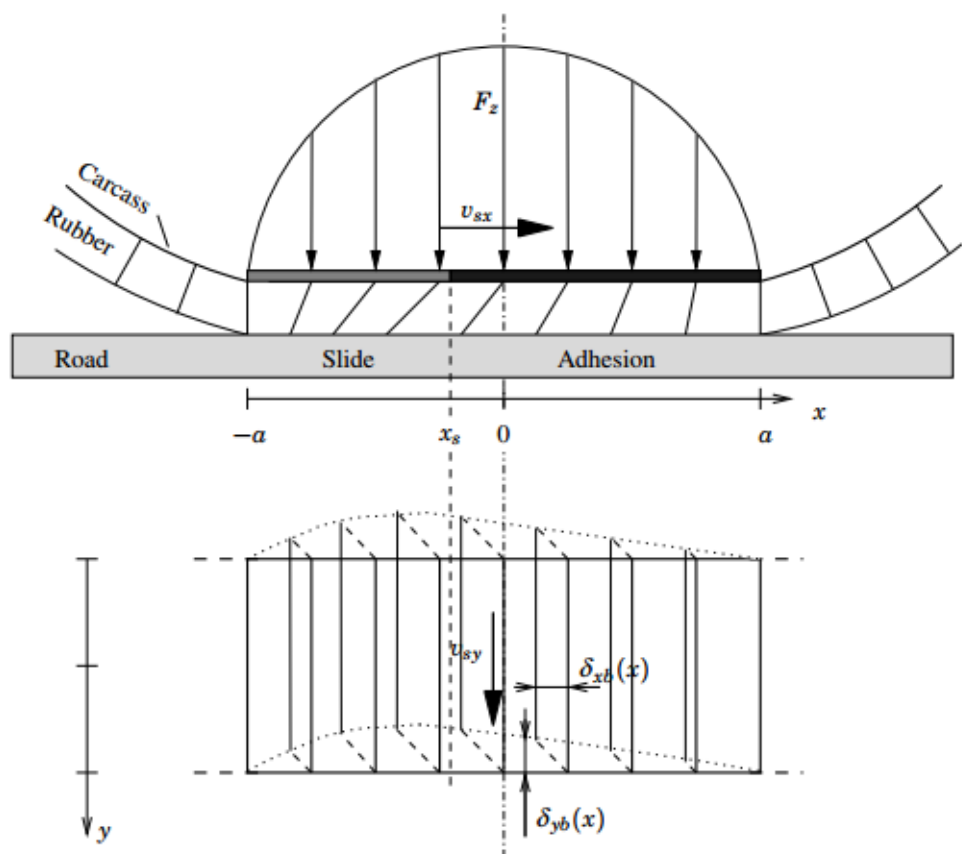


Figure 3.14: Brush tire model side and top view (Pg.40 [15])

3. Methodology

The brush tire model used in this study is from [5], [14], [15] in which ψ is the normalized slip for simplification. s_x^o and s_y^o are the limit slips, this will occur when either of the slips are zero.

$$\psi = \sqrt{\left(\frac{s_x}{s_x^o}\right)^2 + \left(\frac{s_y}{s_y^o}\right)^2} \quad (3.62)$$

$$s_{xy} = \sqrt{s_x^2 + s_y^2} \quad (3.63)$$

$$s_x^o = \frac{3 \cdot F_z \cdot \mu_{sx}}{2 \cdot a^2 \cdot c_{px}} \quad (3.64)$$

$$s_y^o = \frac{3 \cdot F_z \cdot \mu_{sy}}{2 \cdot a^2 \cdot c_{py}} \quad (3.65)$$

If the normalized slip is $\psi < 1$ then both adhesive and sliding forces contribute to the tire forces. If $\psi \geq 1$ then only sliding occurs and the influence of adhesive forces is 0. Assuming a parabolic pressure distribution over the contact length the total force in both the regions is given as

$$F_{tx} = \begin{cases} \text{if } \psi < 1 \\ -c_{px} \cdot s_x \cdot (1 - \psi)^2 - F_z \cdot \left(\frac{s_x}{\max(s, 0.01)}\right) \cdot \mu_k \cdot \psi^2 \cdot (3 - 2 \cdot \psi); \\ \text{else} \\ \mu_k \cdot F_z \cdot \left(\frac{s_x}{\max(s_{xy}, 0.01)}\right) \end{cases} \quad (3.66)$$

$$F_{ty} = \begin{cases} \text{if } \psi < 1 \\ -c_{py} \cdot s_y \cdot (1 - \psi)^2 - F_z \cdot \left(\frac{s_y}{\max(s_{xy}, 0.01)}\right) \cdot \mu_k \cdot \psi^2 \cdot (3 - 2 \cdot \psi); \\ \text{else} \\ \mu_k \cdot F_z \cdot \left(\frac{s_y}{\max(s, 0.01)}\right) \end{cases} \quad (3.67)$$

In the above equations (3.66) and (3.67) c_{px} and c_{py} are the cornering stiffness per unit length, a is the contact patch length, μ_s is the static friction and μ_k is kinematic friction in the above expressions. The total force F at the tire contact patch given below where F_x and F_y are the longitudinal and lateral forces.

$$F = \sqrt{F_{tx}^2 + F_{ty}^2} \quad (3.68)$$

$$F_x = F \cdot \frac{s_x}{\max(s, 0.001)} \quad (3.69)$$

$$F_y = F \cdot \frac{s_y}{\max(s, 0.001)} \quad (3.70)$$

Self-aligning moment (M_z) in the tire is developed due to asymmetric distribution of lateral force and due to deformation of the tire. The self-aligning moment affects the steering torque required which is necessary while designing a steering system. The self-aligning moment in [5] is derived for a uniform pressure distribution using this idea for the current work M_z is derived for a parabolic pressure distribution. The expression for M_z is given by

$$M_z = \begin{cases} \text{if } \psi < 1 \\ a \cdot C_y \cdot (s_y) \cdot (3 \cdot F_z \cdot \mu_k - C_y \cdot \text{abs}(s_y))^3 / (162 \cdot F_z^3 \cdot \mu_k^3) \\ \text{else} \\ 0 \end{cases} \quad (3.71)$$

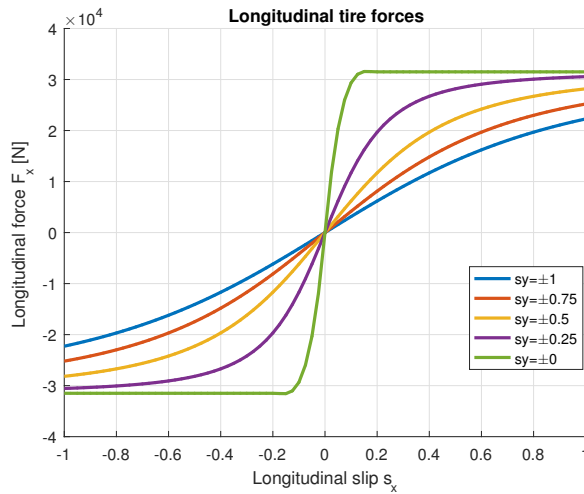


Figure 3.15: Longitudinal force vs longitudinal slip

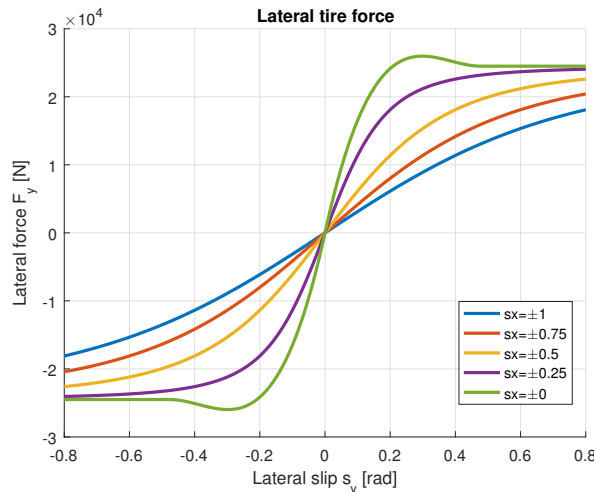


Figure 3.16: Lateral force vs lateral slip

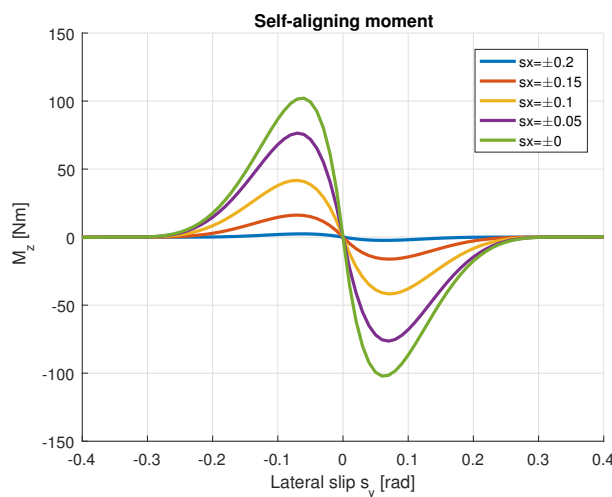


Figure 3.17: Self-aligning moment vs lateral slip

3.5.1.2 Steering

The steering system on the model accepts steering wheel angle from the driver and transmits it to the wheels. For both vehicles a common steering model is used with different design parameters, due to the limited information available regarding the steering systems on the vehicles.

FH16 has an electro-hydraulic power steering [34]. The steering wheel is connected to the steering column. The steering column is connected through one or two universal joints to the hydraulic steering gear which is assisted by an electric motor. This system provides assistance to the driver by providing additional torque called the overlay torque [34]. The steering gear is connected to an arm called the drag or pitman arm which moves the drag link. The drag link causes the upper steering arm to move which rotates the steering knuckle about the kingpin. To transmit the motion of the left wheel over to the right wheel a track rod is used. For this thesis, power steering model is not captured.

The steering is modelled as a second order ODE as shown in equation (3.72) taking into account wheel inertia, damping, aligning torque and torsion bar torque. Ideally, the steering wheel torque is influenced by several factors like steering axis offset, caster, power steering motor or hydraulics and other parameters and components. These are not included due to lack of technical data. However, for the targeted purpose the current steering model is suitable and it can be added extended for to a detailed steering model [23]. In this steering model the torque is resolved about the wheel vertical axis with J_w as the lumped inertia of the wheel along with the remaining moments from the pinion, tire aligning torque and the damping. The equations are as follows

$$J_w \cdot \ddot{\delta}_{wh} = \tau_k \cdot i_s - M_z - c_w \cdot \dot{\delta}_{wh} \quad (3.72)$$

$$\tau_k = k_t \cdot (\delta_{swa} - \delta_p) \quad (3.73)$$

$$\delta_{wh1} = \frac{\delta_p}{i_s} \quad (3.74)$$

$$\delta_{wh2} = \delta_{wh1} \quad (3.75)$$

In the above equations δ_{wh} is the average angle between the two front wheel angles δ_{wh1} and δ_{wh2} . The angles of the pinion and the steering wheel are given as δ_p and δ_{swa} , k_t is the stiffness of the torsion bar and the torque is τ_k . The pinion angle and the wheel angle are related by the steering ratio i_s . A more detailed steering model will be needed if the vehicle models were to operate with a semi-automated function and a driver model (out of the scope of thesis) since the steering model needs to be capable of providing a steering feedback.

3.5.2 FH16

3.5.2.1 Vehicle body

In the vehicle model the body combines all the forces and moments from other subsystem, and translates it into motion. The basic procedure of writing the equations of motion about the CG remains the same, but this approach can be applied to not only the tractor body but also other units with multiple axles. To build up the equation of motion for the body, Newton's law is followed and [33] has been used as reference throughout this section.

In case of a heavy vehicle such as a tractor, the body and the cabin are modelled separately unlike a passenger car. Firstly, the body is studied and the cabin will be looked into in later sections. The body sprung mass has in plane and out of plane motion, the in plane motion are longitudinal, lateral and yaw motion. The roll, pitch and heave motion are the out of plane motion. The body resolves all the forces and moments from the steering, suspension, drivetrain, wheels and axles.

Longitudinal dynamics

All the longitudinal forces that are acting on the chassis are accounted here, the forces from the axles, cab, articulation points if any. These equations not only represent the tractor but it can be used to represent any other units of a combination by changing the respective elements of the forces.

$$m \cdot a_x = F_{x,axles} - F_{x,cab} + F_{x,F} - F_{x,R} - F_g - F_d \quad (3.76)$$

$$a_x = \dot{v}_x - v_y \cdot \omega_z \quad (3.77)$$

The forces $F_{x,axles}$ and $F_{x,cab}$ will be discussed under the respective sub-headings. The articulation forces will be generated by the towed and the towing unit. The driving force such as the axle force and the front articulation point are positive while the opposing forces are negative, from the rear articulation point and cab. The articulation forces need to be resolved about the articulation point, with the point having a kinematic constraint imposed on it. The articulation forces will not be studied in detail in this thesis, detailed explanation can be found in [9] and [33]. The forces F_d and F_g are the aerodynamic drag and road gradient forces which are same as in the simple model as in equation (3.23) and (3.24). All the geometrical lengths are considered positive after the CG and negative if it is measured in front of the CG.

3. Methodology

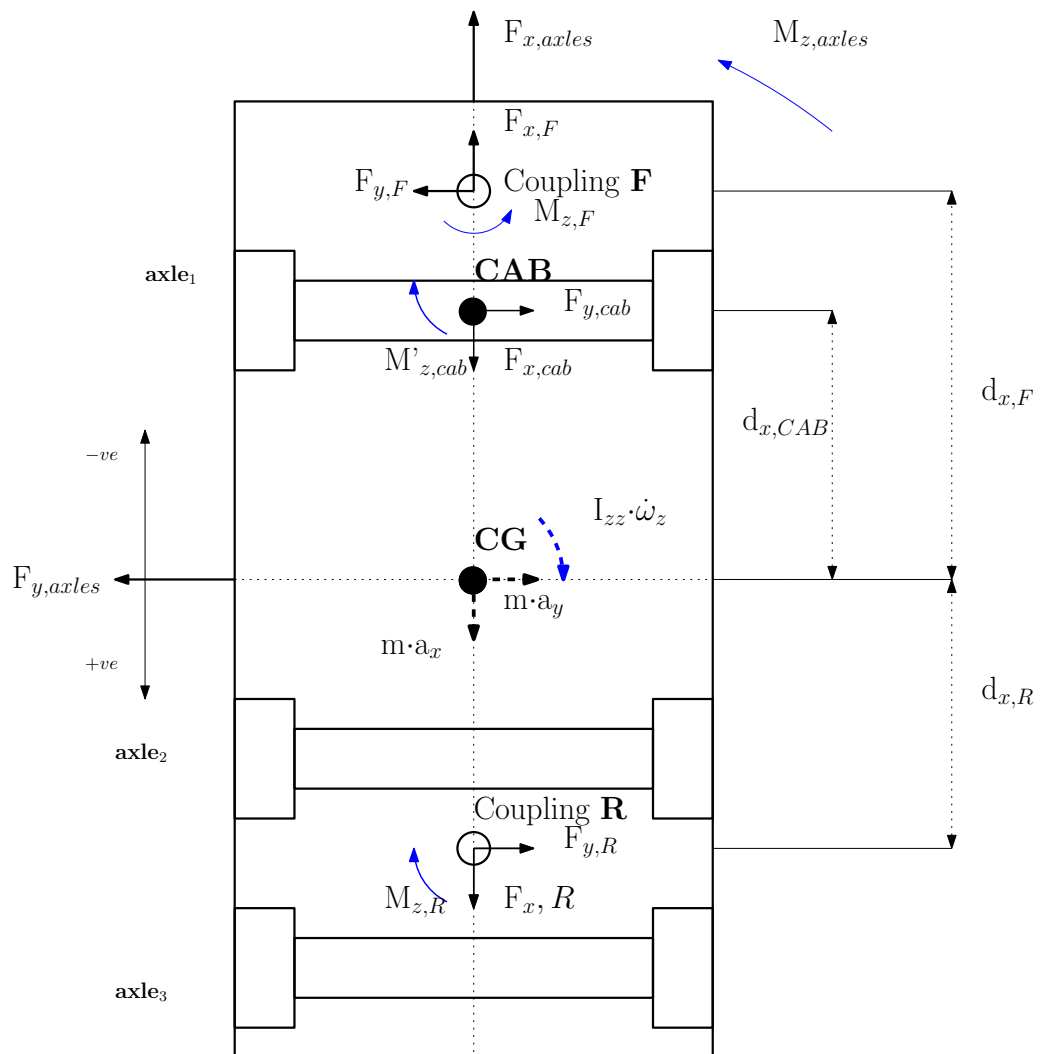


Figure 3.18: Free body diagram of longitudinal forces

Lateral dynamics

The lateral forces are resolved similar to the longitudinal forces by accounting all the lateral forces from each unit like the lateral wheel forces through the axle similarly from the cab and the articulation points.

$$m \cdot a_y = F_{y,axles} - F_{y,cab} + F_{y,F} - F_{y,R} \quad (3.78)$$

$$a_y = \dot{v}_y + v_x \cdot \dot{\varphi}_z \quad (3.79)$$

Vertical dynamics

The vertical force equilibrium of the sprung mass is given as follows:

$$\sum F_{z,s} = m_s \cdot a_z \quad (3.80)$$

$$F_{z,axles} - F_{z,cab} + F_{z,F} - F_{z,R} - m_s \cdot g = m_s \cdot a_z \quad (3.81)$$

$$a_z = \dot{v}_z - v_x \cdot \omega_y \quad (3.82)$$

$$v_z = \dot{z} \quad (3.83)$$

From the above equations, the acceleration of the sprung mass is determined, which on integration gives the displacement of the sprung mass.

Roll dynamics

Rotation about the longitudinal axis is defined as roll motion. The units are assumed to roll about the roll axis, which is the axis through the roll centres. Roll centre is an instantaneous point about which the body rolls and is determined from the geometry of the suspension. The roll angle of the chassis is given by φ_x , the roll rate is given by ω_x and the roll acceleration as $\dot{\omega}_x$. The equilibrium equation is written about the roll center (RC). It is assumed that the roll centre migration is minimal and can be assumed to be a fixed point. The moments from the coupling points, cab, center of gravity (CG) and axle are resolved about the RC as given in equation (3.84). The free body diagram is shown in figure 3.19. The forces from the axle are accounted but shown in figure 3.22. The body moment is resolved about the RC using parallel axis theorem and the moment due to the body is $(I_{xx} + m_s \cdot d_{roll}^2)$.

The cross marks show the CG positions in regular configuration and the solid discs show the respective unit's CG in rolled configuration. The forces $F_{y,CAB}$ and $F_{z,CAB}$ also cause a moment about the chassis CG which is included in the expression $M_{x,CAB}$ this is discussed under the cab dynamics.

$$(I_{xx} + m_s \cdot d_{roll}^2) \cdot \dot{\omega}_x = M_{x,axles} + M_{x,F} - M_{x,R} - M_{x,CAB} - F_{y,F} \cdot d_{zCG,F} - F_{z,F} \cdot d_{zCG,F} \cdot \varphi_x + F_{y,R} \cdot d_{zCG,R} + F_{z,R} \cdot d_{zCG,R} \cdot \varphi_x + m_s \cdot a_y \cdot d_{roll} \quad (3.84)$$

$$\omega_x = \dot{\varphi}_x \quad (3.85)$$

3. Methodology

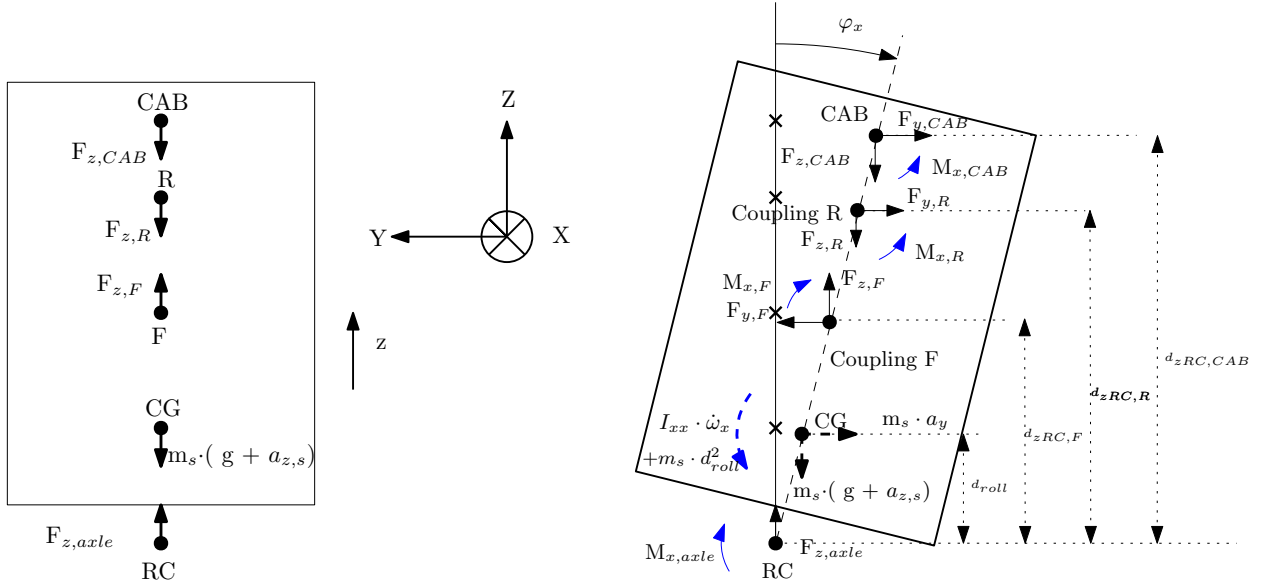


Figure 3.19: Free body diagram for chassis (vertical and roll configuration)

Pitch dynamics

Similar to roll motion, pitch motion is the rotation of the chassis about the lateral axis (y axis) quantified by the pitch angle φ_y . Pitch motion is typically experienced during acceleration, braking and while travelling on uneven roads. In the figure 3.20, the unit in dashed line shows the vehicle at standstill and the solid line show the unit rotated by a pitch angle φ_y . The unit's CG and force transmission points at standstill are represented by cross and by solid discs in pitch configuration. The moments are resolved about the pitch centre PC similar to roll motion, parallel axis theorem is applied with distance between PC and CG given by d_p . Similar assumption is made as in the RC case that the PC migration is minimal and can be assumed to be fixed.

$$(I_{yy} + m_s \cdot d_p^2) \cdot \dot{\omega}_y = M_{y,axles} + M_{y,F} - M_{y,R} - M_{y,CAB} + F_{x,F} \cdot d_{zCG,F} + F_{z,F} \cdot d_{xCG,F} - F_{x,R} \cdot d_{zCG,R} + F_{z,R} \cdot d_{xCG,R} + m_s \cdot a_x \cdot d_{zPC} - m_s \cdot (g + a_z) \cdot d_{xPC} \quad (3.86)$$

$$\omega_y = \dot{\varphi}_y \quad (3.87)$$

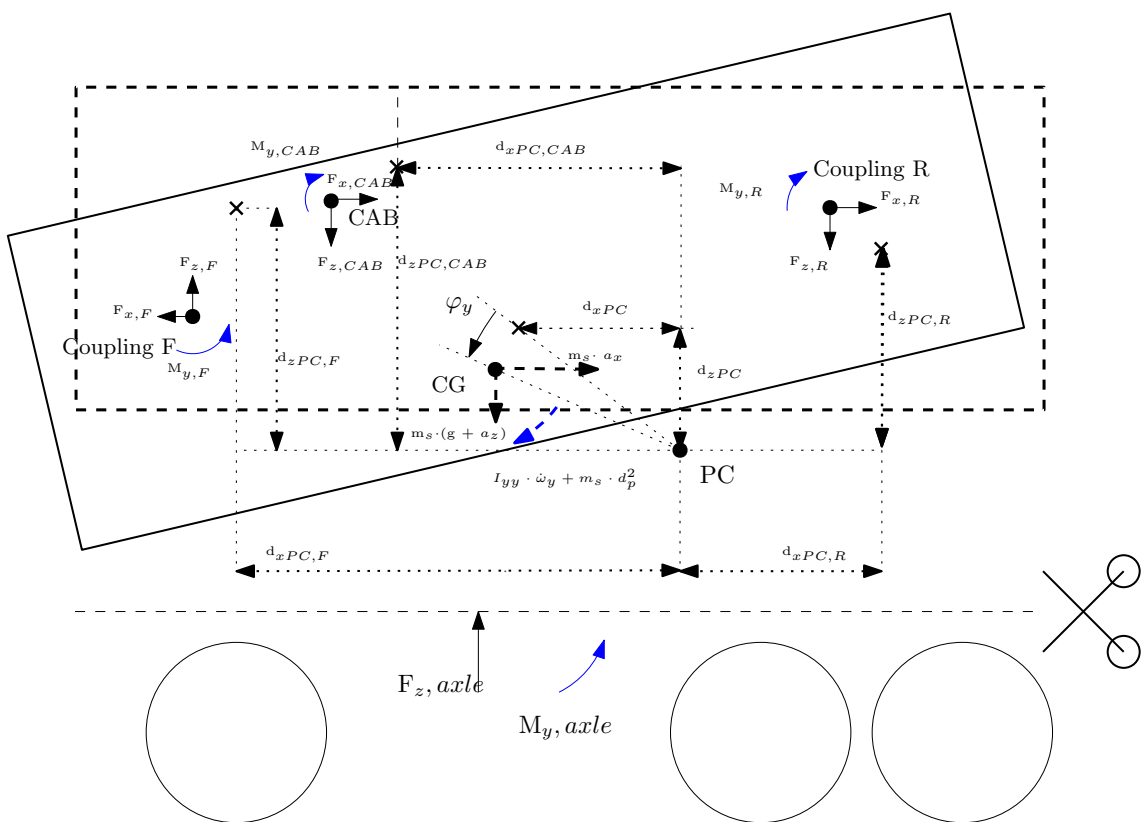


Figure 3.20: Free body diagram for chassis (Pitch configuration)

Yaw dynamics

Rotation about the z axis is considered as yaw motion. Same concept is used here as it was for roll and pitch motion. Forces and moments are resolved about the unit's CG to obtain the yaw acceleration which is given in equation 3.88.

$$I_{zz} \cdot \dot{\omega}_Z = M_{z,axles} - M_{z,CAB} + M_{z,F} \\ - M_{z,R} - F_{y,F} \cdot d_{xCG,F} + F_{y,R} \cdot d_{xCG,R} \quad (3.88)$$

$$\omega_z = \dot{\varphi}_z \quad (3.89)$$

3.5.2.2 Axles

This section describes the axles dynamics including the suspension present on the FH16. One axle is modelled and used for front and rear with suitable parameters. The axle transmits the forces from the wheels to the chassis, it contains the spring, damper and anti-roll bar completing the suspension. The axle has two DOF namely, heave and roll. Firstly, the forces $F_{x,axles}$, $F_{y,axles}$ and $F_{z,axles}$ and moments $M_{x,axles}$, $M_{y,axles}$ and $M_{z,axles}$ are determined followed by the two DOF of the axles. The equation in this section are based on the work done in [33].

The forces and moments from the axle are due to the tire forces and due to the suspension components. The longitudinal and lateral forces in x and y direction are as follows with δ as the wheel steering angle.

$$F_{x,axles} = F_{xl,wh} \cdot \cos(\delta_l) - F_{yl,wh} \cdot \sin(\delta_l) \\ + F_{xr,wh} \cdot \cos(\delta_r) - F_{yr,wh} \cdot \sin(\delta_r) \quad (3.90)$$

$$F_{y,axles} = F_{yl,wh} \cdot \cos(\delta_l) + F_{xl,wh} \cdot \sin(\delta_l) \\ + F_{yr,wh} \cdot \cos(\delta_r) + F_{xr,wh} \cdot \sin(\delta_r) \quad (3.91)$$

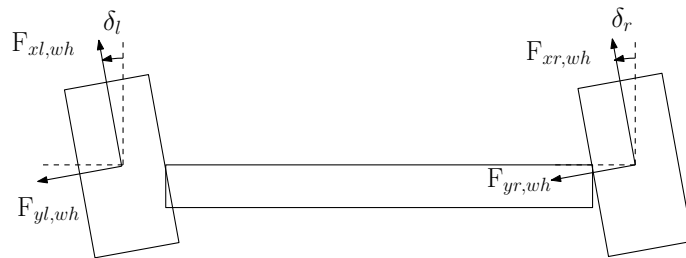


Figure 3.21: Steered axle

$$F_{z,axle} = F_{zs,l} + F_{zs,r} + F_{zd,l} + F_{zd,r} \quad (3.92)$$

$$M_{x,axle} = M_{arb} + F_{zs,l} \cdot \left(\frac{d_s}{2} + d_{zCG,rc} \cdot \theta \right) \\ - F_{zs,r} \cdot \left(\frac{d_s}{2} - d_{zCG,rc} \cdot \theta \right) \\ + F_{zd,l} \cdot \left(\frac{d_s}{2} + d_{zCG,rc} \cdot \theta \right) - F_{zd,r} \cdot \left(\frac{d_s}{2} - d_{zCG,rc} \cdot \theta \right) \quad (3.93)$$

The vertical forces are due to the suspension components spring and damper. The moments from the axle that contribute to the roll motion is given by equation (3.93) and the lateral forces from the axle are assumed to act at the RC. Having considered the moments and forces from the axle the equations (3.91) and (3.93) includes all forces and moments governing roll motion.

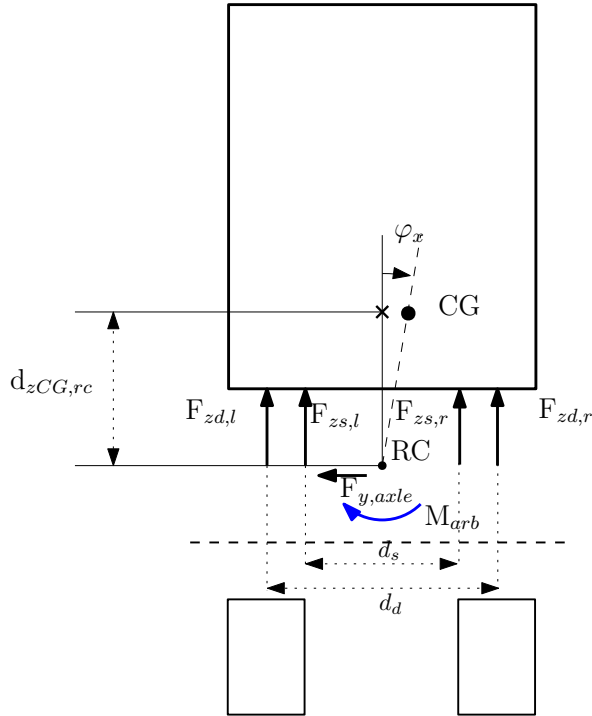


Figure 3.22: Roll moment balance axle and chassis

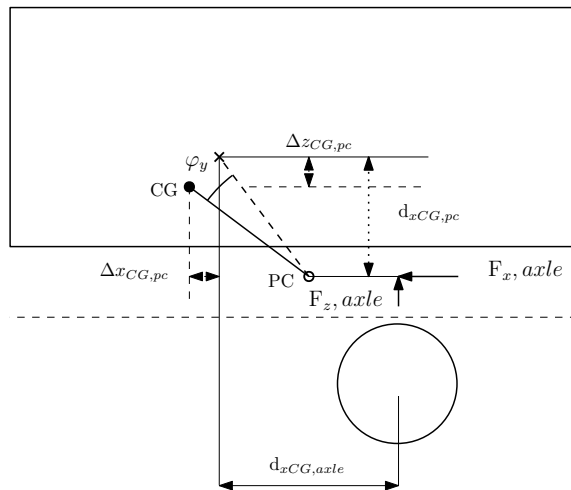


Figure 3.23: Pitch moment balance axle and chassis

3. Methodology

The pitch moment is similarly defined as the roll moment, in the figure 3.23 the forces contributing to the pitch moment from one axle are shown. The forces from the axle act at the pitch centre. Resolving all the forces gives the pitch moment $M_{y,axle}$ from the axle.

$$M_{y,axle} = F_{z,axle} \cdot (d_{xCG,axle} + \Delta x_{CG,pc}) - F_{x,axle} \cdot (d_{zCG,axle} + \Delta z_{CG,pc}) \quad (3.94)$$

The yaw moment of the axle is due to the tire aligning moments and the tire forces. The lateral and longitudinal tires forces generate moments based on the distance between CG to axle and the track width.

$$M_{z,axle} = M_{zl,wh} + M_{zr,wh} + (F_{xr,wh} \cdot \cos(\delta_r) - F_{xl,wh} \cdot \cos(\delta_l) + F_{yl,wh} \cdot \sin(\delta_l) - F_{xr,wh} \cdot \sin(\delta_r)) \cdot \frac{TW}{2} - F_{y,axle} \cdot d_{xCG,axle} \quad (3.95)$$

The axle has two DOF, heave and roll influenced by the tire forces, suspension force and axle inertia. The moments of the axle are resolved about the roll centre RC . The axle can rotate and heave based on the motion of the tire in the vertical direction, modelled as a spring. The vertical displacement of the axle is the mean of the vertical displacements of the left and right tire.

$$m_a \cdot a_{z,axle} = F_{zl,wh} + F_{zr,wh} - m_a \cdot g \quad (3.96)$$

$$I_{x,axle} \cdot \ddot{\theta}_{axle} = (F_{zl,wh} - F_{zr,wh}) \cdot \frac{TW}{2} - M_{arb} + F_{y,axle} \cdot h_{rc} - (F_{zs,l} - F_{zs,r}) \cdot d_s - (F_{zd,l} - F_{zd,r}) \cdot d_d \quad (3.97)$$

$$z_{axle} = R - \frac{z_{l,wh} + z_{r,wh}}{2} \quad (3.98)$$

$$\theta_{axle} = \frac{-z_{l,wh} + z_{r,wh}}{TW} \quad (3.99)$$

Spring and damper

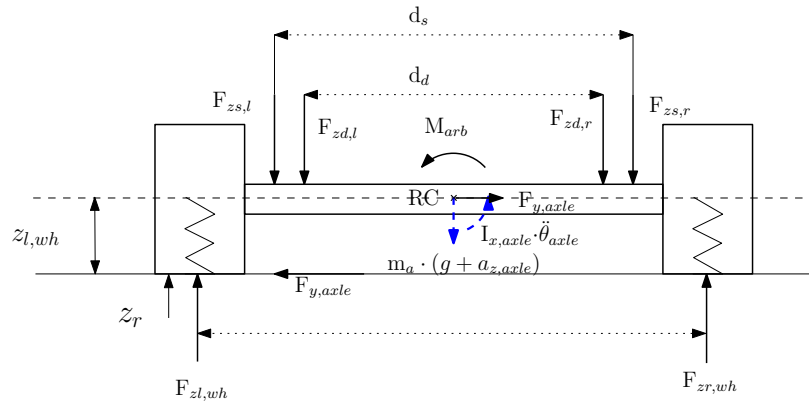


Figure 3.24: Axle free body diagram

The forces $F_{zs,l}$, $F_{zs,r}$, $F_{zd,l}$ and $F_{zd,r}$ due to the springs and dampers are calculated

in equation (3.100) and (3.101). The force is shown for just one side, since it is represented by the same expression for both sides. In the code as well only one model of the spring and damper is made and the equations are called by their class name when needed.

$$F_{zs} = -k_{si} \cdot z_s + F_{static} \quad (3.100)$$

$$F_{zd} = -c_{di} \cdot v_d \quad (3.101)$$

$$M_{arb} = -k_{arb} \cdot \varphi_{x,rel} \quad (3.102)$$

The spring stiffness k_{si} , damping coefficient c_{di} and the anti-roll bar stiffness k_{arb} are assumed to be constants for the model. The force equations remain same at any axle end, the displacements and velocity vary for the left and right ends these are given as follows:

$$z_{s,l} = (z_{sprung} - h_{sprung} - (z_{axle} - r_{wh})) + \varphi_{x,rel} \cdot \frac{d_s}{2} + \varphi_y \cdot d_{xaxle,pc} \quad (3.103)$$

$$z_{s,r} = (z_{sprung} - h_{sprung} - (z_{axle} - r_{wh})) - \varphi_{x,rel} \cdot \frac{d_s}{2} + \varphi_y \cdot d_{xaxle,pc} \quad (3.104)$$

$$v_{d,l} = (v_z - v_{z,axle}) + \dot{\varphi}_{x,rel} \cdot \frac{d_d}{2} + \dot{\varphi}_y \cdot d_{xaxle,pc} \quad (3.105)$$

$$v_{d,r} = (v_z - v_{z,axle}) - \dot{\varphi}_{x,rel} \cdot \frac{d_d}{2} + \dot{\varphi}_y \cdot d_{xaxle,pc} \quad (3.106)$$

$$\varphi_{x,rel} = \varphi - \varphi_{x,axle} \quad (3.107)$$

In the above equations (3.103) to (3.106) d_s and d_d are the distance between the left and right spring and damper, $d_{xaxle,pc}$ is the longitudinal distance of the axle from the pitch centre. The variable v_z and $v_{z,axle}$ are the rate of change of displacements of the sprung mass and of the axle. As shown in the figure 3.24 the tire is modelled as a spring to take into account the vertical motion of the wheels. Both $z_{l,wh}$ or $z_{r,wh}$ are calculated based on the road displacement z_r and the net displacement z_t of the tire spring.

$$z_t = z_r - (z_{l,wh} - r_{wh}) \quad (3.108)$$

$$F_{z,wh} = F_{zstatic,wh} + n_w \cdot k_w \cdot z_t \quad (3.109)$$

The tire vertical displacement equations are added to the tire model such that it does not need to be repeated for each tire.

3.5.2.3 Cab

In most vehicle models for passenger cars the vehicle body and chassis are modelled as a single unit. In the case of heavy vehicles, the cabin needs to be modelled separately due to its significant mass, position and its movement with respect to the chassis of the vehicle. The cab is modelled as a rigid body in a three dimensional (3D) space and the DOF are as shown in the figure 3.25.

The point j is the point that joins the chassis and cab through which the forces and moments are transmitted.

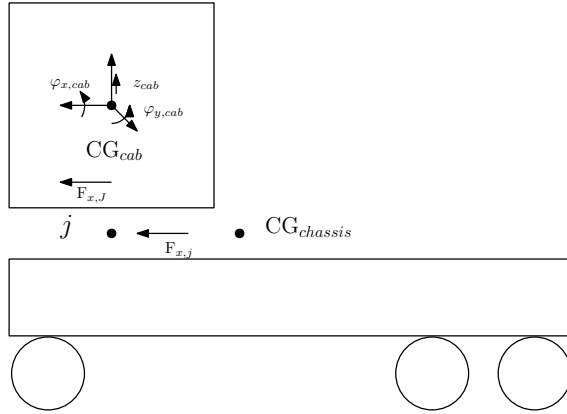


Figure 3.25: Cab and chassis free body diagram

Firstly, the equations of motion of the cab are described, and all the variables with superscript ch are in chassis frame of reference and ca in cab frame of reference. The equations of motion are used from the study [33] which are written based on the Newton's and Euler's equation in 3D:

$$\sum F_i = m \cdot a_i \quad (3.110)$$

$$\sum M_i = J\dot{\omega} + \omega \times (J\omega) \quad (3.111)$$

While resolving the forces small angle approximation is made.

$$(m_{CAB} \cdot a_{x,CAB} = F_{xj} + m_{CAB} \cdot g \cdot \varphi_{y,CAB})^{ca} \quad (3.112)$$

$$(m_{CAB} \cdot a_{y,CAB} = F_{yj} - m_{CAB} \cdot g \cdot \varphi_{x,CAB})^{ca} \quad (3.113)$$

$$(m_{CAB} \cdot a_{z,CAB} = F_{zj} - m_{CAB} \cdot g)^{ca} \quad (3.114)$$

$$(a_{x,CAB} = \dot{v}_{x,CAB} - v_{y,CAB} \cdot \omega_{y,CAB} + v_{z,CAB} \cdot \omega_{z,CAB})^{ca} \quad (3.115)$$

$$(a_{y,CAB} = \dot{v}_{y,CAB} + v_{x,CAB} \cdot \omega_{x,CAB} - v_{z,CAB} \cdot \omega_{z,CAB})^{ca} \quad (3.116)$$

$$(a_{z,CAB} = \dot{v}_{z,CAB} - v_{x,CAB} \cdot \omega_{x,CAB} + v_{y,CAB} \cdot \omega_{y,CAB})^{ca} \quad (3.117)$$

$$\quad (3.118)$$

Moment balance:

$$\begin{aligned} & \left((I_{x,CAB} + m_{CAB} \cdot h_{zCAB,j}) \cdot \dot{\omega}_{x,CAB} + (I_{z,CAB} - I_{y,CAB}) \cdot \omega_{y,CAB} \cdot \omega_{z,CAB} \right)^{ca} \\ & = m_{CAB} \cdot a_{y,CAB} \cdot h_{CAB} + m_{CAB} \cdot g \cdot \varphi_{x,CAB} + M_{x,j} \end{aligned} \quad (3.119)$$

$$\begin{aligned} & \left((I_{y,CAB} + m_{CAB} \cdot h_{zCAB,j}) \cdot \dot{\omega}_{y,CAB} + (I_{x,CAB} - I_{z,CAB}) \cdot \omega_{x,CAB} \cdot \omega_{z,CAB} \right)^{ca} \\ & = m_{CAB} \cdot a_{x,CAB} \cdot h_{CAB} + m_{CAB} \cdot g \cdot \varphi_{y,CAB} + M_{y,j} \end{aligned} \quad (3.120)$$

$$\begin{aligned} & \left(I_{z,CAB} \omega_{z,CAB} + (I_{y,CAB} - I_{x,CAB}) \cdot \omega_{x,CAB} \cdot \omega_{y,CAB} \right)^{ca} \\ & = M_{z,j} \end{aligned} \quad (3.121)$$

The velocity of the cab based on the velocity of the joint in the cab frame of reference is:

$$\begin{bmatrix} v_{x,CAB} \\ v_{y,CAB} \\ v_{z,CAB} \end{bmatrix}^{ca} = \begin{bmatrix} v_{x,j} + \dot{\varphi}_y \cdot h_{zCAB,j} \\ v_{y,j} - \dot{\varphi}_x \cdot h_{zCAB,j} \\ v_{z,CAB} \end{bmatrix}^{ca} \quad (3.122)$$

$$h_{zCAB,j} = h_{zCAB} - h_{zj} \quad (3.123)$$

The chassis transmits the forces and moments through the point "j" as shown in the figure 3.25. The displacement and velocities of the joint are as follows which are in the chassis reference frame:

$$\Delta z_{CAB,jch} = z_{sprg} - h_{sprg} + \varphi_{y,ch} \cdot d_{zCAB,pc} \quad (3.124)$$

$$\begin{bmatrix} v_{xCAB,jch} \\ v_{yCAB,jch} \\ v_{zCAB,jch} \end{bmatrix}^{ch} = \begin{bmatrix} v_{xsprg} \\ v_{ysprg} - \omega_{z,ch} \cdot d_{zCAB,CG} - \omega_x \cdot (h_{zCAB,j} + (z - h_{sprung} - h_{z,rc})) \\ v_{zsprg} - \dot{\varphi}_y \cdot d_{xCAB,pc} \end{bmatrix}^{ch} \quad (3.125)$$

$$\begin{bmatrix} \varphi_{x,j} \\ \varphi_{y,j} \\ \varphi_{z,j} \end{bmatrix} = \begin{bmatrix} \varphi_x \\ \varphi_y \\ \varphi_z \end{bmatrix}^{ch} \quad (3.126)$$

$$\begin{bmatrix} \omega_{x,j} \\ \omega_{y,j} \\ \omega_{z,j} \end{bmatrix}^{ch} = \begin{bmatrix} \omega_x \\ \omega_y \\ \omega_z \end{bmatrix}^{ch} \quad (3.127)$$

The relative angle between the cab and the joint is given by equation (3.128) and the last row of the equation is 0 since the cab is not allowed to rotate about the z axis.

$$\begin{bmatrix} \varphi_x, r \\ \varphi_y, r \\ 0 \end{bmatrix} = \begin{bmatrix} \varphi_{x,CAB} \\ \varphi_{y,CAB} \\ \varphi_{z,CAB} \end{bmatrix}^{ch} - \begin{bmatrix} \varphi_{x,j} \\ \varphi_{y,j} \\ \varphi_{z,j} \end{bmatrix}^{ch} \quad (3.128)$$

To relate the angles, angular velocities, forces and moments between the chassis and cab frame of reference, the rotation matrices are used with first rotation about y and then

3. Methodology

\mathbf{x} given by the matrix R_y and R_x . The product of the two matrices gives the complete rotation matrix.

$$R = R_x \cdot R_y \quad (3.129)$$

$$\begin{bmatrix} \varphi_{x,CAB} \\ \varphi_{y,CAB} \\ \varphi_{z,CAB} \end{bmatrix}^{ch} = R \cdot \begin{bmatrix} \varphi_{x,CAB} \\ \varphi_{y,CAB} \\ \varphi_{z,CAB} \end{bmatrix}^{ca} \quad (3.130)$$

The rotation matrices R_x and R_y are:

$$R_x = \begin{bmatrix} 1 & 0 & 0 \\ 0 & \cos(\varphi_{x,r}) & -\sin(\varphi_{x,r}) \\ 0 & \sin(\varphi_{x,r}) & \cos(\varphi_{x,r}) \end{bmatrix} \quad (3.131)$$

$$R_y = \begin{bmatrix} \cos(\varphi_{y,r}) & 0 & \sin(\varphi_{y,r}) \\ 0 & 1 & 0 \\ -\sin(\varphi_{y,r}) & 0 & \cos(\varphi_{y,r}) \end{bmatrix} \quad (3.132)$$

$$\mathbf{v}_j^{ch} = R \cdot \mathbf{v}_j^{ca} \quad (3.133)$$

$$\mathbf{v}_{CAB}^{ch} = R \cdot \mathbf{v}_{CAB}^{ca} \quad (3.134)$$

$$\mathbf{F}_j^{ch} = R \cdot \mathbf{F}_j^{CAB} \quad (3.135)$$

$$\mathbf{M}_j^{ch} = R \cdot \mathbf{M}_j^{CAB} \quad (3.136)$$

$$(3.137)$$

Since the joint is considered as springs, forces are transmitted to the cab due to the net displacement of the spring proportional to their stiffness k and damping c .

$$(F_{z,j} = -k_{zCAB} \cdot (z_{CAB} - h_{zCAB} - \Delta z_j) - c_{zCAB} \cdot (v_{z,CAB} - v_{z,j}))^{ch} \quad (3.138)$$

$$(M_{x,j} = -k_{\varphi_x CAB} \cdot \varphi_{x,r} - c_{\varphi_x CAB} \cdot \dot{\varphi}_{x,r})^{ch} \quad (3.139)$$

$$(M_{y,j} = -k_{\varphi_y CAB} \cdot \varphi_{y,r} - c_{\varphi_y CAB} \cdot \dot{\varphi}_{y,r})^{ch} \quad (3.140)$$

In the chassis section while resolving the moments about the CG the cab moments were just stated as $M_{x,CAB}$, $M_{y,CAB}$ and $M_{z,CAB}$ these are defined as follows:

$$M_{x,CAB} = (M_{x,j} - F_{y,j} \cdot (h_{zj} - h_{CG}) - F_{z,j} \cdot \varphi_x \cdot (h_{zj} - h_{CG}))^{ch} \quad (3.141)$$

$$M_{y,CAB} = (M_{y,j} + F_{z,j} \cdot (d_{xCAB,CG}) + F_{x,j} \cdot (h_{zj} - h_{CG}))^{ch} \quad (3.142)$$

$$M_{z,CAB} = (M_{z,j} - F_{y,j} \cdot d_{zCAB})^{ch} \quad (3.143)$$

3.5.2.4 Powertrain

Engine

Engine modelling can be based on several methods such as FEM-model, MBS-models, Cycle simulation models and Dynamic engine models [17]. The engine behaviour can be modelled using a set of partial differential equations(PDE) [35] or ordinary differential equations(ODE). The former method gives a better representation of the system since the function variables are related and time dependent. In the case of an ODE, the only variable is time. Using PDE to model the engine would require a lot of data and computational power, while ODE is suitable for quick simulations especially for vehicle dynamics studies. The engine model is represented by a set of state variables, this can further be classified based on the state variables - primary (mechanical, engine speed, torque) and secondary (thermodynamics, flow rate, and temperature) [17]. For this thesis, the engine model is based on ODE using primary variables.

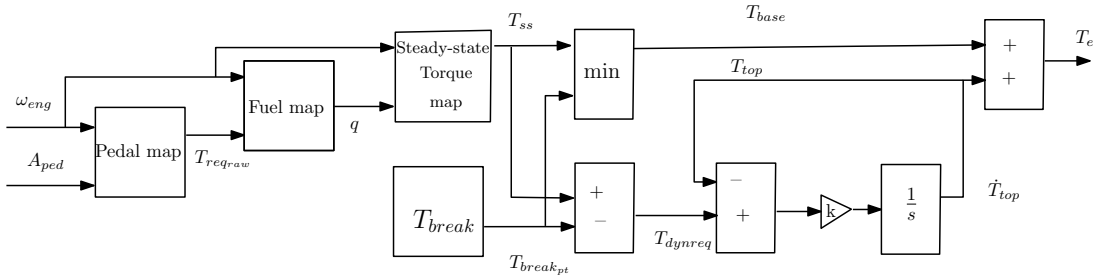


Figure 3.26: Engine flow diagram

Using the engine speed (ω_e) and torque T_e as dynamic states the engine model is developed. The initial request torque is generated based on accelerator pedal position (Aped) and engine speed using a 2D look-up table (pedal map). The torque generated from the pedal map is fed to the fuel map along with the current engine speed to determine the fuel injected q . The steady-state torque T_{ss} is obtained from another look-up table based on fuel injected and engine speed. The steady state torque is split into two portions a base torque T_{base} and top torque T_{top} based on a break-point torque value. Using this break-point torque the steady state torque is split, to mimic the boost pressure build-up. The rise of the torque from the base region is modeled as a first order differential equation with build-up coefficient $k = 1 \text{ s}^{-1}$.

$$T_{reqraw} = f(A_{ped}, \omega_{eng}) \quad (3.144)$$

$$q = f(T_{reqraw}, \omega_{eng}) \quad (3.145)$$

$$T_{ss} = f(q, \omega_{eng}) \quad (3.146)$$

$$T_{base} = \min(T_{ss}, T_{break_{pt}}) \quad (3.147)$$

$$T_{dynreq} = T_{ss} - T_{break_{pt}} \quad (3.148)$$

$$\dot{T}_{top} = k \cdot (T_{dynreq} - T_{top}) \quad (3.149)$$

$$T_e = T_{base} + T_{top} \quad (3.150)$$

The variable q is fuel injected per stroke to determine the fuel consumed in litres, it needs to be converted to mass flow rate and then the volume can be calculated. The

3. Methodology

relationship between q and \dot{m} is given as [36]:

$$\dot{m} = c \cdot \frac{N \cdot \omega_{eng}}{n \cdot 2\pi} \cdot q \quad (3.151)$$

N is six which is the number of cylinders on the engine and n is two because fuel is injected once every second stroke, for a four-stroke engine. The parameter c is the unit conversion from milligrams to kilograms. Once the mass flow rate is calculated, determining the volume of fuel is rather straight forward as given below:

$$V_{fuel} = \frac{1}{\rho} \cdot \int \dot{m} \cdot dt \quad (3.152)$$

Clutch

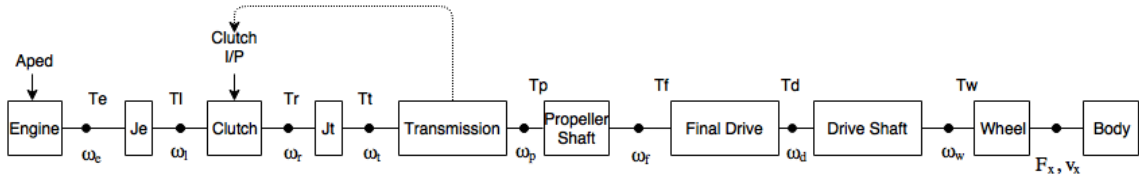


Figure 3.27: Powertrain node diagram for advanced model

The next component of the powertrain is the clutch, which connects and disconnects the engine from the transmission when necessary. The Revere FH16 is equipped with a single clutch which is modeled using the clutch model in the Modelica standard library. The input to the clutch model is normalized input force f_n that varies from 0 to 1. A maximum allowable force $f_{n,max}$ is calculated for the clutch such that the maximum clutch torque is 1.5 times the maximum engine torque taking into account the geometric coefficient c_{geo} for the clutch.

$$f_{n,max} = \frac{1.5 \cdot T_{eng,max}}{c_{geo}} \quad (3.153)$$

When operating during gear shift or start-up the clutch model determines the modes of operation based on the torque and the relative angular velocity between the discs. The standard Modelica clutch during operation can take up 4 modes which are - free, stuck, forward, and backward. As the name indicates when in free mode the clutch discs are not in contact, when in contact they are in the stick mode. If the ω_{rel} is positive then forward rotation and if negative then backward rotation. Based on these operating modes Modelica determines three other parameters which are locked, startForward and startBackward. When locked, the model transmits the torque from the engine to the transmission. The other two cases are for slipping clutch, for which the torque is calculated based on the mode and the normalized input force f_n . During operation, the clutch torque τ is determined based on the demanded clutch force f_{nc} , which is linearly proportional to the normalized input f_n and the maximum force $f_{n,max}$ as in equation (3.157). Based on the force f_{nc} the clutch torque is determined as in equation (3.158).

The nodal approach is applied for moment balance equation for the node between engine flywheel and clutch disc left. The engine torque T_e is balanced by the clutch left disc torque T_l and the engine inertia.

$$J_e \cdot \dot{\omega}_e = T_e - T_l \quad (3.154)$$

The actuation force input is controlled by the clutch control block which is discussed later along with the gear shift manager.

$$\omega_e = \omega_l \quad (3.155)$$

$$T_l = \tau \quad (3.156)$$

$$f_{nc} = f_{n_{max}} \cdot f_n \quad (3.157)$$

$$\tau = c_{geo} \cdot f_{nc} \cdot f(\mu, \omega_{rel}) \quad (3.158)$$

$$T_r = \tau \quad (3.159)$$

$$\omega_{rel} = \omega_l - \omega_r \quad (3.160)$$

Gearbox

The clutch module is followed by the transmission or gearbox. The gearbox reduces the engine speed and increases the torque by the selected gear ratio. The gearbox receives the gear number from the gear shift manager, based on which the appropriate gear ratio is selected. T_t is the torque at the transmission node that is resolved based on the clutch right disc torque T_r and the gearbox inertia J_t . The angular speed at the transmission node is given by ω_t .

$$J_t \cdot \dot{\omega}_r = T_r - T_t \quad (3.161)$$

$$\omega_t = \omega_r \quad (3.162)$$

Following the gearbox is the propeller shaft, which is modelled as a rotational member with no inertia, and it is possible to add damping, stiffness to propeller shaft if sufficient parameters are available. The propeller shaft connects the gearbox to the final drive. η_{tr} is the transmission efficiency. The torque from the gearbox is multiplied by the gear ratio i_{gear} to give the propeller shaft torque T_p while the angular speed ω_t is stepped down by the gear ratio to the propeller shaft speed ω_p .

$$T_p = \eta_{tr} \cdot T_t \cdot i_{gear} \quad (3.163)$$

$$\frac{\omega_t}{i_{gear}} = \omega_p \quad (3.164)$$

The torque at the final drive is T_f which is multiplied by the final drive ratio i_f which gives the drive shaft torque T_d .

$$T_p = T_f \quad (3.165)$$

$$\omega_p = \omega_f \quad (3.166)$$

$$T_d = \eta_{fd} \cdot T_f \cdot i_f \quad (3.167)$$

$$\omega_f = \omega_d \cdot i_f \quad (3.168)$$

Final Drive

The final drive gear box is modelled like the transmission gearbox with gear ratio multiplying the torque leaving the final drive to the wheels. In the case of Revere's FH16 it is of 6x4 type with a lift-able rear axle. Both the rear axles are capable of being powered, hence two different setups will be made. The first case when the 3rd axle is lifted which means the tractor will have two axles in use. The front axle that is steerable and non-powered and 2nd axle is driven. The second configuration is when both 2nd and 3rd axle are driving axles. For the simulation models when the third axle is lifted it is assumed that the final drive torque is equally distributed to the wheels on either side. Similarly, when then the third axle is lowered it is assumed that the drive torque is equally distributed making it 25% to each side of the two axles.

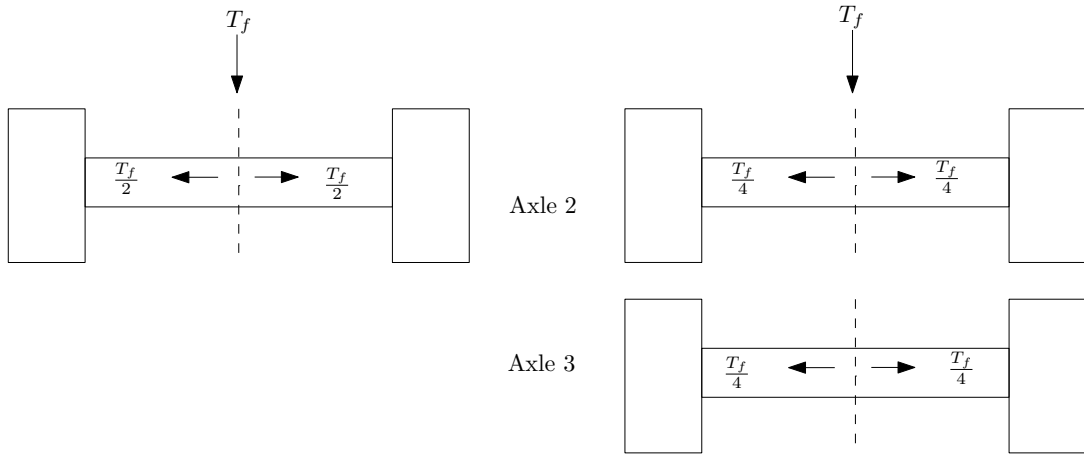


Figure 3.28: Torque distribution for axle configurations

$$\omega_w = \omega_d \quad (3.169)$$

$$T_{wl1} = 0.5 \cdot T_d \quad (3.170)$$

$$T_{wr1} = 0.5 \cdot T_d \quad (3.171)$$

The above equations are applicable when the second axle is driven, but when both rear axles are driven the torque is distributed as follows:

$$T_{wl1} = 0.25 \cdot T_d \quad (3.172)$$

$$T_{wr1} = 0.25 \cdot T_d \quad (3.173)$$

$$T_{wl2} = 0.25 \cdot T_d \quad (3.174)$$

$$T_{wr2} = 0.25 \cdot T_d \quad (3.175)$$

Gear shift manager

The FH16 has an *I-shift* gearbox which is an automated manual gearbox or in other words a manual gearbox with a shifting robot. The *I-Shift* gearbox is a non-sequential gear shifting system that takes into account several vehicle parameters before making a gearshift. For this thesis, the gearshift manager will take into account vehicle cargo mass, velocity, previous gear and A_{ped} accelerator pedal position while making a gearshift. These variables are chosen based on the observations made from the collected log data and discussion with experts. The first parameter chosen is the cargo mass, the load that is being hauled by the vehicle dictates the start gear and the shift number which is the number of gears to shift up is determined based on the remaining parameters. The logic is as follows:

```

if m > 12000
    stagear = 1;
    when vxv > upshift[pre(agear)]
        agear = pre(agear) + 2;
    elsewhen vxv < downshift[pre(agear)]
        agear = pre(agear)-1;
    else
        agear = pre(agear);
    end when
else
    when vxv > up[pre(agear)]
        agear = pre(agear) + shftnum;
    elsewhen vxv < dw[pre(agear)]
        agear = max(pre(agear)-1,6);
    else
        agear = pre(agear);
    end when
    stagear = 6;
    if Aped > 45
        g2 = 3;
    else
        g2 = 1;
        if agear >= g1
            shftnum = 1;
        else
            shftnum = g2
        end if
    end if

```

The arrays `up[]` and `dw[]` of length twelve, contain the velocity shift points for the 12 gears for up and down shift respectively. The array index gives the gear number. Based on the array index the minimum gear that can be attained is one and in this work, the neutral gear is not modelled. In the case of downshifting for cargo mass less than 12000 kg the

3. Methodology

minimum gear that can be reached is six as in the real vehicle. The variable $shft_{num}$ and the shift points decide the number of gears to shift up and this captures the non-sequential gear shifts. The variable g_1 decides beyond which gear shifting needs to be sequential. As seen in the shifting logic if the current gear represented by the variable `agear` is greater than g_1 then shifting is sequential else the shifting varies by the variable g_2 . The variable g_1 is set not to exceed ten. The magnitude of the accelerator pedal position (Aped) governs the up-shift number. This logic is chosen because this indicates that the driver wants to speed-up at least for the case with low cargo mass but for the high cargo mass case it is set to skip two gears. This is done because of lack of information on how gearshift are made under loaded scenarios. It should be noted that the gear-shifting logic would require the user to provide shifting points to match the gear-shifting on the real vehicle. In reality, the shifting logic is far more complicated since the gearshift manager takes a lot of variables into account and trying to capture it, is beyond the scope of this work.

Clutch Control

Previously the clutch model was explained, here the clutch actuation control will be explained. The actuation has been divided into three stages:

- Starting from standstill
- Reaching standstill
- Gear changes

For the above cases, the clutch model needs to be controlled and to do so the actuation is divided into two parts. First part controls the first two of the above and the second for gear changes.

When the vehicle starts from standstill and as the Aped request is given, the clutch needs to be smoothly engaged to avoid stalling of the engine or revving up. The engine stalls if the clutch is engaged too quickly. If the clutch is engaged too slowly then the discs slip and no torque is transmitted which causes the engine to rev-up. While the vehicle is braking, as its velocity approaches zero and as the engine speed approaches the idle speed the clutch has to disconnect the engine from the transmission to avoid engine stall. To handle these two cases a conditional function block is written, that generates an output that is either zero or one, this is called clutch trigger. The conditional function generates the clutch trigger output based on four input variables: accelerator pedal, brake pedal position, engine speed and longitudinal velocity.

$$clutch_{trig} = \begin{cases} \text{if } A_{ped} == 0 \ \& \ B_{ped} == 0 \ \& \ \omega_{eng} < \omega_{eng,idl} \ \& \ v_x < 2.5 \\ \parallel \\ A_{ped} \leq 0 \ \& \ B_{ped} > 0 \ \& \ \omega_{eng} < \omega_{eng,idl2} \ \& \ v_x < 2.5 \\ 1 \\ \text{else} \\ 0 \end{cases} \quad (3.176)$$

When the clutch trigger is one the clutch is disengaged and engaged when it is zero. In condition (3.176), the first statement checks if the vehicle is at standstill and the second statement check if it is going to reach standstill on braking. For these cases, the clutch has

to be disengaged such that the engine idles on reaching standstill. When an acceleration request is made trigger value switches to zero which connects the clutch disc. When the vehicle is running the clutch remains connected. The parameter $\omega_{eng,idl}$ is engine idle speed and $\omega_{eng,idl2}$ is a value that is marginally greater than the idle speed. This is done to prevent engine stall while braking.

The next function block as shown in figure 3.29 is for start-up actuation and is activated when trigger output switches from one to zero. As prior to starting from standstill the clutch discs are not connected. This generates the required clutch actuation profile to be followed for smooth engagement of the clutch discs. Along with the start-up function, a engine speed controller is modelled. During start-up, if the engine speed falls below the reference idle speed the controller generates a proportional torque to make up for the difference in engine speed.

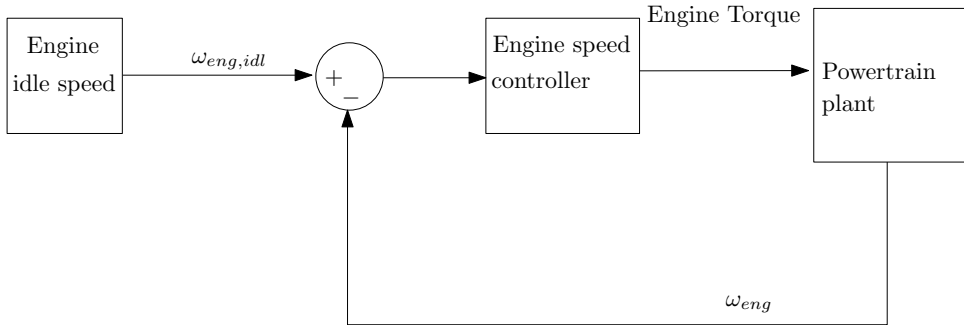


Figure 3.29: Engine speed clutch controller

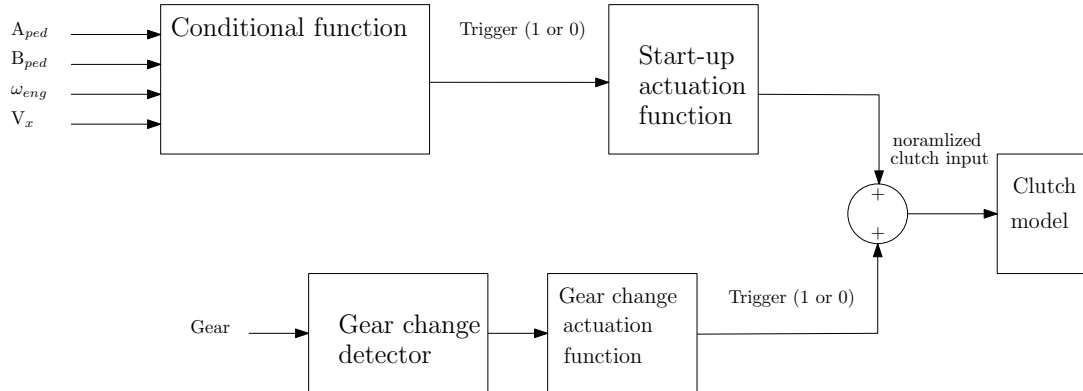


Figure 3.30: Clutch actuation flow diagram

The clutch actuation is different for the case when gear shifts are made, as in the real vehicle a single clutch model is implemented. When the vehicle is running the clutch normalized input is in zero state. When a gear change is made the clutch should be disengaged and re-engaged smoothly. Based on the gear-shifting logic it is identified that a shift will be made, using this condition the normalized input is made one at a predefined slope. After the input reaches its maximum value of one it is held for a time period of 0.5s to emulate the synchronization of the gears. Finally, it is dropped down to zero at a certain predefined slope which indicates completion of a gear change. The gear changes are seen as small steps on the velocity plots or as drop in engine torque. In reality, the

3. Methodology

slopes of the input changes from zero to one are not predefined, it is influenced by the torque request that generally depends on the road gradient and cargo mass and for this study it assumed to be constant as testing is conducted with solo tractor and on relatively flat roads.

The current logic is suitable for all of the test cases recorded at the track. For some test cases, the engine speed during start-up varies from the experimental data and this will be further discussed under the results and discussion chapter.

3.5.3 XC90

The passenger car model in this thesis is modelled a little differently when compared to the commercial heavy vehicle FH16. The main reasons are the lack of a cabin, having four wheels and the difference in the powertrain system. The representation of the equations are different but the idea of resolving forces and moments based on Newton and Euler equation remains the same and the equations in [19] have been used as references in this section.

3.5.3.1 Vehicle body

The vehicle body including the frame and cabin have six DOF, three planar and three out of plane similar to the truck chassis. The planar equations are as follows:

$$m_{sp} \cdot a_x = \sum_{i=1}^4 F_{x,i} \cdot \cos(\delta_{wh,i}) - \sum_{i=1}^4 F_{y,i} \cdot \sin(\delta_{wh,i}) - F_d - F_g + F_{ext,x} \quad (3.177)$$

$$m_{sp} \cdot a_y = \sum_{i=1}^4 F_{y,i} \cdot \cos(\delta_{wh,i}) + \sum_{i=1}^4 F_{x,i} \cdot \sin(\delta_{wh,i}) + F_{ext,y} \quad (3.178)$$

$$a_x = \dot{v}_x - v_y \cdot \omega_z \quad (3.179)$$

$$a_y = \dot{v}_y + v_x \cdot \omega_z \quad (3.180)$$

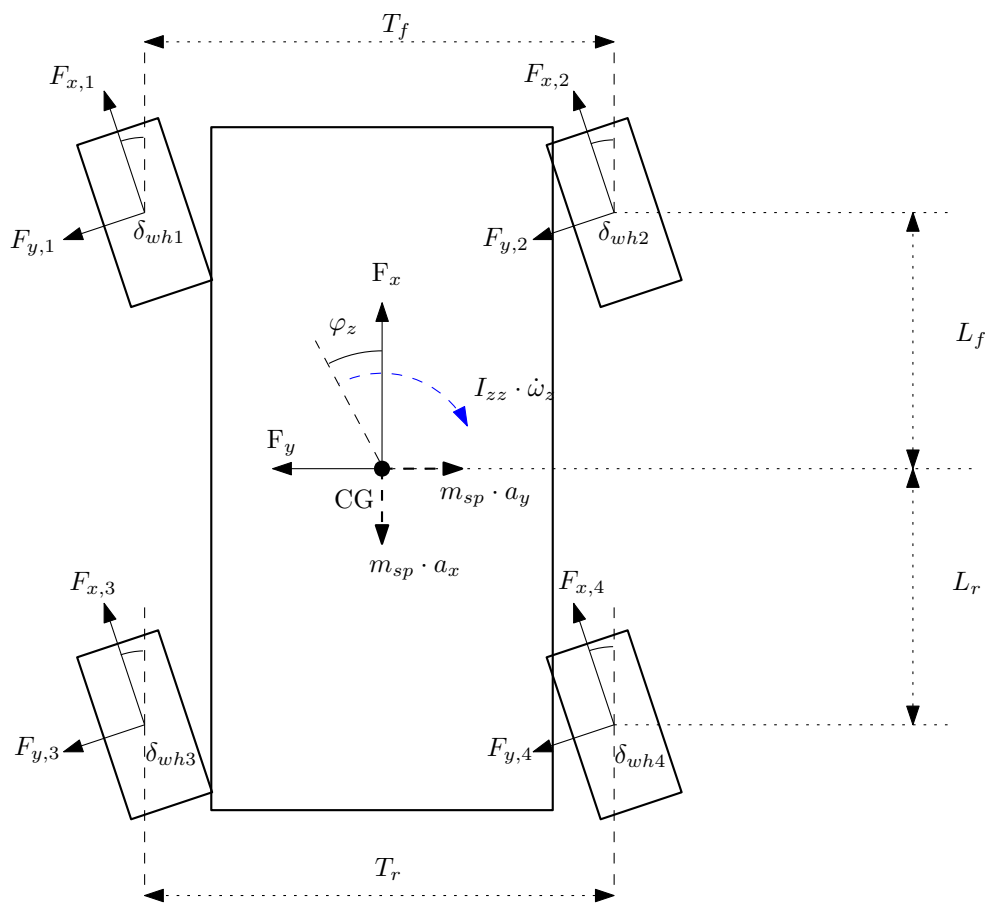


Figure 3.31: Planar free body diagram for passenger car

3. Methodology

$$\begin{aligned}
I_{zz} \cdot \dot{\omega}_z &= \sum_{i=1}^2 (F_{x,i} \cdot \sin(\delta_{whi}) + F_{y,i} \cdot \cos(\delta_{whi})) \cdot L_f \\
&- \sum_{i=3}^4 (F_{x,i} \cdot \sin(\delta_{whi}) + F_{y,i} \cdot \cos(\delta_{whi})) \cdot L_r \\
&- (F_{x,1} \cdot \cos(\delta_{wh1}) - F_{y,1} \cdot \sin(\delta_{wh1})) \cdot \frac{T_f}{2} \\
&+ (F_{x,2} \cdot \cos(\delta_{wh2}) - F_{y,2} \cdot \sin(\delta_{wh2})) \cdot \frac{T_f}{2} \\
&- (F_{x,3} \cdot \cos(\delta_{wh3}) - F_{y,3} \cdot \sin(\delta_{wh3})) \cdot \frac{T_r}{2} \\
&+ (F_{x,4} \cdot \cos(\delta_{wh4}) - F_{y,4} \cdot \sin(\delta_{wh4})) \cdot \frac{T_r}{2} \\
&+ \sum_{i=1}^4 M_{z,i}
\end{aligned} \tag{3.181}$$

Equations (3.177) to (3.180) are the force balance equations for longitudinal and lateral motion. The resistive forces F_d and F_g are same as in equation (3.23) and (3.24). Unlike the truck model, modular approach is followed only for the wheel because the axle modular equations are not useful here. The equation (3.181) gives the yaw moment balance about the z axis similar to the model of the truck. The out of plane motions like roll pitch and heave are studied under the suspension section.

$$v_{x,wh1} = v_x - \omega_z \cdot \frac{T_f}{2} \tag{3.182}$$

$$v_{x,wh2} = v_x + \omega_z \cdot \frac{T_f}{2} \tag{3.183}$$

$$v_{x,wh3} = v_x - \omega_z \cdot \frac{T_r}{2} \tag{3.184}$$

$$v_{x,wh4} = v_x + \omega_z \cdot \frac{T_r}{2} \tag{3.185}$$

$$v_{y,wh1} = v_y + \omega_z \cdot \frac{L_1}{2} \tag{3.186}$$

$$v_{y,wh2} = v_y + \omega_z \cdot \frac{L_1}{2} \tag{3.187}$$

$$v_{y,wh3} = v_y - \omega_z \cdot \frac{L_2}{2} \tag{3.188}$$

$$v_{y,wh4} = v_y + \omega_z \cdot \frac{L_2}{2} \tag{3.189}$$

$$\beta = \arctan\left(\frac{v_y}{v_x}\right) \tag{3.190}$$

The velocities at each wheel corner is influenced by the body velocity and yaw rate which is given by the equations (3.182) – (3.189).

3.5.3.2 Suspension

For a 14DOF passenger car model the individual wheel displacements are accounted. At each corner of the car, the wheel assembly is modelled as an un-sprung mass connected to the chassis (sprung) mass through spring and damper. The un-sprung mass is connected to the ground through tires also modeled as a spring. The equations for the suspension have been written based on the equation in [19].

$$m_u \cdot \ddot{z}_u = F_z - F_{z,c} - m_u \cdot g \quad (3.191)$$

$$F_{zi} = k_t \cdot (z_r - z_u + r_{wh} + \frac{m_s \cdot m_u \cdot g}{k_t}) \quad (3.192)$$

$$F_{z,c} = -(F_{spring} + F_{damp}) - F_{arb} \quad (3.193)$$

$$z = -(z_u - z_s - r_{wh} + h_{cg} + \frac{m_s \cdot g}{k_i}) \quad (3.194)$$

$$F_{spring} = k_{si} \cdot z, \text{ for } i=1,2,3,4 \quad (3.195)$$

$$F_{damp} = c_{di} \cdot \dot{z}, \text{ for } i=1,2,3,4 \quad (3.196)$$

In equation (3.195) and (3.196) k_{si} is the spring stiffness and c_{di} is the damping coefficient. The anti-roll bar forces at each corner is as follows where K_{arb} is the anti-roll bar stiffness:

$$F_{arb,f1} = K_{arb} \cdot (z_{s,1} - z_{s,2}) \quad (3.197)$$

$$F_{arb,f2} = -K_{arb} \cdot (z_{s,1} - z_{s,2}) \quad (3.198)$$

$$F_{arb,r3} = K_{arb} \cdot (z_{s,3} - z_{s,4}) \quad (3.199)$$

$$F_{arb,r4} = -K_{arb} \cdot (z_{s,3} - z_{s,4}) \quad (3.200)$$

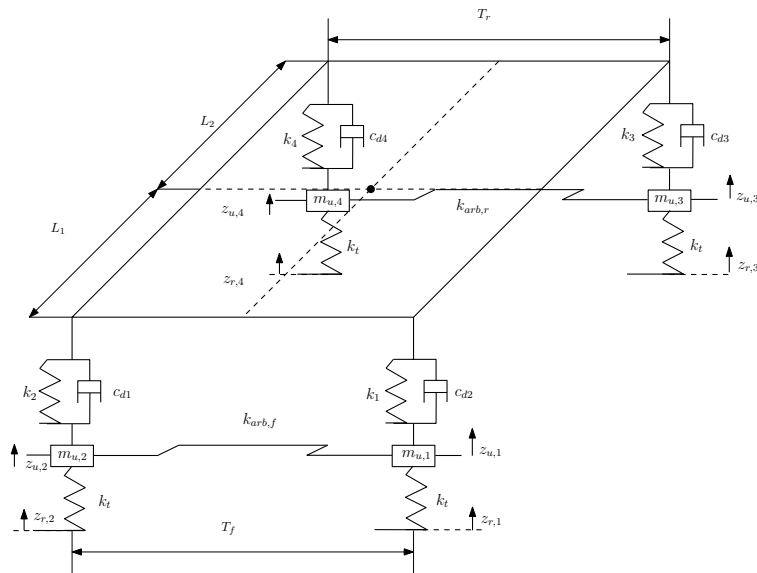


Figure 3.32: Vertical DOF for a passenger car

3. Methodology

The displacement of the unsprung mass is given by z_u and the equation of motion for the unsprung mass is as follows:

$$m_u \cdot \ddot{z}_u = k_t \cdot (z_r - z_u + r_{wh}) - k_{si} \cdot (z_u + r_{wh} + h_{cg}) \quad (3.201)$$

The above equations are for one corner of the car. At each corner the sprung mass displacement is given by the following equations:

$$z_{s1} = z_{cg} - L_1 \cdot \varphi_y + \frac{T_f}{2} \cdot \varphi_x \quad (3.202)$$

$$z_{s2} = z_{cg} - L_1 \cdot \varphi_y - \frac{T_f}{2} \cdot \varphi_x \quad (3.203)$$

$$z_{s3} = z_{cg} + L_2 \cdot \varphi_y + \frac{T_r}{2} \cdot \varphi_x \quad (3.204)$$

$$z_{s4} = z_{cg} + L_2 \cdot \varphi_y - \frac{T_r}{2} \cdot \varphi_x \quad (3.205)$$

Having determined the displacements at each wheel corner the heave motion of the vehicle body is captured by the following equation summing up the vertical forces.

$$m_s \cdot \ddot{z}_{cg} = \sum_{i=1}^{(4)} F_{c,i} - m_s \cdot g \quad (3.206)$$

The distance between the CG to the roll centre and CG to pitch centre are calculated based on simple geometry.

$$d_{zrc,CG} = z_{cg} - \frac{L_2 \cdot h_{frc} + L_1 \cdot h_{rrc}}{L_1 + L_2} \quad (3.207)$$

$$d_{zpc,CG} = z_{cg} - h_{pc} \quad (3.208)$$

The individual wheel motions affect the roll and pitch dynamics of the vehicle body, as shown in figure 3.33 and 3.34.

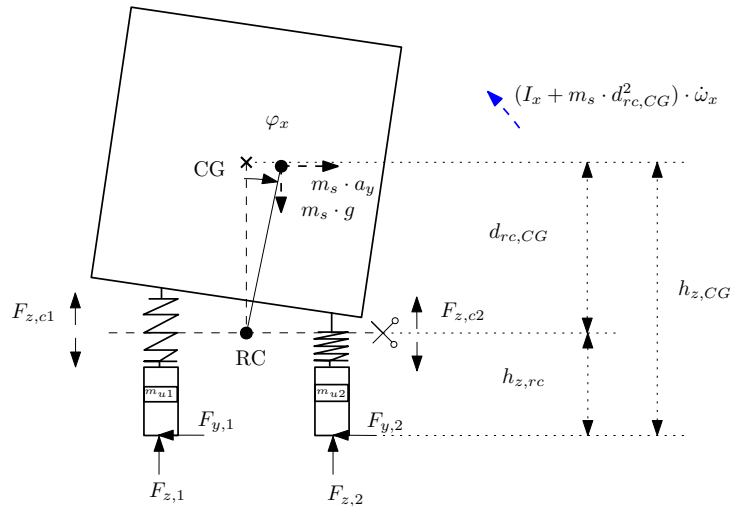


Figure 3.33: Roll moment balance for a passenger car

The roll moment is resolved about the roll centre RC of the car. The equation is as given in (3.209). The roll moment due to the suspension forces are accounted by the forces at the corner 1,3 and 2,4.

$$\begin{aligned}
 & (I_x + m_{sp} \cdot d_{rc,CG}) \cdot \dot{\omega}_x + (I_z - I_y) \cdot \omega_y \cdot \omega_z = \\
 & (F_{z,c1} - F_{z,c2}) \cdot \frac{T_f}{2} + (F_{z,c3} - F_{z,c4}) \cdot \frac{T_r}{2} \\
 & + (F_{y,1} \cdot \cos(\delta_{wh1}) + F_{y,2} \cdot \cos(\delta_{wh2}) \cdot h_{zrc} \\
 & + (F_{y,3} \cdot \cos(\delta_{wh3}) + F_{y,4} \cdot \cos(\delta_{wh4}) \cdot h_{zrc} + m_{sp} \cdot a_y \cdot d_{rc,CG}
 \end{aligned} \tag{3.209}$$

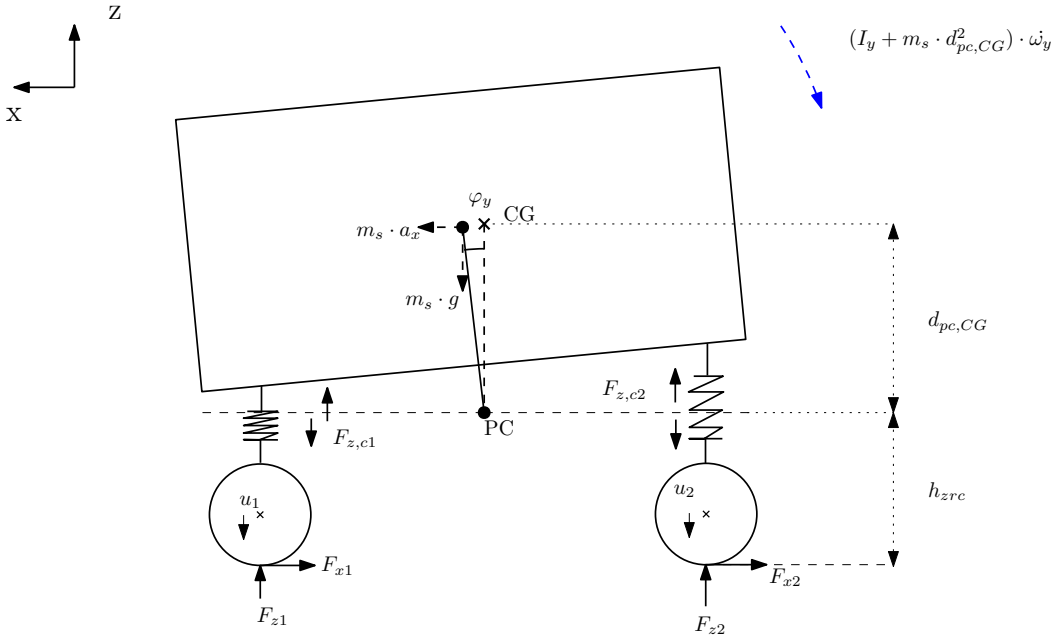


Figure 3.34: Pitch moment balance for a passenger car

$$\begin{aligned}
 & (I_y + m_{sp} \cdot d_{pc,CG}) \cdot \dot{\omega}_y + (I_x - I_z) \cdot \omega_x \cdot \omega_z = \\
 & (F_{z,c3} + F_{z,c4}) \cdot L_r - (F_{z,c1} + F_{z,c2}) \cdot L_f \\
 & \sum_{i=1}^4 (F_{x,i} \cdot \cos(\delta_{wh,i}) \cdot h_{z,pc} + m_{sp} \cdot a_x \cdot d_{zpc,CG}
 \end{aligned} \tag{3.210}$$

3.5.3.3 Powertrain

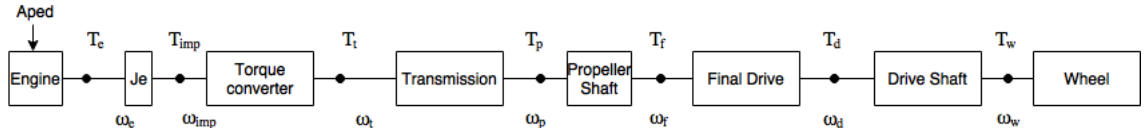


Figure 3.35: Driveline node diagram for XC90

The driveline of the XC90 follows a similar structure as the advanced FH16 model, the only difference is that instead of a dry friction clutch a torque converter is present

3. Methodology

in the driveline. The torque converter's purpose is same as that of a clutch but using fluid coupling. It consists of three elements, an impeller which is a centrifugal pump, a turbine and a stator. The pump uses mechanical energy from the engine and converts it to fluid coupling power. The turbine is coupled to the impeller through fluid coupling which rotates the turbine and its shaft, that is connected to the transmission. The fluid is redirected by the stator onto the impeller or pump. This completes one fluid cycle in the torque converter. Based on the impeller and turbine characteristics, torque amplification is provided. The torque from the engine is related as follows:

$$\nu = \frac{\omega_{turbine}}{\omega_{impeller}} \quad (3.211)$$

$$T_{impeller} = \omega_{impeller}^2 \cdot \lambda(\nu) \quad (3.212)$$

$$T_{turbine} = T_{impeller} \cdot \mu_{tur}(\nu) \quad (3.213)$$

In the above equations ν is the speed ratio of the turbine to the impeller and μ_{tur} is torque ratio which is a function of the speed ratio. The Kfactor also known as $\lambda(\nu)$ is the characteristic of the torque converter relating the impeller torque to the impeller speed. This ratio is a function of speed ratio and is dependent on the fluid properties and geometry of the torque converter [5]. The relationship is of ν with the other two variables is set up as a look-up table in the model. Since the data for the look-up tables is not easily available, for the thesis the torque converter characteristics from a MATLAB example [37] is modified such that the test data and model velocity are comparable.

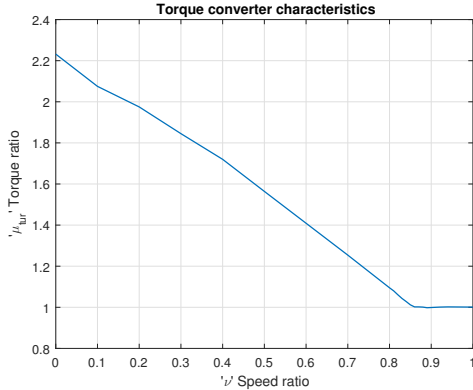


Figure 3.36: Torque ratio vs speed ratio

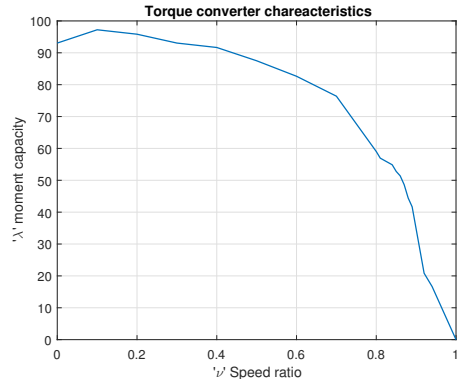


Figure 3.37: K factor vs speed ratio

3.6 Summary

Two types of vehicle models for each of the test vehicles with their respective control interface are elucidated in this chapter. All the models are developed using the programming tool *Modelica* on Dymola. The simple model developed is a quick simulation model that is suitable for online prediction. The simple model is represented by a single-track model with the body having three DOF and each wheel having rotational DOF. The advanced model has additional degrees of freedom to give a more realistic representation of the real vehicle. In the case of the FH16, the vehicle body has six DOF, each axle has two DOF, each wheel has two DOF namely rotational and vertical (no contact loss for wheel vertical

DOF), and the cabin with three DOF. Since the FH16 advanced model has two rear axles, the two possibilities are modelled. One with six wheels and the other with ten wheels, in the former configuration the 2nd rear axle is raised. While for the XC90 the body has six DOF, each wheel has two DOF rotational and vertical.

The powertrain models in both the vehicles have a similar engine model with a pedal map and boost-pressure build-up. The differences in the powertrain system are in the coupling unit and transmission. The FH16 has a clutch model and automated manual transmission which is a manual transmission with a shifting robot. A clutch control logic and non-sequential shifting logic needed within the FH16 powertrain model are implemented. The XC90 model has a conventional automatic transmission model with a simplified torque converter model. All the models are capable of starting and re-starting from a standstill. In addition to the generic vehicle model the control interface models are developed and this maps the generic driver inputs like steering wheel angle, accelerator and brake pedal position to the test vehicle specific inputs. In the next chapter, the models are validated with testing data and compared against each other.

3. Methodology

4

Results and Discussion

In this chapter, the simple and advanced vehicle models of the test vehicles are validated against experimental data and compared against each other. The experimental results are collected using two testing methods. First, open-loop tests with the control interface and the second with manual driving with the recorded driver inputs being fed to the models. The open-loop tests are designed based on the previously discussed control interface actuation requests. A set of csv files containing the actuation requests are built and sent through the OpenDLV interface or the vehicle network toolbox interface on Simulink. Both the interfaces connect to the vehicle CAN bus.

Under section 4.1 and 4.2, the test inputs and the resulting plots for the longitudinal and lateral tests can be found. The plots illustrating the outcome of the inputs will have the following pattern, a red line for the simple model, a blue line for the advanced model and a black line for the log data. To examine the error, the difference between the log and the simulation data is represented with a histogram plot.

The x axis indicates the error and the y axis, the normalized sample counts. On a histogram plot, if the bars are skewed to the left of zero it indicates that the simulation data exceeds the log data. The red bars indicate the error with the simple model and the blue bars for the advanced model. As the sample counts are normalized adding all the counts represented by all the bars of a particular color results to 1. If a bar is of height 0.4 then it represents 40% of the total sample count. The error magnitude represented with a histogram will be explained in detail with a test result.

All tests start from a standstill and braking input is present for each test to bring the vehicles to a standstill. If the braking input was not sufficient to bring the vehicle to a complete stop, the csv inputs were overridden by the driver input to ensure safety. Following the test results some comments will be made on the computational performance of the models. Finally, a use-case with the advanced XC90 model is discussed.

4.1 Results FH16

The actuation input signals for the FH16 were discussed in the section 3.3.1, but will be restated here:

- Road wheel angle request [rad]
- Accelerator pedal position request [%]
- Brake deceleration request [m/s^2]

4.1.1 Longitudinal test

4.1.1.1 Test 1 FH16: Slow acceleration to 8–10 m/s

In this test, the accelerator pedal position is gradually increased as a ramp to reach a velocity of 8–10 m/s or 30–40 km/h starting from a standstill. This test is defined to study the influence of gradual accelerator pedal input on the powertrain model and compare it against other tests. The test inputs are shown in the figure 4.1. The same inputs are given to test vehicle and to the models.

Figure 4.2 illustrates the results with a graphical comparison and an error histogram. It can be seen in figure 4.2a that the distance covered by the simple model is within 5m of the log data while the advanced model exceeds it by 40m. In figure 4.2b the velocity error between the simple model and log data is significantly low. In the normalized error distribution of velocity the histogram bars in red show that 85% of the sample counts are within an error magnitude of $\pm 0.5 \text{ m/s}$ which means that 85% of the total number of samples of the simple model velocity differ from the log data by only $\pm 0.5 \text{ m/s}$. For the advanced model the normalized error distribution of velocity represented by the blue bars show that approximately 50% of the sample counts lie within an error magnitude of -2 to -1 m/s. This shows that about 50% of the total number of samples of the velocity differ from the log data by -2 to -1 m/s thus indicating that advanced model velocity has a comparatively large error. In the case of the acceleration plots in figure 4.2b the normalized error distribution for both models is concentrated about zero where 50% of sample counts for both the models lie within an error magnitude of $\pm 0.5 \text{ m/s}^2$. Further discussion can be found under the section 4.1.3.

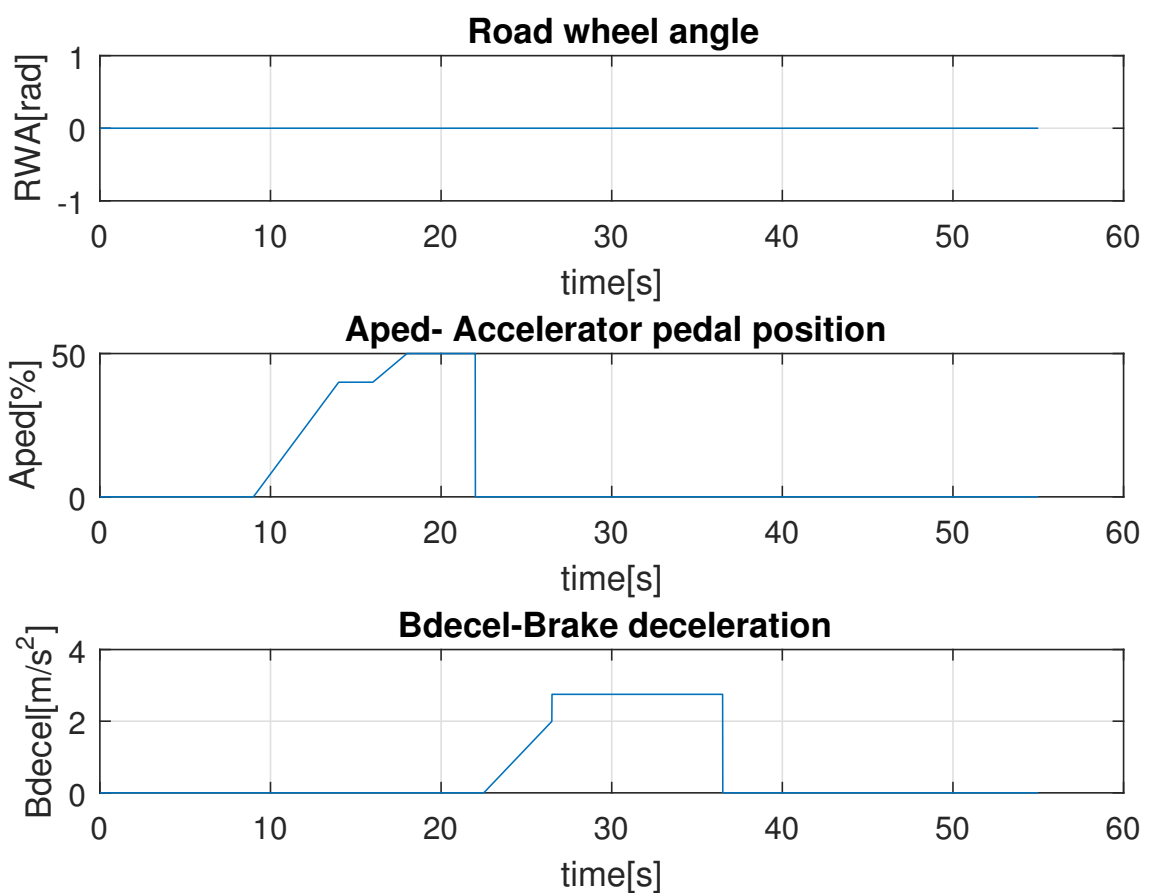
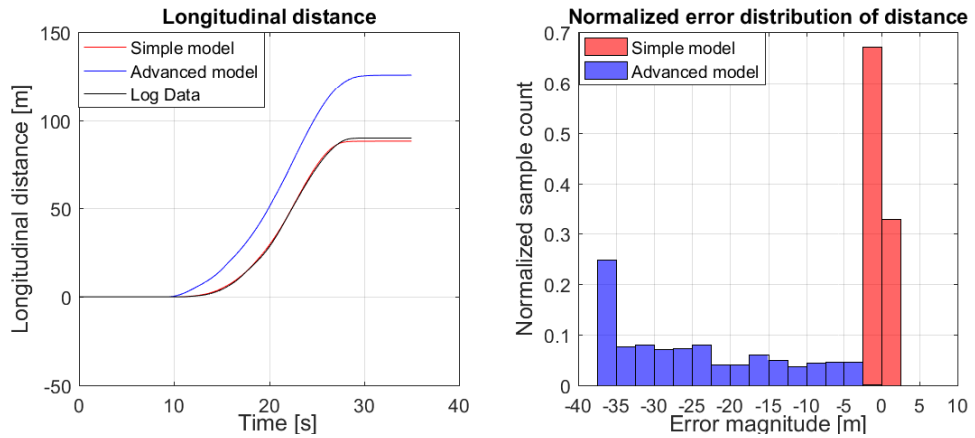
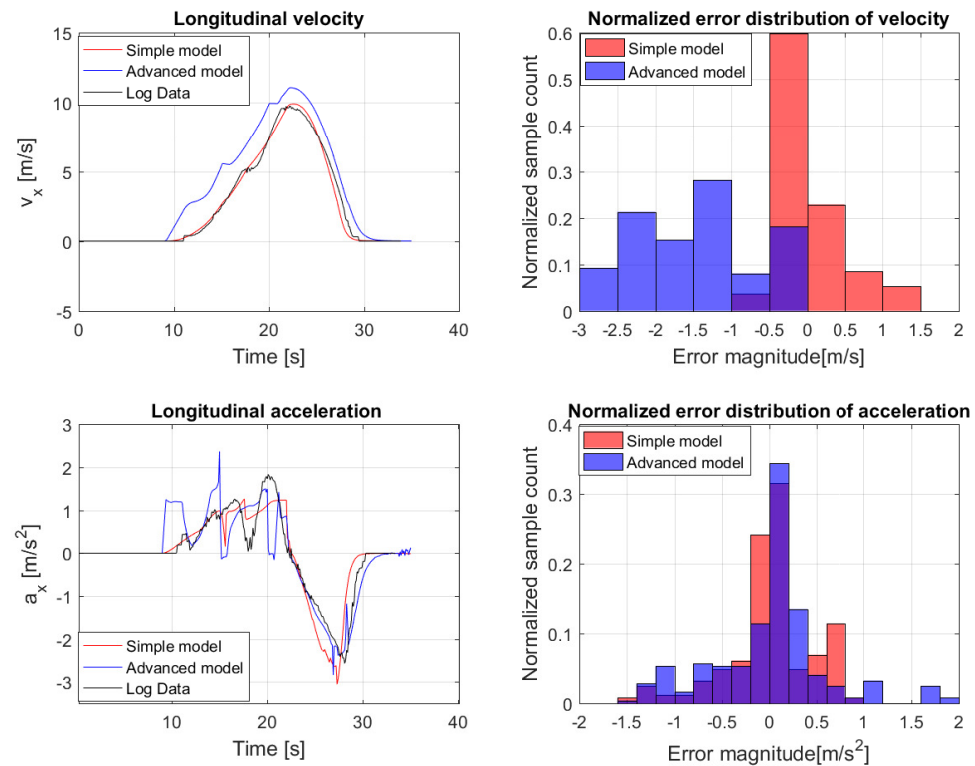


Figure 4.1: Actuation input for slow acceleration to 8–10 m/s

4. Results and Discussion



(a) Longitudinal distance of test 1 FH16



(b) Longitudinal velocity and acceleration of test 1 FH16

Figure 4.2: Longitudinal results for test 1 FH16

4.1.1.2 Test 2 FH16: Step acceleration to 13–15 m/s

In this test, a higher velocity of 13–15 m/s or 50-60 km/h is targeted in comparison to test 1. The accelerator pedal input is steadily increased in the form of steps upto 80%. The test inputs are as shown in figure 4.3. This test is defined to evaluate its outcome against test 1.

In figure 4.4 the longitudinal results are illustrated with a graphical comparison and an error histogram. The distance covered by the simple model as shown in figure 4.4a exceeds the log data by 25m and the advanced models is within 5m. In the figure 4.4b for the advanced model the normalized error distribution of velocity indicates a relatively low error as (blue bars) 80% of the sample counts are within an error magnitude of ± 0.5 m/s while for the simple model (red bars) it is 45%. This shows that the advanced model velocity error is insignificant compared to the simple. For the acceleration plots the normalized error distribution indicates that 50-60% of the sample counts are within an error magnitude of ± 0.5 m/s² (blue bars) for the advanced model. For the simple model it is skewed with more than 40% between 0.2 to 0.6 m/s² (red bars). Additional discussion and comparison can be found in section 4.1.3.

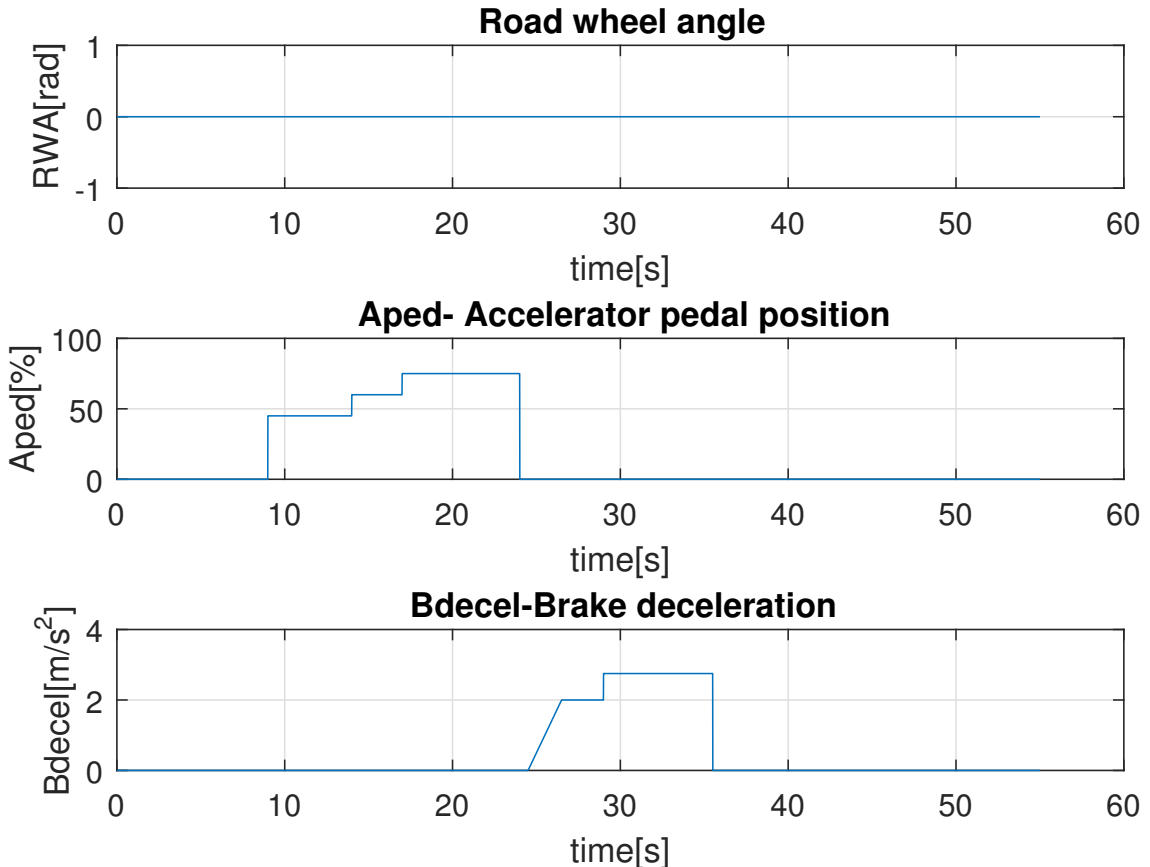
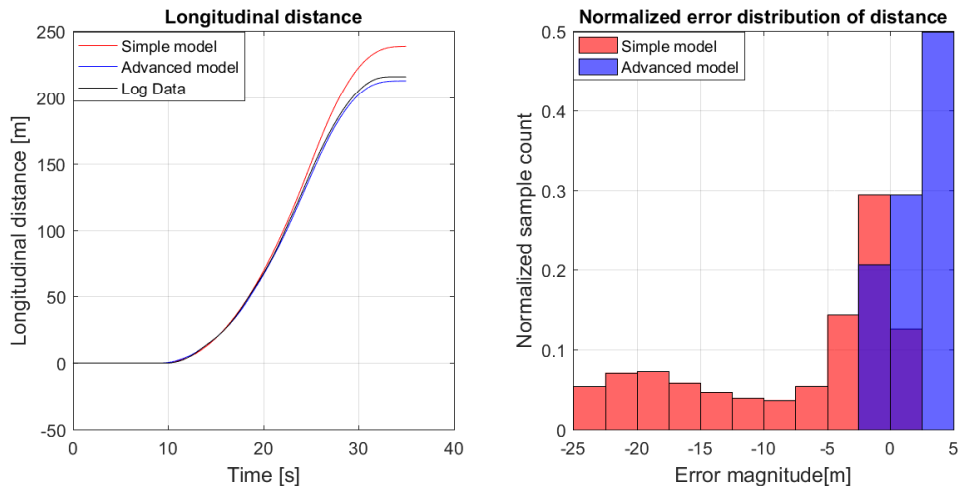
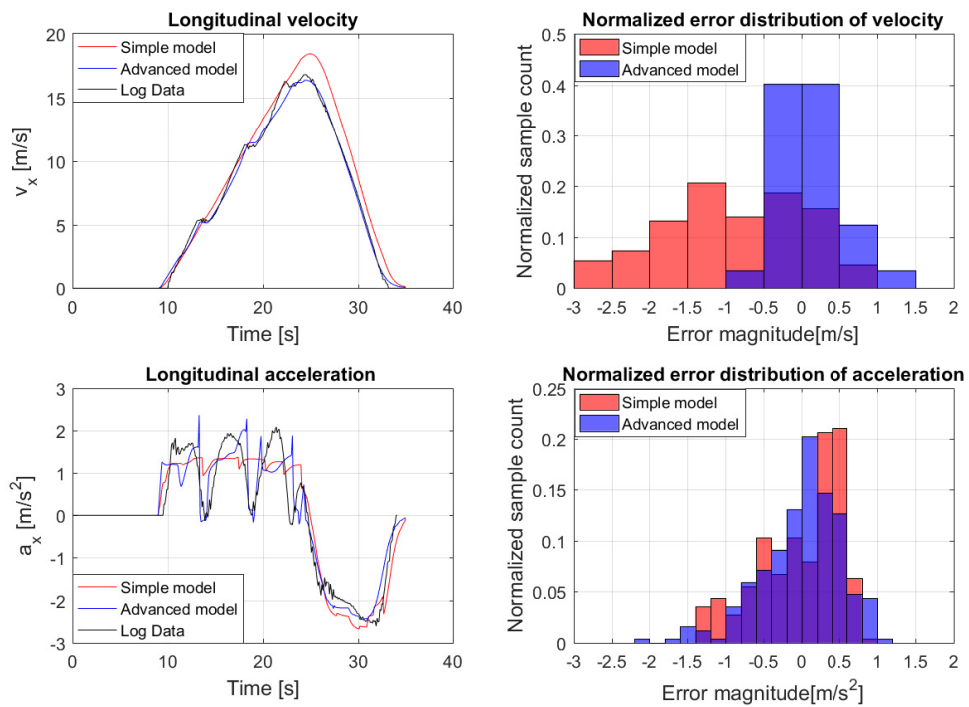


Figure 4.3: Actuation input for step acceleration to 13–15 m/s

4. Results and Discussion



(a) Longitudinal distance of test 2 FH16



(b) Longitudinal velocity and acceleration of test 2 FH16

Figure 4.4: Longitudinal results for test 2 FH16

4.1.1.3 Test 3 FH16: Step acceleration of 100 %

In this test, as shown in figure 4.5, 100% accelerator pedal input is given to examine the behaviour of the models at full-throttle.

The figure 4.6 illustrates the results with a graphical comparison and an error histogram. In figure 4.6a the distance covered by the simple and the advanced models are within 10m of the log data. In the figure 4.6b the normalized error distribution of velocity shows that for both models about 60% of the sample counts are within an error magnitude of ± 0.5 m/s indicating an insignificant error in velocity. In the case of the acceleration plots about 40% sample counts are within an error magnitude of ± 0.3 m/s² for both models. In the figure 4.6b the acceleration saturates during the start of the maneuver this because the clutch actuation controller delivers a proportional torque to avoid engine stall. Additional discussion is under the section 4.1.3.

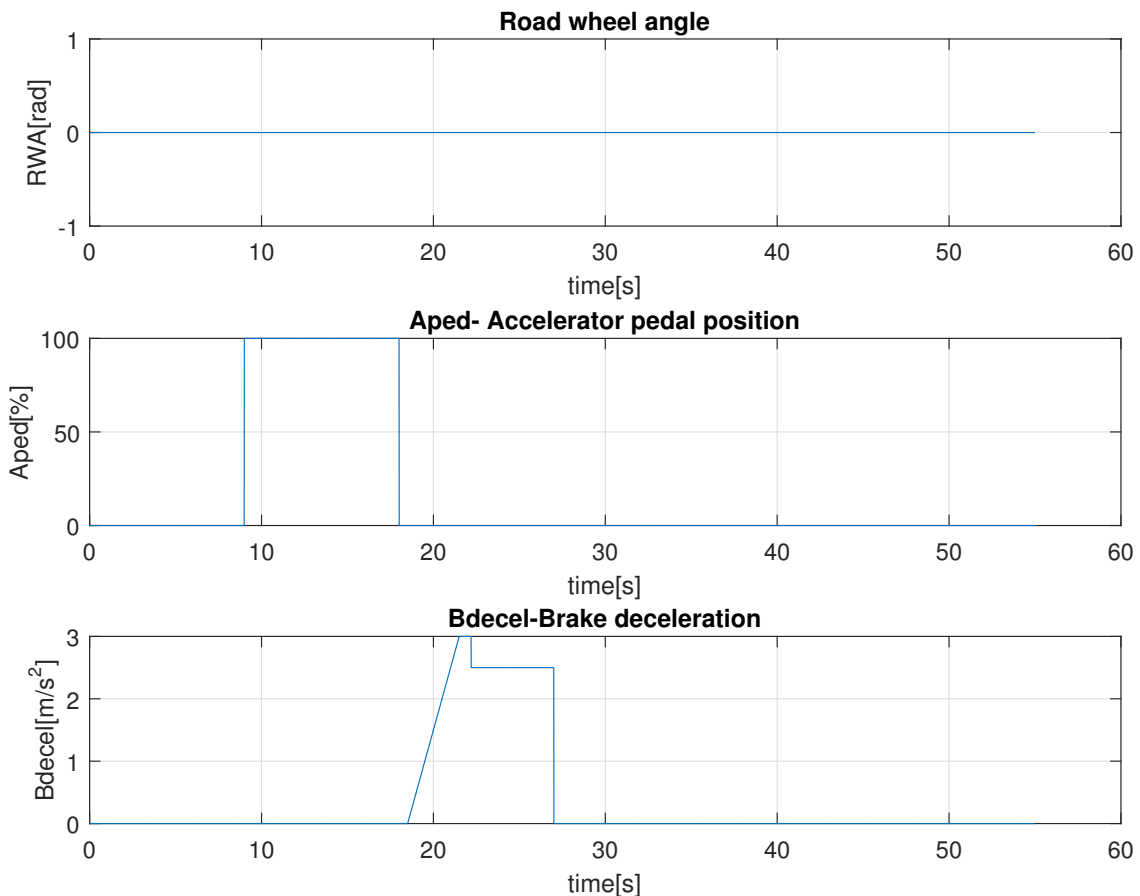
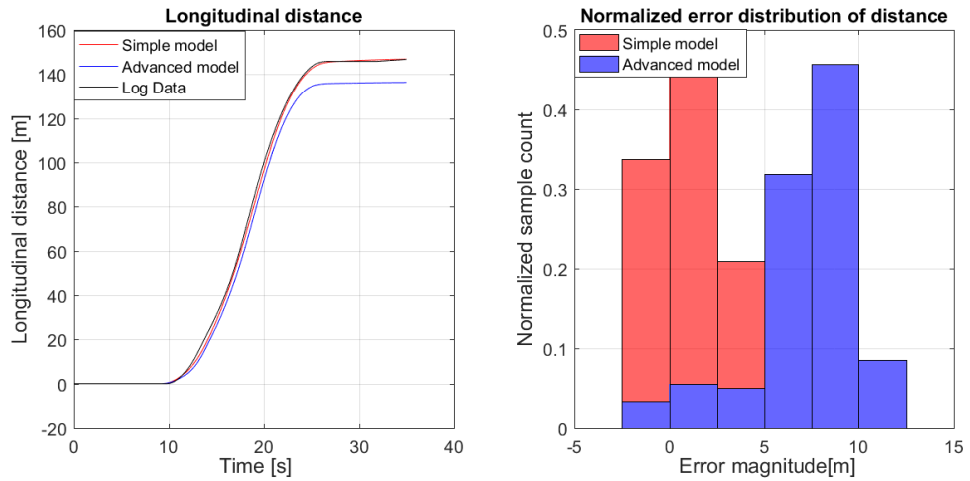
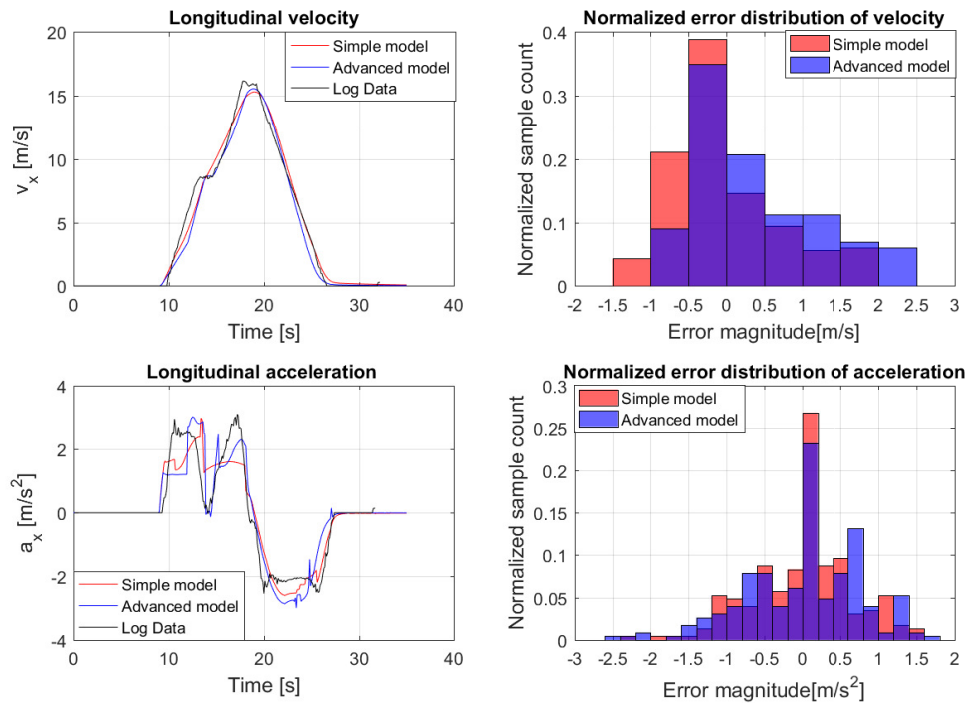


Figure 4.5: Actuation input for step acceleration of 100 %

4. Results and Discussion



(a) Longitudinal distance of test 3 FH16



(b) Longitudinal velocity and acceleration of test 3 FH16

Figure 4.6: Longitudinal results for test 3 FH16

4.1.1.4 Test 4 FH16: Manual driving of driving cycle 1

In this test recorded manual driving inputs as shown in figure 4.7 are sent to the simulation models. The driving scenario is aimed to capture a city driving cycle lasting six minutes. With this test it is aimed to highlight the differences between the simple and advanced models. Though the steering input is given due to model due to technical difficulty the lateral acceleration and yaw rate of the test vehicle were not recorded.

The figure 4.8 illustrates the longitudinal results with a graphical comparison and an error histogram. In figure 4.8a the distance covered by the advance model is within 150 m of the log data while for the simple model it is within 350 m. In the figure 4.8b, the normalized distribution of velocity for the advanced model (blue bar) show that 40% of the sample counts are within an error magnitude of ± 1 m/s. For the simple model (red bar) 30% of the sample counts are within an error range of ± 1 m/s and the total error magnitude range is significantly large ranging from -10 to 6 m/s. The reason for the large difference is the lack of clutch model due to which the engine speed and torque rise instantaneously and attain a higher value. The spikes in the acceleration plot of advanced model is because of the abrupt change in the angular velocity during a gearshift. Additional discussion is under the section 4.1.3.

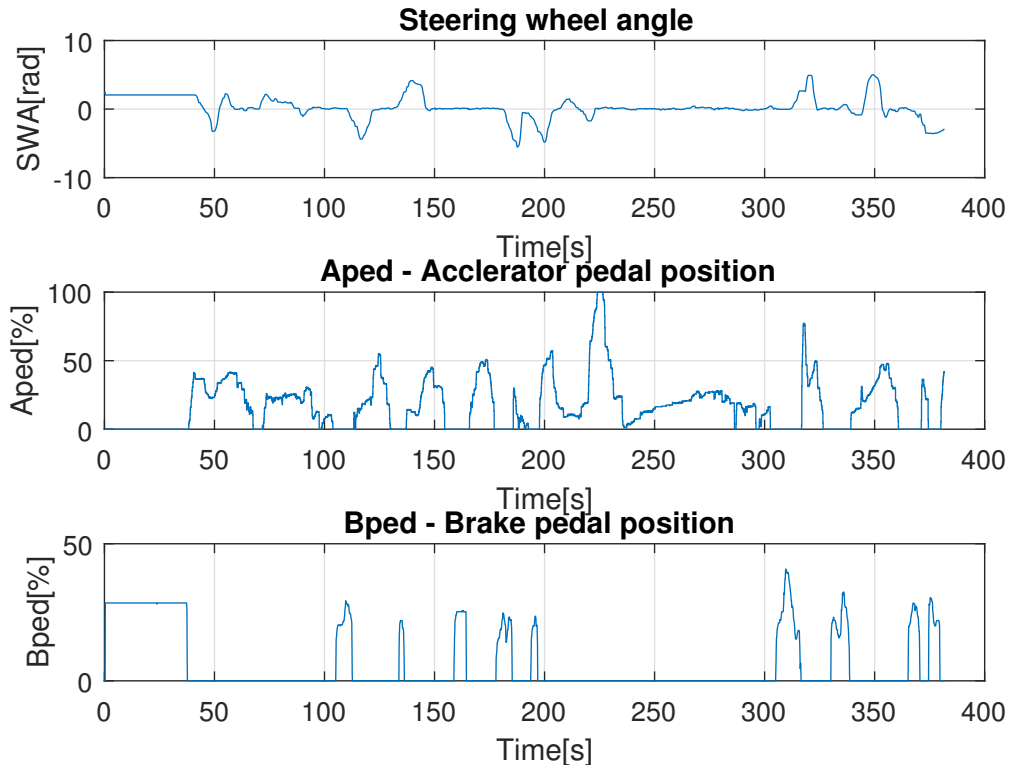
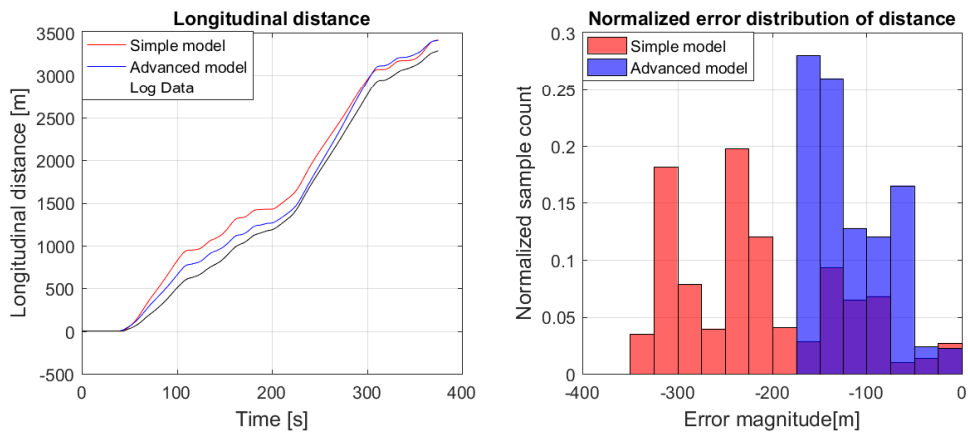
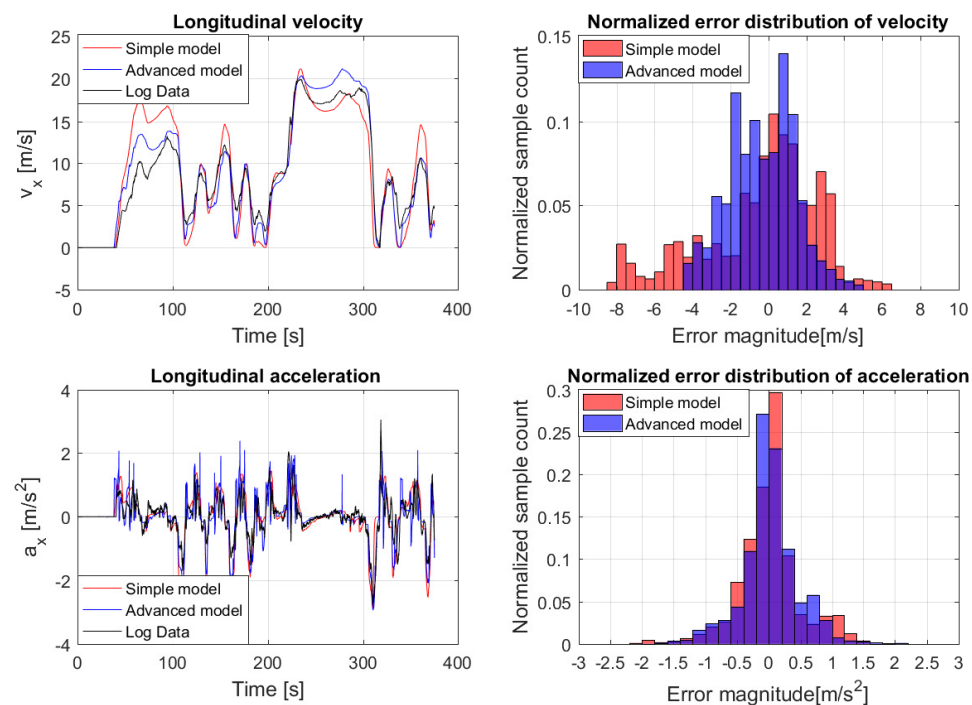


Figure 4.7: Recorded test inputs for the driving cycle

4. Results and Discussion



(a) Longitudinal distance of driving cycle 1



(b) Longitudinal velocity and acceleration for driving cycle 1

Figure 4.8: Longitudinal results of test 4 FH16

4.1.1.5 Test 5 FH16: Manual driving of driving cycle 2

In this test figure 4.9 shows the recorded manual driving inputs of the second driving cycle. As in the previous test, it is aimed to highlight the differences between the simple and the advanced model. In this test only the region of interest is plotted the initialization data was unimportant hence the plots start from 95 seconds.

The figure 4.10 illustrates the results with a graphical comparison and an error histogram. In figure 4.10a the distance covered by the simple model exceeds the log data by 1200 m and the advanced model exceeds it by only 300 m. Similar trend is observed in the normalized distribution of velocity in figure 4.10b, the error for the simple model is comparatively large with (red bars) 50% of the sample counts having an error magnitude greater than -4 m/s. For the advanced model same number of sample counts are within an error magnitude of ± 1 m/s (blue bars). In the case of acceleration plots it can be seen that the error magnitude is concentrated about ± 0.5 m/s² because of the deceleration sections. The comparatively large error for the simple model is due to the absence of a clutch model due to which the power disruptions are not captured by the model. The net engine torque throughout the maneuver is significant higher than the log data.

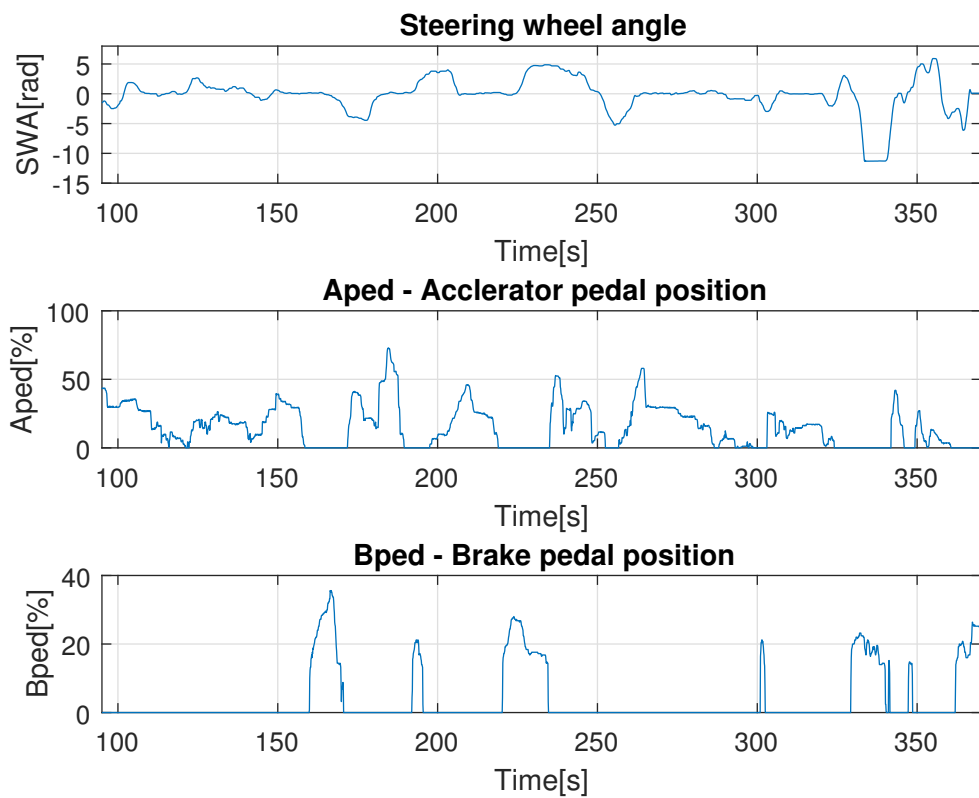


Figure 4.9: Recorded test inputs for the driving cycle 2

4. Results and Discussion

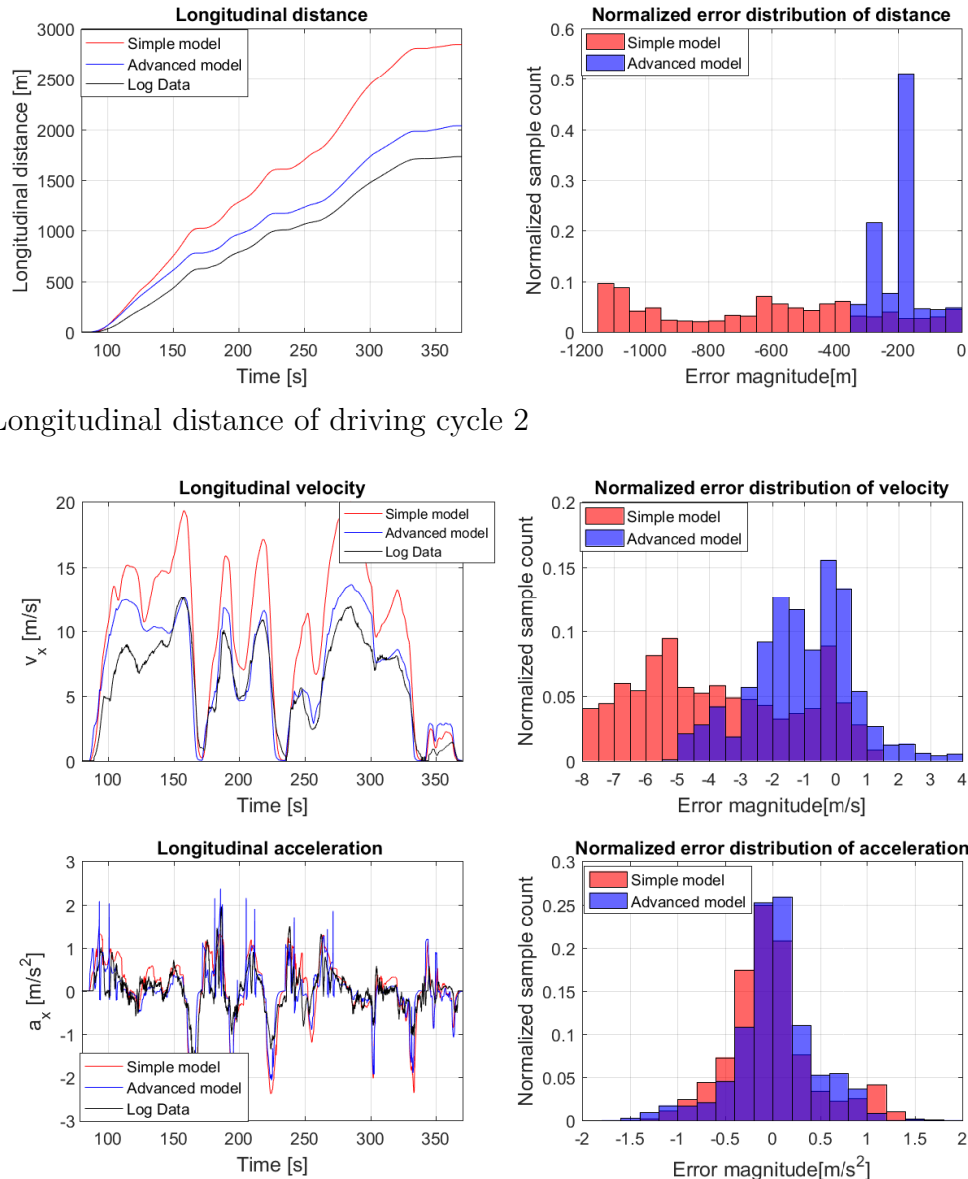


Figure 4.10: Longitudinal results of test 5 FH16

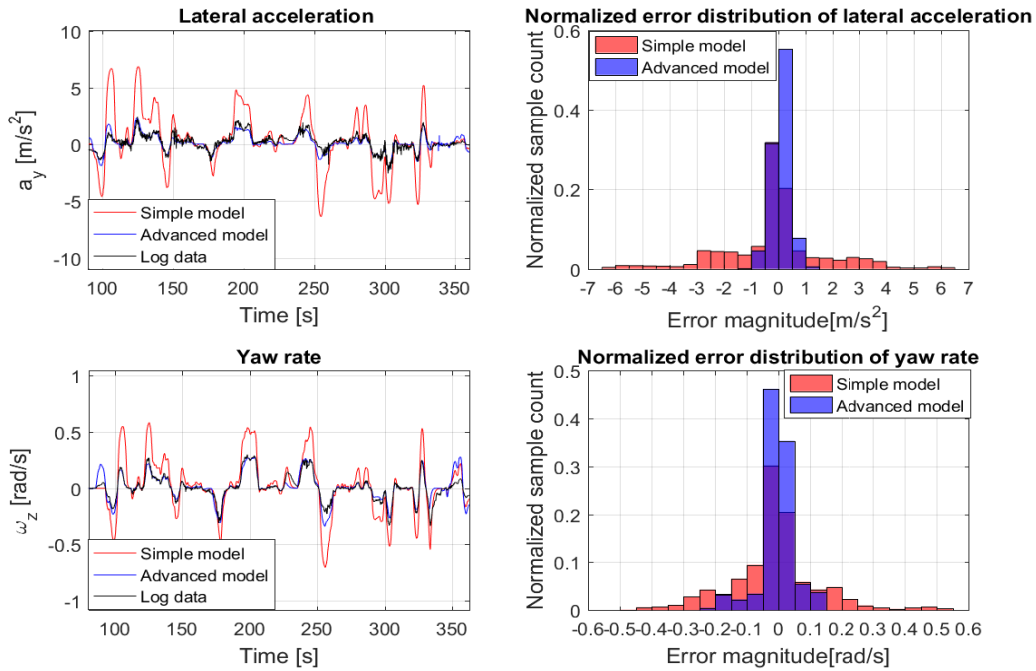


Figure 4.11: Lateral acceleration and yaw rate for driving cycle 2

The lateral acceleration and yaw rate error is relatively large for the simple model with only (red bars) 25% of the sample counts within an error magnitude of $\pm 0.5 \text{ m/s}^2$. For yaw rate only 30% of sample counts are within an error magnitude of $\pm 0.05 \text{ rad/s}$. The main reason for the difference is because of the high velocity attained by the simple model, isotropic tire model and absence of load transfer. For the advanced model (blue bar) in the normalized error distribution of lateral acceleration more than 80% of the sample counts are within an error magnitude of $\pm 0.5 \text{ m/s}^2$ indicates that the difference with respect to the log data is insignificant. Similar trend is observed for the yaw rate as well. Additional discussion is under the section 4.1.3.

4.1.2 Lateral test

4.1.2.1 Test 6 FH16: Manual lane change test

In this test lateral behaviour of the model is evaluated using recorded manual driving inputs for a lane change as seen in figure 4.12. The vehicle is steadily accelerated to a velocity of about 30 km/h or 8.3 m/s, on reaching the targeted velocity three lane changes are performed.

The figure 4.13 illustrates the results with a graphical comparison and an error histogram. Figure 4.13a indicates the longitudinal distance covered by both the models is within 10 m of the log data. The normalized error distribution of velocity for the simple model in the figure 4.13b indicates that the error is marginally small for both models. It slightly skewed for simple model (red bar) with 70% of the sample counts within an error magnitude of -0.1 to -0.9 m/s. For the advanced model 70% of sample counts are within an error magnitude of ± 0.4 m/s (blue bar). The acceleration normalized error distribution is concentrated around zero because a significant section of the data shows that the vehicle is travelling at a constant velocity (low acceleration). In figure 4.14 the lateral results are illustrated. In the normalized error distribution of lateral acceleration for the simple model (red bar) 40% of the sample counts are within an error magnitude of ± 0.2 m/s² while it is more than 50% for the advanced model indicating a relatively low error for the advanced model. Additional discussion is under the section 4.1.3.

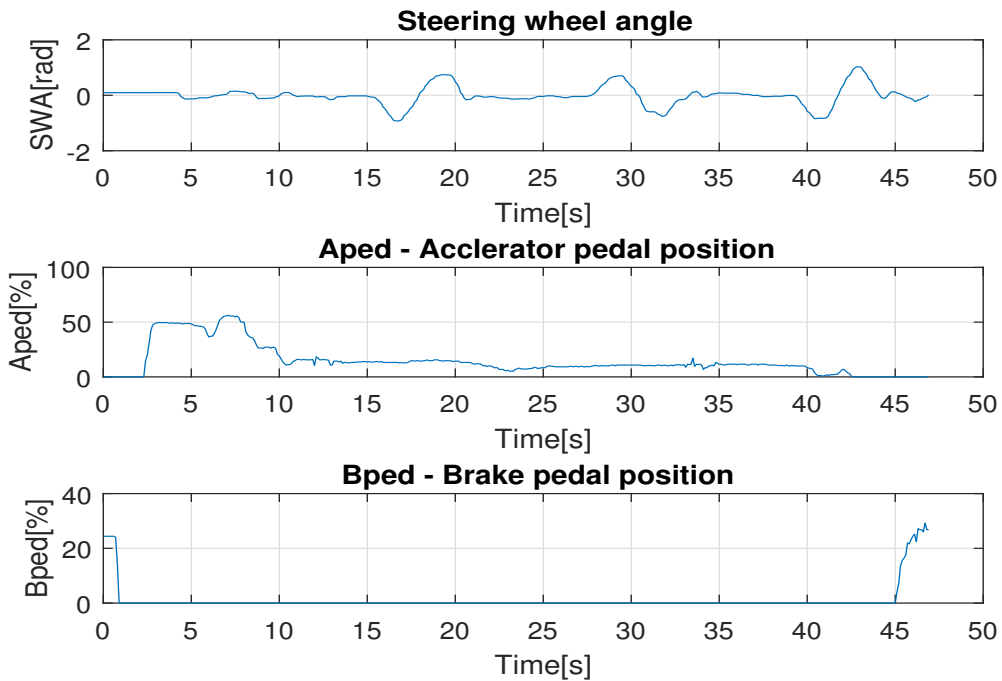
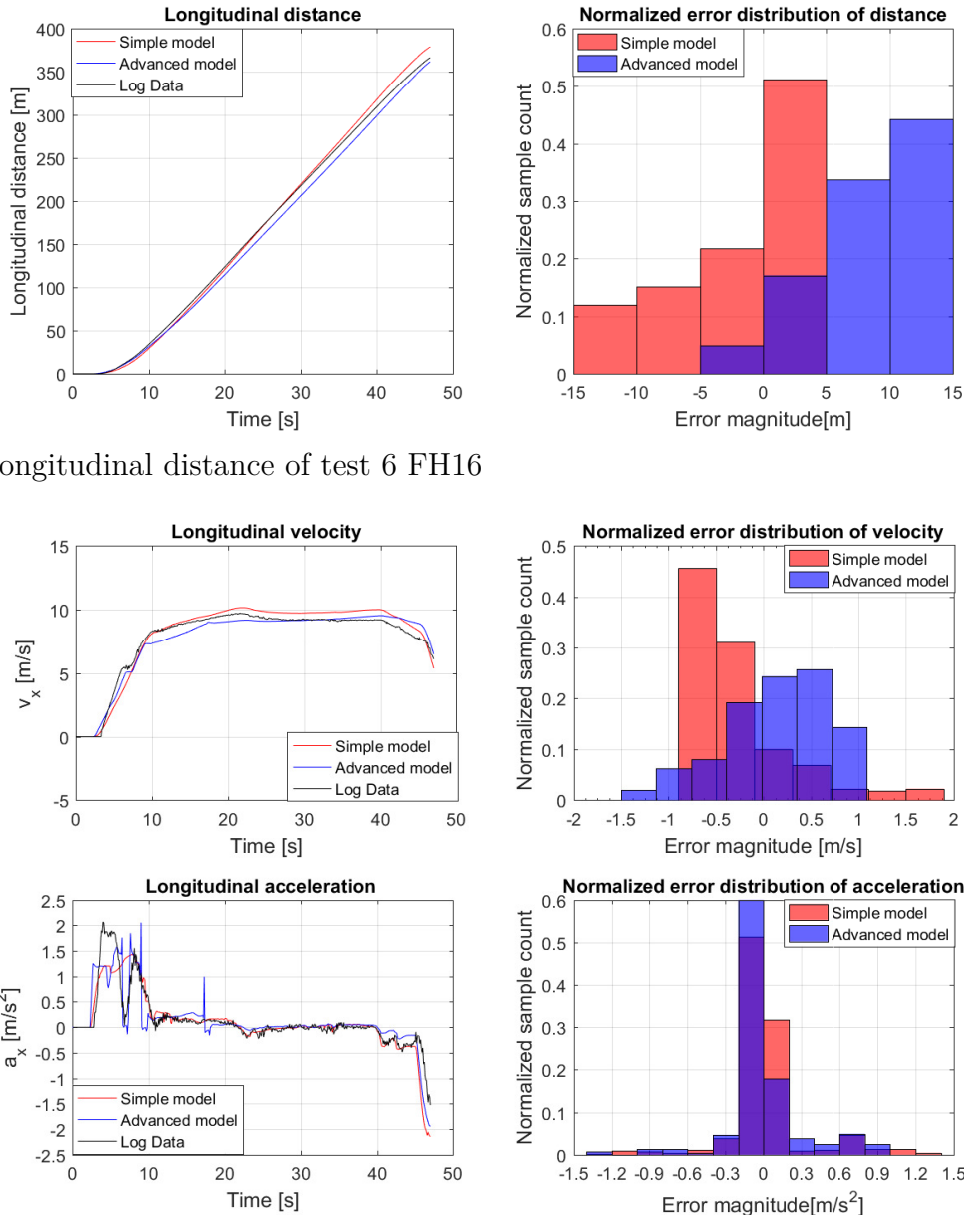


Figure 4.12: Input for Test 6 FH16



(b) Longitudinal velocity and acceleration for test 6

Figure 4.13: Longitudinal results of test 6 FH16

4. Results and Discussion

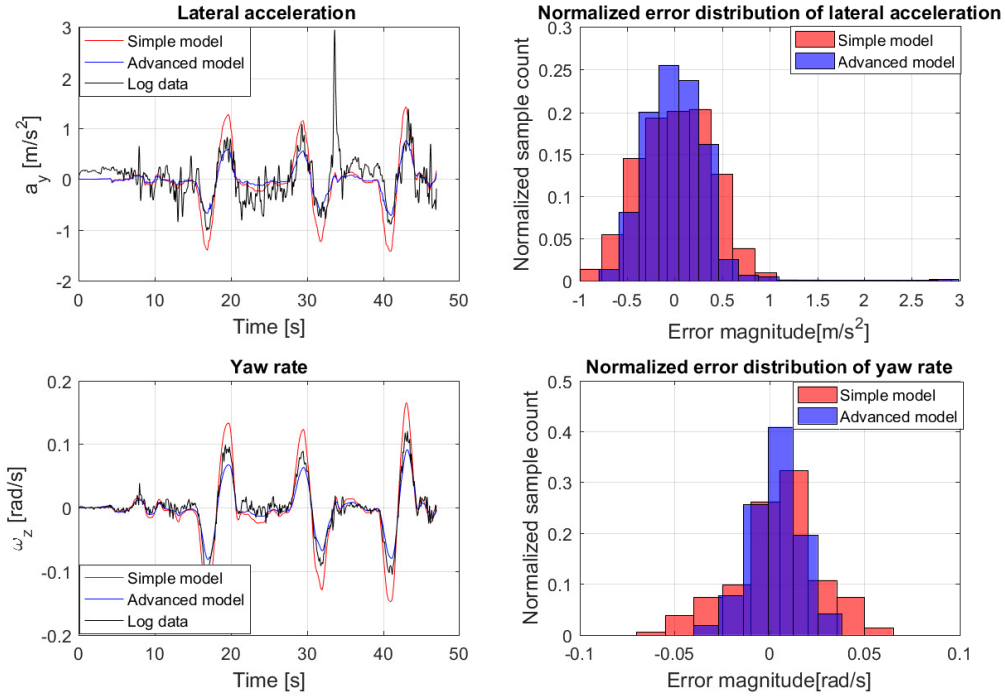


Figure 4.14: Lateral results of test 6 FH16

4.1.3 Discussion FH16

In this section, more discussion on the longitudinal and lateral tests is done. Figure 4.2 illustrates the results of test 1, where the error in the velocity plot for the advanced model is significantly large. This difference arises due to the clutch start-up logic, when the clutch discs engage the engine speed drops as seen in figure 4.15a because the torque from the transmission side is larger than the engine side torque and if the engine speed further drops it can lead to engine stall or engine-kill. Based on the difference between the current engine speed and the reference engine a proportional torque is fed which is seen in figure 4.15c and clearly this not as in reality. In this work the rate of disengagement and engagement of the clutch is fixed and an engine speed based controller feeds the deficit torque to prevent engine stall. It should be noted that the logic is better suited for test 2 with a step accelerator pedal input than for test 1. This logic is chosen because step accelerator pedal input is a more realistic input as seen from the recorded manual tests in figure 4.8 and 4.10. Test 1 is chosen to highlight the possible limitation of clutch actuation logic, in reality the clutch actuation logic is complicated and beyond the scope of this work. In this work based on the collected log data, the clutch actuation rate is kept constant and a engine speed based controller is added to prevent engine stall and surge.

To highlight the difference between the two models, the two driving cycle tests are compared. For the first driving cycle both models closely follow the experimental data as seen in section 4.1.1.4. While, in the second driving cycle as in section 4.1.1.5 the error in the longitudinal variables for the simple model is significantly large. The main reason is due to the absence of the clutch model in the simple vehicle model. As seen in figure

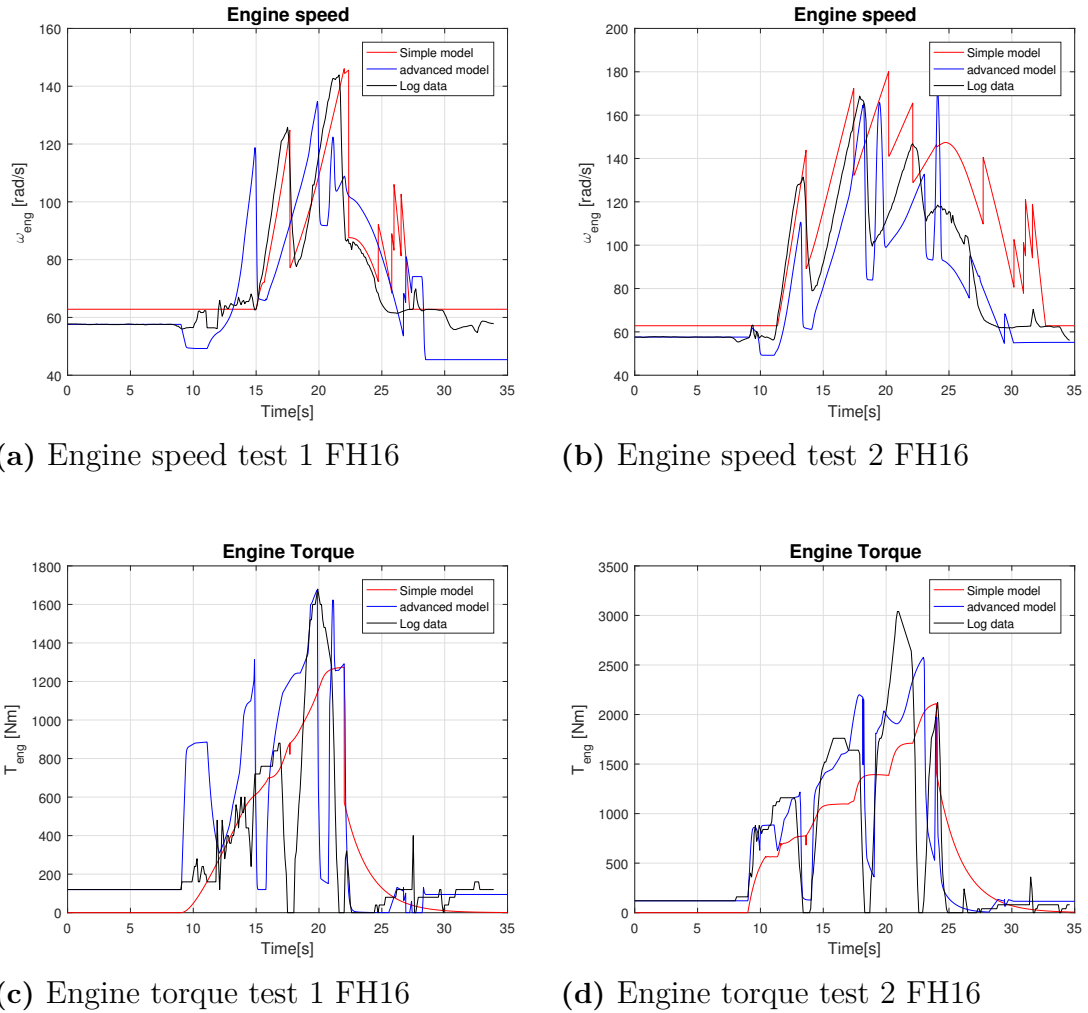
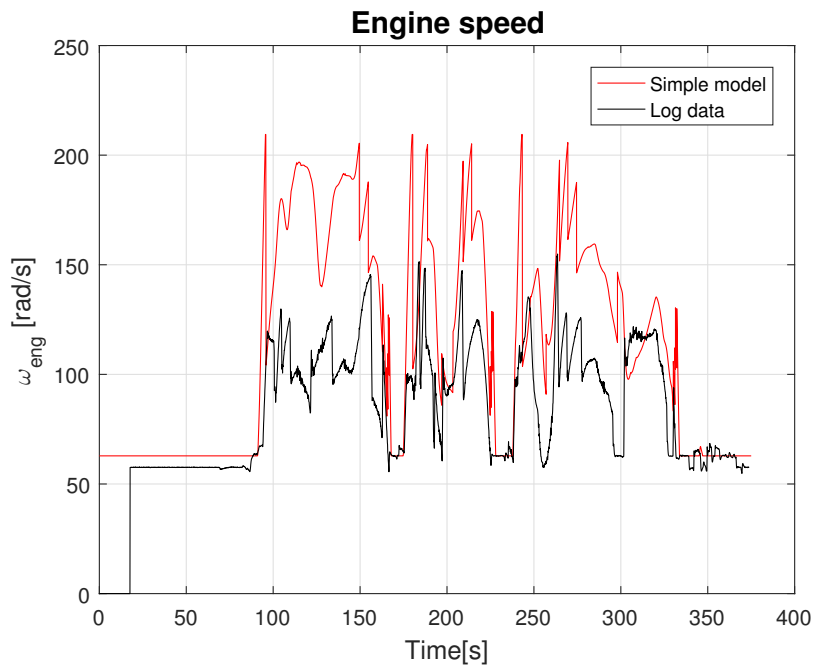


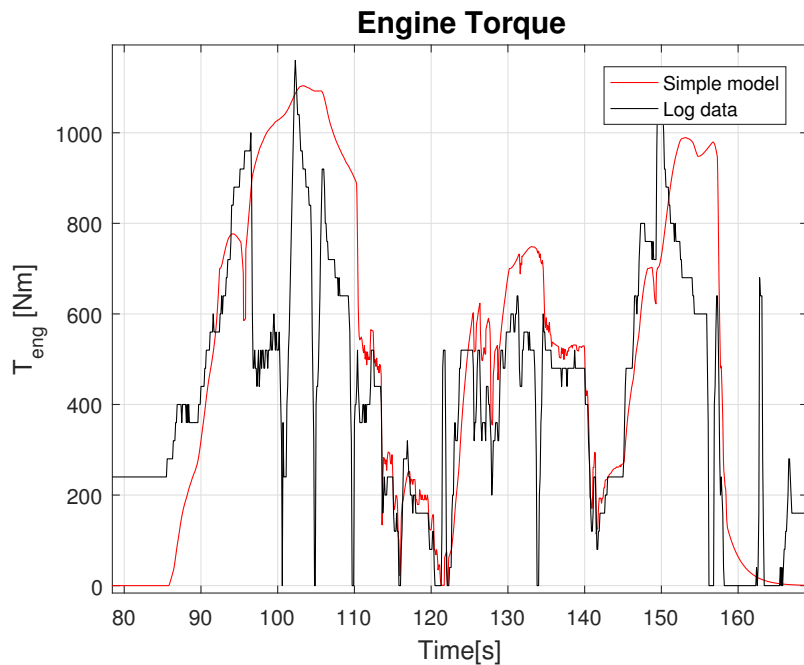
Figure 4.15: Comparison of Engine speed and torque for test 1 and 2 FH16

4.16a the engine speed rises instantaneously with the accelerator pedal input as a result of which the engine torque delivered is also higher and the power disruptions during gear change are also absent in figure 4.16b. This error is seen throughout the simulation and builds up due to which the total distance covered by the simple model is 1200 m more than the experimental data in contrast to 300 m by the advanced model. In figure 4.8b and 4.10b for the advanced model the spikes in the acceleration are due to gearshifts as there is an instantaneous change in the angular velocity. Unlike in reality the elasticity and damping in the powertrain elements are not considered but to add such features to the model more data is necessary.

4. Results and Discussion



(a) Engine speed test 5



(b) Engine torque of a small section of test 5

Figure 4.16: Engine speed and torque for test 5 Fh16

Due to limitations at the testing facility only a few lateral tests were conducted, out of which the manual lane change test gave good lateral behaviour with respect to the test vehicle. In the figure 4.14 at 35 seconds there is a spike in the log data for lateral acceleration, which persisted after filtering. It can be said that the spike is due to sensor noise. The modelling differences between the simple and the advanced model that can influence the lateral behaviour are the tire model, out of plane degrees of freedom, load transfer and suspension model. The error in the lateral acceleration and yaw rate of the advanced model is insignificant compared to the simple model. This is because the simple model does not capture out of plane DOF and load transfer, and it has an isotropic tire model. Figure 4.11 also illustrates the lateral behaviour, where again the error for the advanced model is significantly lower than the simple model. For this particular test case the longitudinal velocity of the simple model is 5-6 m/s higher than the log data as seen in figure 4.10b, due to this and the aforementioned reasons the lateral acceleration and yaw rate error is comparatively large.

As an additional point to validate the models the energy consumption is calculated. Integrating the power generated over time gives the energy consumed. Power is given as the product of engine speed and engine torque. Since these variables were logged from the vehicle CAN bus for the tractor, the approximate energy consumption is calculated for the experimental data and simulation models and is presented in the table 4.1. Similar trend is observed with energy consumption as it was with velocity. The test results for which the error in velocity plots is low, the simulated energy consumption is also close to the actual energy consumption. The error in velocity and distance covered as seen in figure 4.10b is significantly large this is also reflected in the energy consumed as well, showing a large difference for test 5 FH16.

Table 4.1: Energy consumed

Test case	Energy Consumed [J]		
	Log data	Simple model	Advanced model
Test 1	8.712e5	10.07e5	1.084e6
Test 2	2.419e6	2.32e6	2.457e6
Test 3	2.107e6	1.878e6	2.827e6
Test 4	1.6061e7	2.131e7	1.624e7
Test 5	1.11e7	1.752e7	9.64e6
Test 6	1.53e6	2.161e6	1.30e6

4.2 Results XC90

To control the vehicle in automated driving mode the cruise control interface is used. The vehicle is driven to a velocity of 7 km/h (3 m/s) by the driver after which the vehicle can be controlled with the control interface. This can be seen in the test results, until $t < 17\text{s}$ the vehicle is controlled by the driver and beyond 17 s the vehicle is under the control of the open-loop tests.

4. Results and Discussion

The actuation input signals were discussed in section 3.3.2 and they are stated again below:

- Steering wheel angle request [rad]
- Acceleration request [m/s^2]
- Brake deceleration request [m/s^2]

4.2.1 Longitudinal test

Test 1 XC90: Ramp acceleration test to 8–10 m/s

In this test, acceleration input is gradually increased as a ramp to attain a velocity of 8–10 m/s or 30–40 Km/h followed by a deceleration input as shown in figure 4.17. This test is defined to evaluate the longitudinal behaviour of the models with a gradually increasing acceleration input.

Figure 4.18a indicates the distance covered by the models and it can be seen that both the models are within 15 m of the log data. In figure 4.18b illustrates that the simple model velocity marginally exceeds the log data. In the normalized error distribution (red bar) 60% of the sample counts are within an error magnitude of -0.2 to -0.6 m/s. For the advanced model 60% of sample counts are within an error magnitude of ± 0.4 m/s. The total range of the error magnitude is only ± 1.5 m/s which indicates relatively low velocity error for both models. The log data vehicle velocity does not reach zero because the vehicle was on a downhill and the deceleration input was not sufficient.

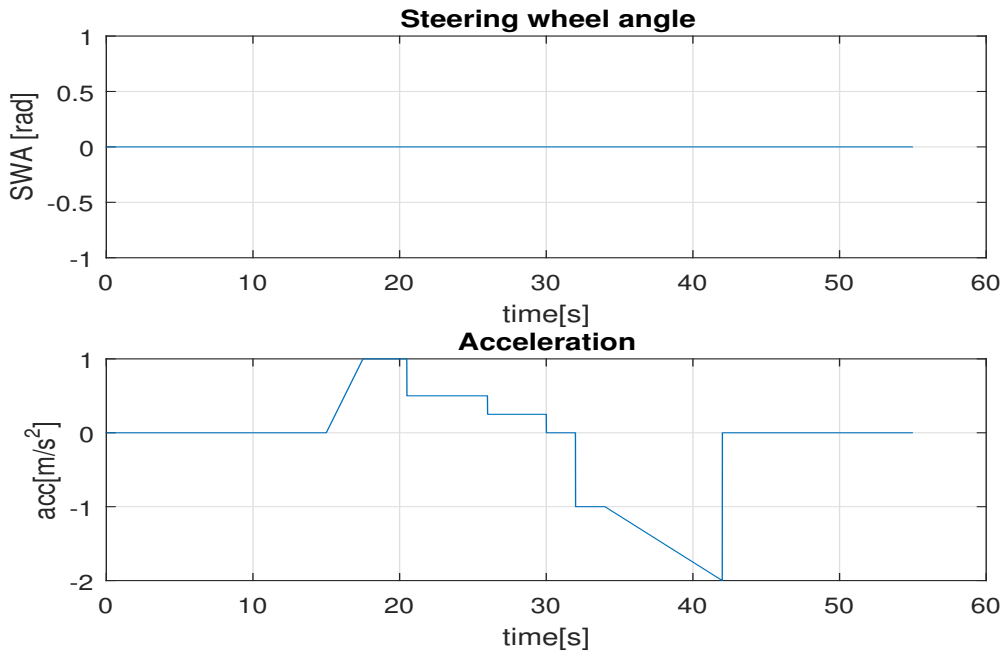
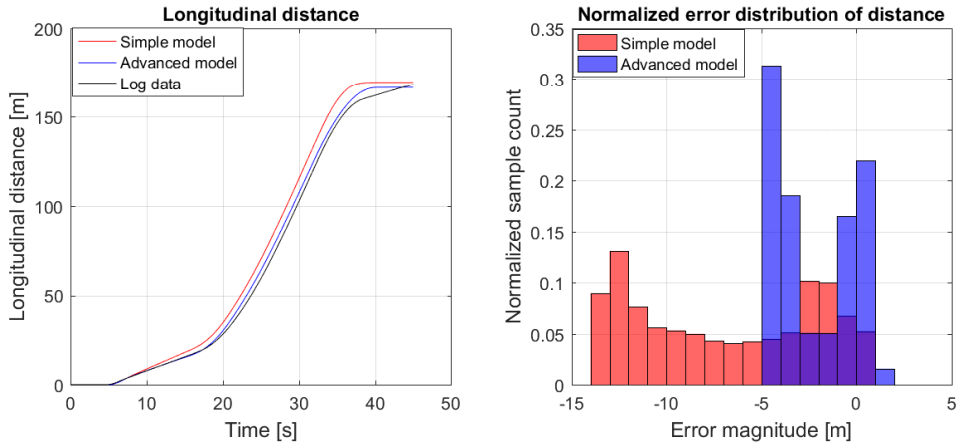
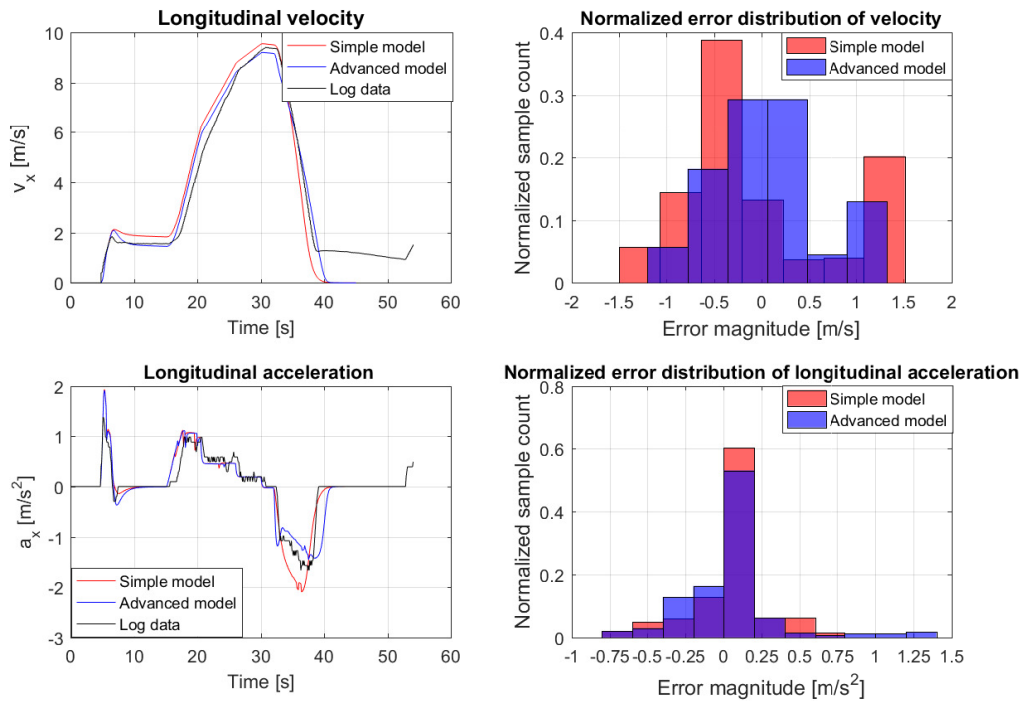


Figure 4.17: Input for Test 1 XC90



(a) Longitudinal distance of test 1 XC90



(b) Longitudinal velocity and acceleration for test 1

Figure 4.18: Longitudinal results of test 1 XC90

4.2.2 Lateral test

Test 2 XC90: Step acceleration and sine steer

In this the lateral behaviour of the model is evaluated with a step acceleration and braking input as shown in figure 4.19. The steering input is a sine wave of magnitude 1 rad and frequency 0.3 Hz.

The total distance covered by both the models exceeds the log data by 15 m which is seen in figure 4.20a. The trend in the velocity plot is same as in the previous test for the simple model, as 55% of the sample counts are within an error magnitude of -0.75 to -0.25 m/s. For the advance model in the normalized error distribution of velocity 70% of sample counts are within an error magnitude of 0 to -0.5 m/s indicating an insignificant error. For both models the longitudinal behaviour is good with a total error magnitude range of ± 1.25 m/s. In case of the acceleration plots for both models the sample counts are concentrated about zero, with 60 % of sample counts within an error magnitude of ± 0.25 m/s².

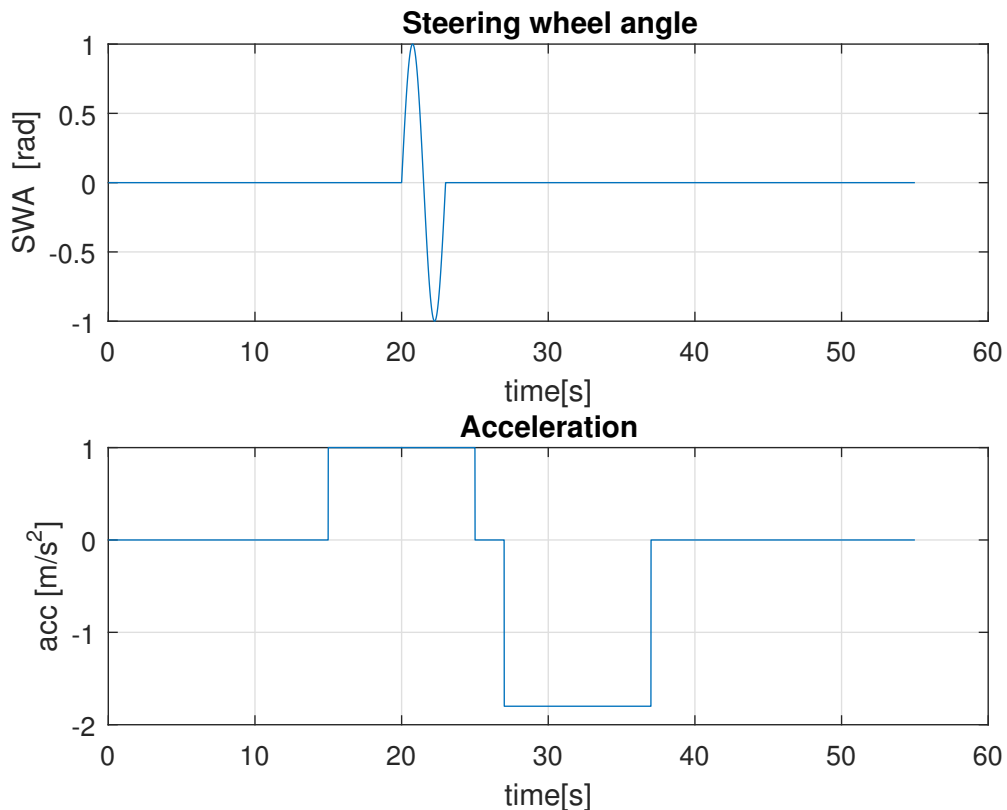


Figure 4.19: Input for Test 2 XC90

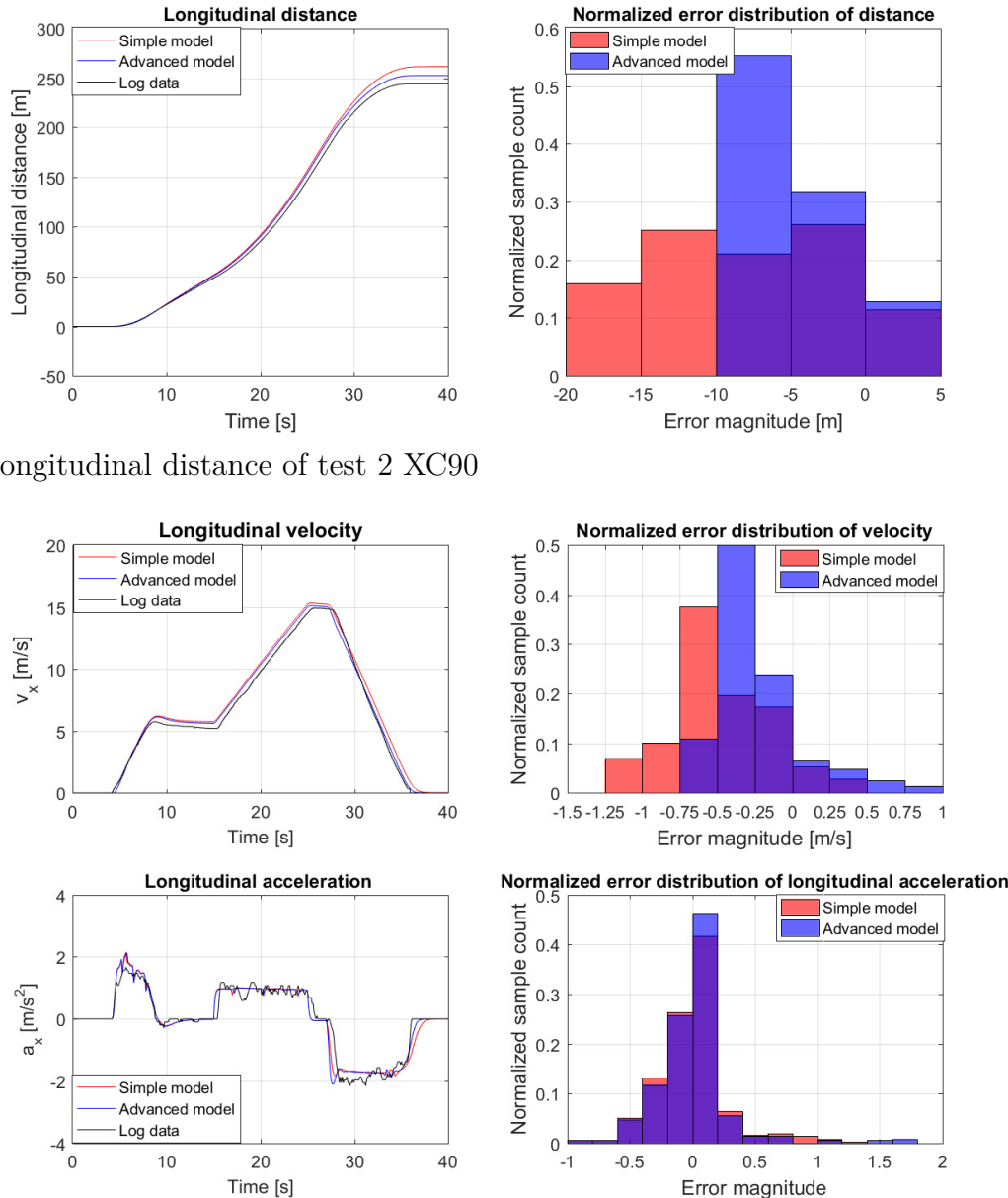


Figure 4.20: Longitudinal results of test 2 XC90

4. Results and Discussion

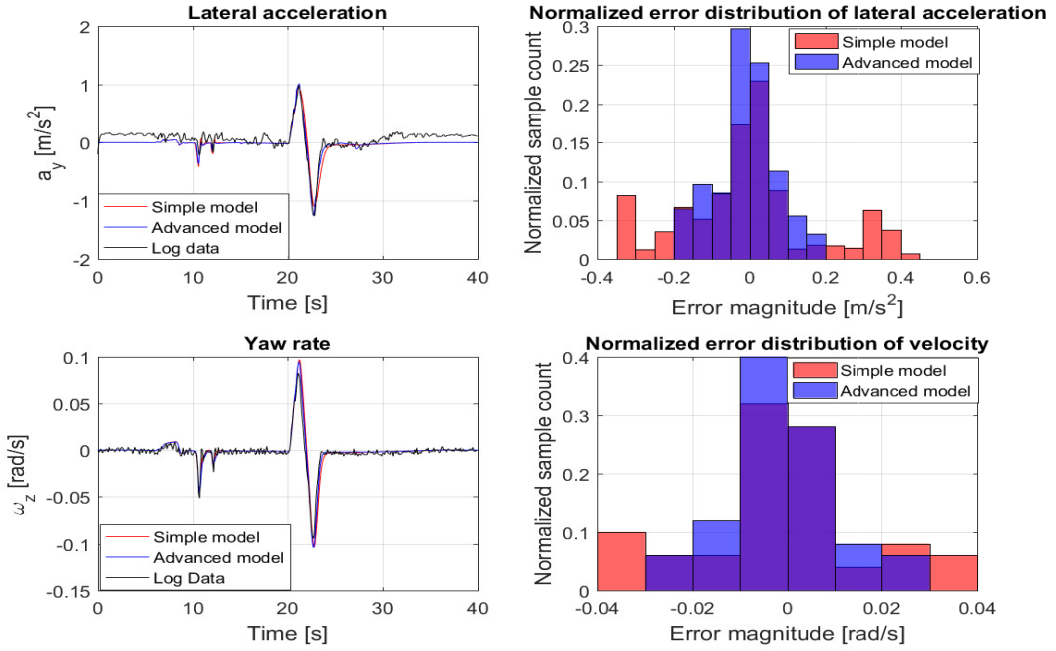


Figure 4.21: Lateral results of test 2 XC90

The results of the sine steering input are shown in the figure 4.21. For the simple and advanced model the lateral acceleration is error insignificant, as 50% of the sample are within an error magnitude of $\pm 0.1 \text{ m/s}^2$. In the case of Yaw rate as well, the error is low for both the models with 65% of it within an error magnitude of $\pm 0.01 \text{ rad/s}$.

4.2.3 Discussion XC90

The longitudinal behaviour of the model is validated based on the test results in figure 4.18 and 4.20. In test 1, as shown in figure 4.18b both models velocity accuracy is high with a total error range of $\pm 1.5 \text{ m/s}$ and for the advanced model 50% of the error sample counts are in the range of $\pm 0.4 \text{ m/s}$.

The lateral test is a mild test, with sine steering input. The velocity of the vehicle is below 60km/h during the lateral test and at such low velocities the tire model remains in the linear range of operation, and the effects of out plane DOF and load transfer are insignificant. The model variables lateral acceleration and yaw rate follow the experimental data with a minimal error of $\pm 0.1 \text{ m/s}^2$. At such low speeds and mild steering maneuver, the additional modelling features such as the out of plane DOF and suspension cannot be validated. These extra DOF were added such that models can be used for future research. To validate the additional DOF more experimental data is needed.

4.3 Computational efficiency

The simple model is targeted to be used within controllers for online predictions. To check the computational performance of the model, one of the open-loop test scenario is simulated multiple times using a *for* loop. The scenario chosen has a simulation time of 35s. The simulations are conducted with MATLAB and Simulink using a fixed step of 0.01s and RK4 as solver. The simulation is run in loops for 5, 10, 20 and 30 times the simulation time and these iterations have been repeated 10 times to check its consistency. To conduct the simulation a standard computer with i-7 processor clocking 2.5GHz and 8 GB RAM has been used. The run time is determined using the *tic-toc* function on MATLAB. The run-time and simulated time are reported in the table 4.2, which indicates that the model is faster than real time (wall-clock time).

Table 4.2: Simple model run-times

Simulated time [s]	Run-time [s]
35	0.44
175	2.21
350	4.40
700	8.67
1050	13.02

For the advanced model to evaluate simulation performance, the real-time Simulink toolbox has been used. The simulation is conducted on the same computer using the same test scenario lasting for 35s. A fixed step size of 0.01s and RK4 solver is used to conduct the simulation. The simulations conducted were approximately close to real-time as using the function *tic-toc* and *sim* commands, the time including the initialization time was 35.8s averaged over 10 iterations. The 0.8s can be assumed to be set for initialization. The method adopted is not entirely accurate for better results the models should be simulated in hard Real-time.

4.4 Use-case: GPS-based autonomous navigation

In this use-case, GPS-based autonomous navigation on the runway of the Umeåairport. The actual controller was implemented in the C++ software framework OpenDLV, which includes a generic UDP-based interface that can be used with the model in Simulink. Here are some functions of OpenDLV:

- Sending and receiving vehicle sensor data and actuation requests
- Hosts control algorithm for the AI needed for automated driving
- Vehicle to Vehicle communication
- Processing sensor data (Example: Using camera feed for Lane detection)

This use-case is demonstrated with the advanced XC90 vehicle model. The controller predicts a path for the vehicle to follow based on predefined latitude–longitude and determines the inputs to the model based on the current GPS position and vehicle speed. The inputs to the model are acceleration request and steering wheel angle request. The lateral

4. Results and Discussion

control is based on the current angle to the next waypoint with a speed-dependent gain, and the longitudinal control is implemented as a simple PI controller.

The same controller is used with the real vehicle as well, only adaptation blocks are necessary for simulation. First adaptation is to setup communication for which UDP send and receive blocks in Simulink library are used along with functions to pack and unpack the data. The next adaptation is to transform xy to GPS coordinates using WGS84 standards.

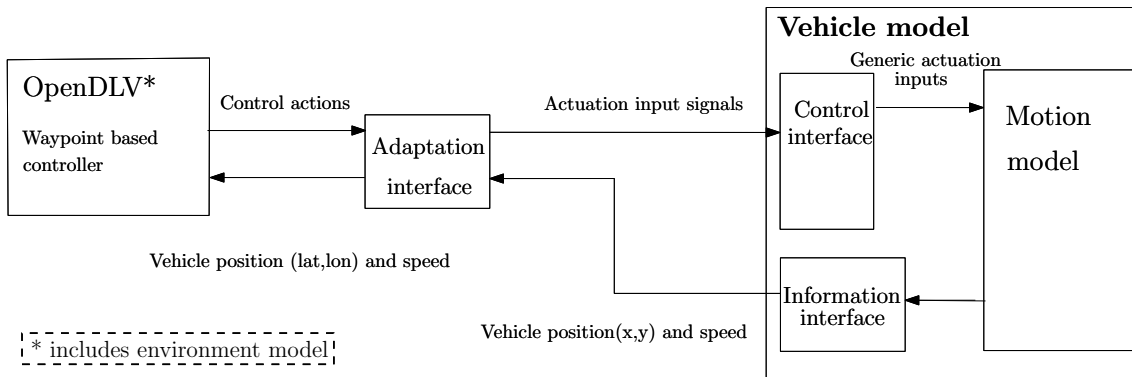


Figure 4.22: Model architecture followed with GPS based autonomous navigation

The trajectory of the real vehicle log and the simulation is shown in figure 4.23. Start point is indicated by a circle marker 'o' and finish is marked by a star '*'. The black dashed line indicates the trajectory of the test vehicle and the blue solid line is of the advanced XC90 model. It is observed that there is negligible difference between the two trajectories. Figure 4.24 is the velocity comparison plot, the simulation time prior to 106s is for initialization and is unimportant hence plots begin from 106s and end at 500s. The test vehicle and the model are at a low initial velocity at the start their location, which on the trajectory plot in figure 4.23 would be just before the curve (heading downwards) joining the straight.

Figure 4.24 shows the longitudinal velocity comparison between the log data and simulation. At 220 s, 350 sec there is an offset because the model has a more responsive steering due to which the vehicle model negotiates the curve faster than the test vehicle. This is also seen in the figures 4.25 and 4.26, which show the comparison of the controller inputs to the real vehicle and the model. In the figure 4.27 green line is the recorded vehicle steering angle, black line is of the actuation input from the controller and the blue line is for the model steering wheel angle. It is observed that the reduced rate and magnitude of the steering wheel angle results in sluggish behaviour of the test vehicle. This behaviour is not captured as the Revere lab is working towards removing this limitation and making the system more responsive. Though the magnitude of acceleration input is same for both the cases there exists a difference in velocity, and the possible reason can be that the vehicle and model were operating at different gears but no experimental data is available to validate this reason.

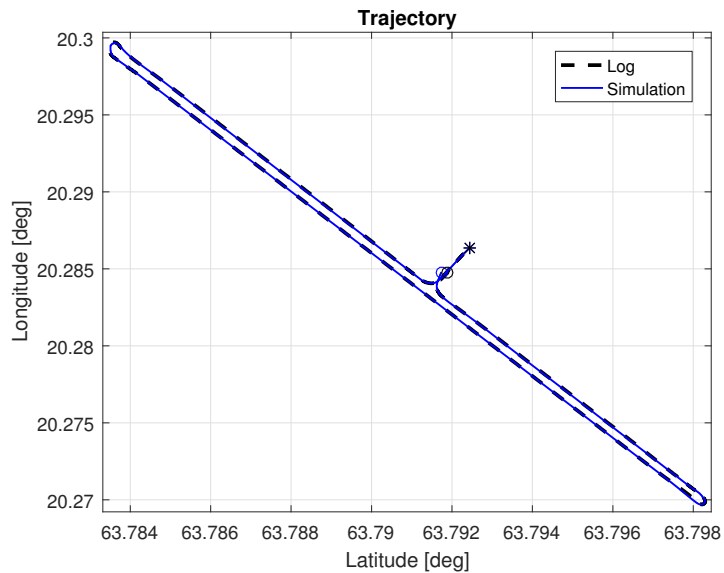


Figure 4.23: Trajectory in lat–lon for GPS-based autonomous navigation

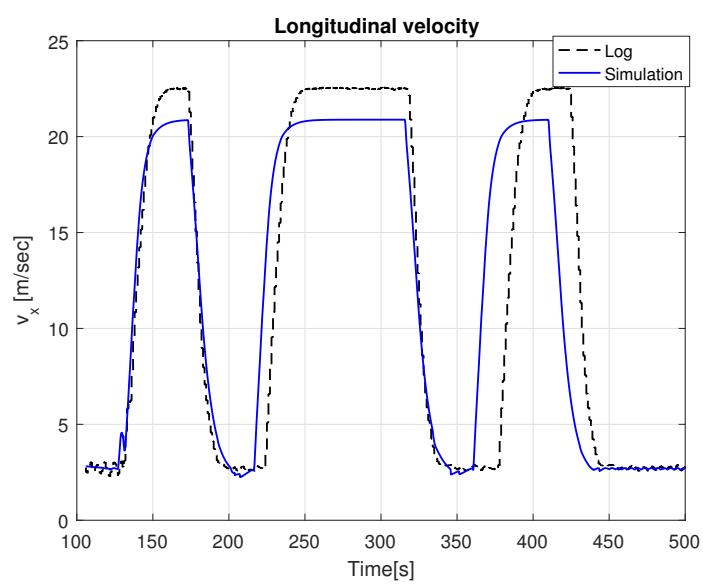


Figure 4.24: Longitudinal velocity in m/s for GPS-based autonomous navigation

4. Results and Discussion

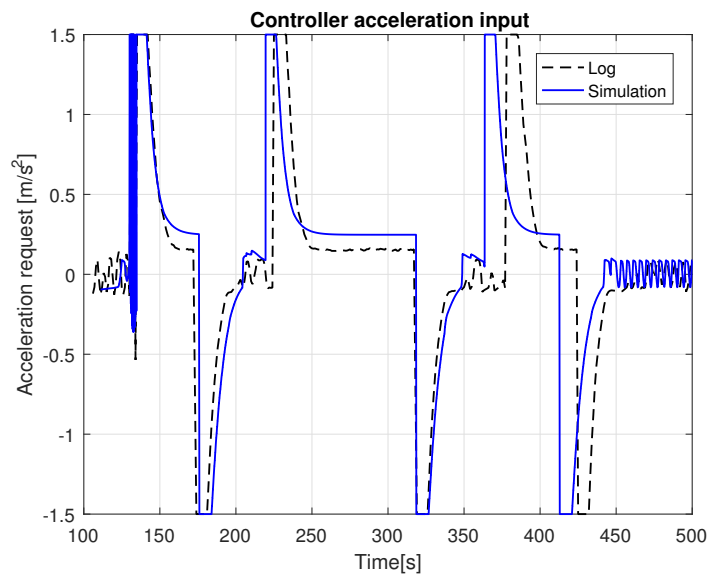


Figure 4.25: Controller acceleration input

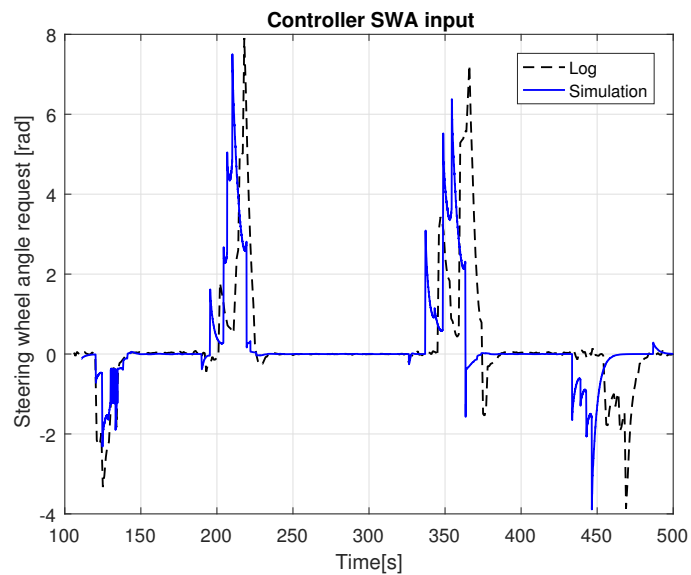


Figure 4.26: Controller steering input

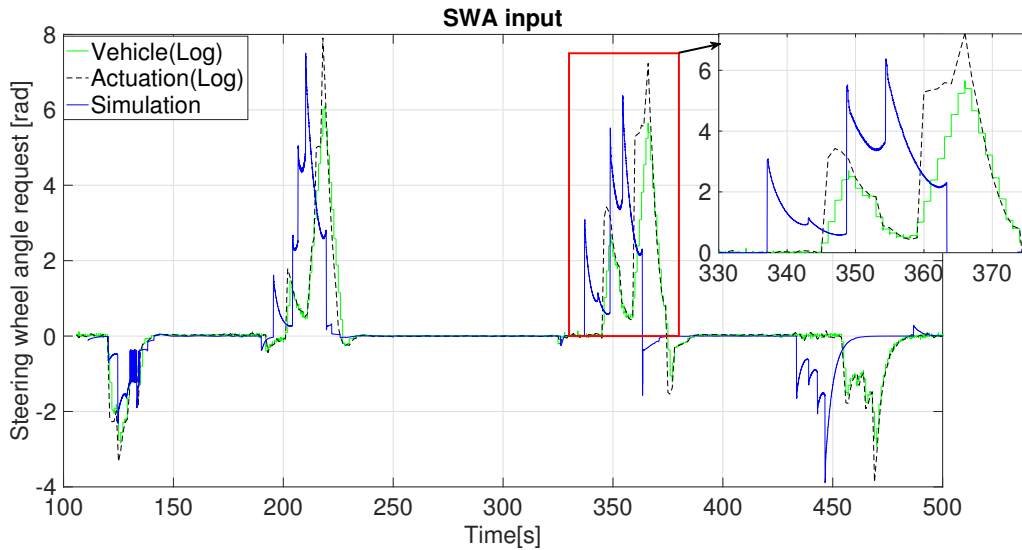


Figure 4.27: Comparison of vehicle steering input with model and actuation input

4.5 Summary

Each of the vehicle models developed are validated and compared in this chapter. Several open loop and manual tests are conducted with the test vehicles. For comparison and validation graphical method has been used. The error between the experimental and the simulated data is calculated and represented as a histogram which gives the error range and distribution.

Different open-loop longitudinal test scenarios are set-up to highlight the differences between the test vehicles and the models. From the graphical comparison and error distribution plots it is seen that for most tests the velocity of the models is within ± 1 m/s of the logged velocity. The plots also highlighted the modelling differences between the two models. Adding the clutch model to the powertrain improved the longitudinal behaviour of the advanced model in comparison to the simple model. The engine speed and torque gave a good representation of the real vehicle by capturing the gear shifts and the start-up behaviour. The differences in modelling between the models is evident in driving cycle 2 in section 4.1.1.5. Additionally, both the XC90 models exhibited a good longitudinal behaviour with minimal error. In case of the lateral behaviour, the conducted tests indicated that the error is rather insignificant. As the lateral acceleration is within ± 0.2 m/s² to ± 0.5 m/s² and the yaw rate is within ± 0.01 rad/s for all the developed models. It should be noted that additional experimental data is needed to validate the lateral behaviour of the models for transient maneuvers. Additionally, from the powertrain model developed the energy consumed can be calculated as seen in table 4.1 but the same is not shown with the XC90 because of the required data is not available.

In the use-case section of this chapter with the XC90 advanced model is tested with a GPS based autonomous navigation controller. The results of the simulation models are validated against collected experimental data. Based on the proposed architecture a

4. Results and Discussion

simulation is setup between the controller on Linux platform and the model on Simulink as shown in figure 4.22. The figure 4.23 shows that the error in the trajectories is insignificant. The offset in the velocity plot in figure 4.24 and the actuation inputs in figure 4.25 and 4.26 is due to the rate limitation in the steering software system that results in a sluggish behaviour. This is not captured by the model because the steering software on the test vehicle is a prototype and is being updated to overcome the limitation.

5

Conclusion and Recommendation

5.1 Conclusion

To reach the targeted deliverable and answer the research question an iterative approach (real testing and modelling) was used in this thesis. The deliverables set were:

- Develop open-source models of test vehicles:
 - Volvo FH16
 - Volvo XC90
- For each test vehicle
 - Control interface model
 - Set 1 simple model
 - Set 2 advanced model
- Model validation through track testing.

The research questions were

- What level of model detail is suitable for autonomous driving for:
 - Non-critical highway driving (*)
 - Non-critical city driving
- What is a suitable model architecture for simulation of automated driving function?

For vehicle model development Modelica was used which is an open-source tool. Its object oriented nature resulted in modular vehicle model that can be easily extended for further development. All the equations of motion for different components on the vehicle can be easily understood because of the acausal modelling nature and text based approach of Modelica. The control interface model, quick simulation simple model and advanced models were developed from scratch. In case of the simple model it was based on a single track model with three DOF. The advanced model was a more detailed model. It was based on a two track model with 14 DOF and an isotropic brush tire model. A detailed powertrain model was included in the vehicle model, for the FH16 tractor model a clutch model and non-sequential gear shifting logic were implemented and in case of the XC90 model a simplified torque converter model was implemented. A suspension model based on spring-mass-damper, a second order steering model and a simplified brakes model were also considered in the advanced vehicle model. Additionally, a cabin with three DOF was modelled for the FH16 tractor model.

5. Conclusion and Recommendation

Different open loop and manual driving tests were specified to validate and compare the vehicle models. The results showed that all models are capable of starting standstill and give a good representation of the longitudinal behaviour for different test maneuvers. Both the vehicle models showed good accuracy in terms of velocity for both the open-loop tests and the manual driving cycle tests. From these validation results it can be highlighted that while modelling an automated manual transmission, adding a clutch model and a gear shifting logic improved the longitudinal performance of the model. This is because capturing the clutch behaviour during the start-up process and during gearshift resulted in a more realistic representation of the engine torque and the speed in comparison to the simple model.

A limited number of lateral tests were conducted with both the test vehicles. Firstly, in the FH16 advanced model at low longitudinal velocity both the models gave good representation of the test vehicle behaviour. However, in case of the simple model for one of the driving cycle tests it was observed that the lateral acceleration and yaw rate were significantly larger than the log data because of the higher longitudinal velocity. While for the XC90 model error in the lateral variables was rather insignificant. The differences between the simple and advanced model were minimal this is because the longitudinal velocity was low, and the vehicle was operating in the linear regions of tire model. Furthermore, the influence of load transfer and out of plane DOF on the lateral behaviour at a such low velocity is minimal or unnoticeable. To highlight such differences in the models, transient maneuvers like double lane change must be conducted at relatively higher velocities [5].

Following the validation of the models, the computational efficiency of the models was studied. The results showed that the simple model is faster than real-time. Simulation with the real-time toolbox on Simulink showed that the advanced model follows real-time. This method is more suitable for soft real-time validation but for complete real-time evaluation it should be done in hard real-time.

The demonstration with the GPS based autonomous navigation highlighted the use of the simulation architecture specially its sub-function like the adaptation interface which allowed the interaction between the model and the controller that were operating on different platforms. Additionally, the simulation results were compared with experimental data, it showed that the trajectories followed by the model and test vehicle were very well matched. The test vehicle steering control interface compared to the model exhibited a sluggish behaviour. This is not captured because this behaviour is a limitation and is under development to improve its response. In conclusion, validation of the models with several test maneuvers implied there is minimal difference in the behaviour of the models and the test vehicles. However further improvement can be added to the models. Simulation of the advanced model with the controller demonstrated that the model is suitable to be used as a tool for development and testing of controllers.

5.2 Recommendations

Though the vehicle models developed in this thesis are good representation of the real vehicles, there are some areas that can be further developed. A general advice would be to develop vehicle models that are driven by needs from different research/product development. Here are some recommendation to further improve the models:

- Adding models of semi-trailer, dolly (even propelled dolly) to the solo tractor for full combination models.
- A low-speed brush tire model to capture parking maneuvers.
- FMU export to C-code to extend usability with different tools
- Translation of model components developed in MATLAB/Simulink into *Modelica* to make it completely open-source.
- More track data to validate out of plane DOF of the models.

5. Conclusion and Recommendation

Bibliography

- [1] Dassault Systèmes AB, “Dymola. dynamic modeling laboratory. fmi support in dymola”, vol. 2, no. September, pp. 1–40, 2014.
- [2] D. Fischer and R. Isermann, “Mechatronic semi-active and active vehicle suspensions”, *Control Engineering Practice*, vol. 12, no. 11, pp. 1353–1367, 2004.
- [3] C. Ghike and T. Shim, “14 degree-of-freedom vehicle model for roll dynamics study”, SAE Technical Paper, Tech. Rep., 2006.
- [4] G. Venture, P.-J. Ripert, W. Khalil, M. Gautier, and P. Bodson, “Modeling and identification of passenger car dynamics using robotics formalism”, *IEEE Transactions on Intelligent Transportation Systems*, vol. 7, no. 3, pp. 349–359, 2006.
- [5] B. Jacobson, *Vehicle Dynamics Compendium*. 2016, pp. 223–245.
- [6] R. Jazar, *Vehicle dynamics: theory and application*. 2008, p. 1015.
- [7] J. Kong, M. Pfeiffer, G. Schildbach, and F. Borrelli, “Kinematic and dynamic vehicle models for autonomous driving control design”, pp. 1094–1099, 2015.
- [8] K. Kritayakirana and J. C. Gerdes, “Autonomous vehicle control at the limits of handling”, *International Journal of Vehicle Autonomous Systems*, vol. 10, no. 4, pp. 271–296, 2012.
- [9] S. Kharrazi, “Steering based lateral performance control of long heavy vehicle combinations”, PhD thesis, 2012.
- [10] P. Nilsson and K. Tagesson, “Single-track models of an a-double heavy vehicle combination”, Chalmers University of Technology, Tech. Rep., 2014.
- [11] J. D. Demerly and K. Youcef-Toumi, “Non-linear analysis of vehicle dynamics (navdyn): A reduced order model for vehicle handling analysis”, SAE Technical Paper, Tech. Rep., 2000.
- [12] B. Shyrokau, D. Wang, D. Savitski, and V. Ivanov, “Vehicle dynamics control with energy recuperation based on control allocation for independent wheel motors and brake system”, *International Journal of Powertrains*, vol. 2, no. 2-3, pp. 153–181, 2013.
- [13] J. G. Fernández, “A vehicle dynamics model for driving simulators(master thesis)”, p. 115, 2012.
- [14] H. Pacejka, *Tire and vehicle dynamics*. Elsevier, 2005.
- [15] J. Svendenius, “Tire modeling and friction estimation”, *PhD Theses*, 2007.
- [16] B. Jacobson, *Gear shifting with retained power transfer*. Chalmers University of Technology, 1993.
- [17] S. Berglund, *Modeling complex engines as dynamic powertrain members*. Chalmers University of Technology, 1999.

- [18] H. Naunheimer, B. Bertsche, J. Ryborz, and W. Novak, *Automotive Transmissions-Fundamentals, Selection, Design and Application*. 2013, vol. 53, pp. 1689–1699.
- [19] E. Obialero, “A refined vehicle dynamic model for driving simulators”, 2013.
- [20] J. He, D. A. Crolla, M. Levesley, and W. Manning, “Coordination of active steering, driveline, and braking for integrated vehicle dynamics control”, *Proceedings of the Institution of Mechanical Engineers, Part D: Journal of Automobile Engineering*, vol. 220, no. 10, pp. 1401–1420, 2006.
- [21] M. Zanon, J. V. Frasch, M. Vukov, S. Sager, and M. Diehl, “Model predictive control of autonomous vehicles”, in *Optimization and Optimal Control in Automotive Systems*, Springer, 2014, pp. 41–57.
- [22] F. Bruzelius, J. Gomez Fernandez, and B. Augusto, “A basic vehicle dynamics model for driving simulators”, *International Journal of Vehicle Systems Modelling and Testing*, vol. 8, no. 4, pp. 364–385, 2013.
- [23] B. Shyrokau, J. Loof, O. Stroosma, M. Wang, and R. Happee, “Effect of steering model fidelity on subjective evaluation of truck steering feel”, in *Proceedings of the 14th Driving Simulation Conference and Exhibition, DSC 2015 Europe, Tubingen (Germany) 16-18 Sept. 2015*, Max Planck Institute for Biological Cybernetics, 2015.
- [24] D. K. Fisher, “Brake system component dynamic performance measurement and analysis”, SAE Technical Paper, Tech. Rep., 1970.
- [25] B. Shyrokau, D. Wang, K. Augsburg, and V. Ivanov, “Vehicle dynamics with brake hysteresis”, *Proceedings of the Institution of Mechanical Engineers, Part D: Journal of automobile engineering*, vol. 227, no. 2, pp. 139–150, 2013.
- [26] S. Türkay and H. Akçay, “Multi-objective control design for a truck cabin”, *IFAC Proceedings Volumes (IFAC-PapersOnline)*, vol. 19, no. 1988, pp. 8793–8798, 2014.
- [27] K. Abdelgawad, M. Abdelkarim, B. Hassan, M. Grafe, and I. Gräßler, “A modular architecture of a pc-based driving simulator for advanced driver assistance systems development”, in *Research and Education in Mechatronics (REM), 2014 15th International Workshop on*, IEEE, 2014, pp. 1–8.
- [28] J. E. Stellet, M. R. Zofka, J. Schumacher, T. Schamm, F. Niewels, and J. M. Zollner, “Testing of advanced driver assistance towards automated driving: a survey and taxonomy on existing approaches and open questions”, *IEEE Conference on Intelligent Transportation Systems, Proceedings, ITSC*, vol. 2015-Octob, pp. 1455–1462, 2015.
- [29] M. R. Zofka, J. M. Zöllner, M. Ren, S. Klemm, F. Kuhnt, T. Schamm, and J. Z. Marius, “Testing and validating high level components for automated driving : simulation framework for traffic scenarios testing and validating high level components for automated driving : simulation framework for traffic scenarios”, 2016.
- [30] J. Ziegler, P. Bender, M. Schreiber, *et al.*, “Making bertha drive-an autonomous journey on a historic route”, *IEEE Intelligent Transportation Systems Magazine*, vol. 6, no. 2, pp. 8–20, 2014.
- [31] M. Montemerlo, J. Becker, S. Bhat, *et al.*, “Junior: The stanford entry in the urban challenge”, *Journal of field Robotics*, vol. 25, no. 9, pp. 569–597, 2008.

- [32] K. Yi, S. Lee, and Y. D. Kwon, “An investigation of intelligent cruise control laws for passenger vehicles”, *Proceedings of the Institution of Mechanical Engineers*, vol. 215, no. 2, p. 159, 2001.
- [33] S. Sedran, “A truck dynamics model for driving simulators”, 2016.
- [34] K. Tagesson, “Truck steering system and driver interaction”, 2014.
- [35] R. Festila and V. Tulbure, “Numerical simulation of a diesel engine in railway traction using partial differential equations”, *Automation Quality and Testing Robotics (AQTR), 2010 IEEE International Conference on*, vol. 1, no. 8, pp. 1–5, 2010.
- [36] P. Pettersson, B. Jacobson, and S. Berglund, “Model for automatically shifted truck during operating cycle for prediction of longitudinal performance”, pp. 1–34, 2016.
- [37] MathWorks. (2016). Modeling an automatic transmission controller, [Online]. Available: <https://se.mathworks.com/help/simulink/examples/modeling-an-automatic-transmission-controller.html> (visited on 04/25/2017).

Bibliography

A

Appendix 1

Notations

T	Torque[Nm]
F	Force[N]
J	Mass moment of inertia[kg· m ²]
ω	Rotational speed [rad/s]
A_{ped}	Accelerator pedal position [%]
B_{ped}	Brake pedal position [%]
B_{dec}	Brake deceleration [m/s ²]
x, y, z	Vehicle position [m]
v_x, v_y, v_z	Vehicle velocity [m/sec]
a_x, a_y, a_z	Vehicle acceleration [m/s ²]
$\varphi_x, \varphi_y, \varphi_z$	Roll, Pitch and Yaw angle [rad]
$\omega_x, \omega_y, \omega_z$	Roll, Pitch and Yaw rate [rad/s]
$\dot{\omega}_x, \dot{\omega}_y, \dot{\omega}_z$	Roll, Pitch and Yaw acceleration [rad/s ²]
s_x, s_y	Longitudinal and lateral wheel slip
A_f	Frontal area [m ²]
a_x	longitudinal acceleration[m/s ²]
a_y	lateral acceleration[m/s ²]
C_d	Coefficient of drag
F_d	Drag force [N]
F_g	Road gradient force[N]
F_x, F_y, F_z	Longitudinal,Lateral and vertical force [N]
I_{xx}, I_{yy}, I_{zz}	Moment of inertia of vehicle body [kg·m ²]
l_f	distance from CG to front track [m]
l_r	distance from CG to rear track [m]
δ_f, δ_r	Front and rear wheel angle [rad]
$agear$	Gear number
i_{gear}	Gear ratio
i_{final}	Final drive ratio
M_z	Tire aligning torque [Nm]
m	Mass of the body [kg]
R	Radius of circular road[m]
r_w	Wheel radius [m]
c_{px}, c_{py}	Longitudinal and lateral tire cornering stiffness [N]
μ	Friction coefficient
μ_{sx}	Adhesion friction coefficient
μ_k	Sliding friction coefficient
β	body slip angle [rad]
k_{si}	Spring stiffness [N/m]
c_{di}	Damping coefficient [N/(m/s)]